REPORT NO. ARD-284

ADVANCED RESEARCH

DIVISION OF
HILLER AIRCRAFT CORP

Report No. ARD-284

December 1960

FINAL REPORT CONTRACT NONR 3023(00)

INVESTIGATION OF SPECIAL GROUND EFFECT MACHINE CONFIGURATIONS

M. F. Gates
Principal Investigator

C. L. Cochran
Research Assistant

ADVANCED RESEARCH
DIVISION HILLER AIRCRAFT CORP.

1. SUMMARY

This program has continued the evaluation of two unique GEM configurations (diffuser-recirculation and diffuser-plenum) conceived by this contractor and originally disclosed in Reference 1. The prime emphasis under this contract has been to investigate and document the performance and stability characteristics of the two concepts, and to determine means of achieving the required positive stability characteristics. This investigation has been accomplished with 2-dimensional model tests and supporting mathematical studies. The stability has been demonstrated with 3-dimensional, free-flight model tests.

Static 3-dimensional model tests have documented the performance of an inherently stable configuration of the original concept. The 3-dimensional model static test data of the diffuser-plenum GEM indicates that a performance of 4.20 air horsepower per square foot of gap area can be attained at a planform loading of 20 psf. The theoretical performance that can be attained with this configuration is 2.36. A concerted effort to improve diffuser efficiency, which was not made under this program, would obviously result in superior performance. The off-design hover performance is also presented.

Data is presented which describes the characteristics of the diffuser edge seal and exit gap as components of the GEM. This data describes the hover performance, the pitch and heave stability characteristics, the lifting efficiency, the diffuser efficiency, the diffuser pressure rise and a continuity parameter, which is the ratio of diffuser exit flow to the flow supplied to the diffuser.

ACKNOWLEDGEMENTS

This study was sponsored by the Office of Naval Research, United States Navy.

The authors also wish to acknowledge the help and guidance afforded by E. R. Sargent, Manager, Propulsion Department and F. A. Heileman, Director, Advanced Research, in the performance of this study. They also wish to thank D. A. Graber for his interest and invaluable assistance in the test phase, H. Wichers for his photographic coverage, and W. Churchill for his editorial assistance.

TABLE OF CONTENTS

TABLE OF CONTENTS (CON'T)

FIGURE LIST

FIGURE LIST (CON'T)

SYMBOL LIST

a	=	Horizontal length of flap	ft.
A_d	=	Planform area of diffuser	ft.^{2}
A_g	=	Total peripheral sealed gap	ft.^{2}
A_{gr}	=	Rearward projected sealed gap DP-3 model	ft.^{2}
A_{gr}	=	Exit rear gap area DP-2 model	ft.^{2}
A_j	=	Jet Nozzle area	ft.^{2}
A_1	=	Diffuser inlet area	ft.^{2}
A_2	=	Diffuser outlet area	ft.^{2}
A_p	=	Planform area	ft.^{2}
A_x	=	Duct cross sectional area at station x	ft.^{2}
b	=	Vertical height of flap	ft.
C_c	=	Contraction coefficient	
C_d	=	Discharge coefficient $\frac{\dot{w}_e \text{ actual}}{\dot{w}_e \text{ theo.}}$	
F	=	Horizontal propulsive thrust	lb.
G	=	Inlet jet thickness	in. (0.75)
G.W.	=	Model gross weight	lb.
h	=	Front lip ground clearance, DP-2	in.
h/D	=	Effective ground clearance, $\left(\frac{A_p}{hA_g}\right)$, DP-3	
HP	=	Air horsepower, supply	
$HP_{S.L.}$	=	Air horsepower sea level standard	

SYMBOL LIST (CON'T)

h_r	=	Ground clearance at rear gap or exit flap	in.
K	=	General loss coefficient, $\frac{\text{pressure loss}}{q}$	
K_D	=	Sum of nozzle-gap spanning loss, general friction and diffuser loss coefficients	
K_L	=	Sum of K_D, duct loss and residual velocity loss coefficients	
L	=	Lift	lb.
ℓ	=	Characteristic length of JP-3 model	in. (30)
ℓ'	=	Apparent diffuser length JP-2 model	in. (22)
m	=	$\frac{\ell}{h}\left(\frac{L}{q_a a}\right)$	
M	=	Moment, positive nose-up	in.lb.
P_a	=	Static pressure at station a, flap exit	psf
P_b	=	Base pressure (pressure at end of diffuser)	in. H_2O
P_o	=	Ambient pressure	in. H_2O
$P_{S.L.}$	=	Ambient pressure, sea level standard	in. H_2O
P_t	=	Total pressure, = "P + q"	psf
P_{te}	=	Exit total pressure	in. H_2O
P_{tr}	=	Reverse flow total pressure	in. H_2O
P_{ts}	=	Supply total pressure	in. H_2O
P_x	=	Static pressure at station x	psf
q	=	Dynamic pressure	psf

SYMBOL LIST (CON'T)

q_a	=	Dynamic pressure at station a, flap exit	psf
q_x	=	Dynamic pressure at station x	psf
T_s	=	Temperature, air supply	^oR
$T_{S.L.}$	=	Temperature, sea level standard	^oR
V	=	Velocity	ft./sec.
$\dot{w}_e$	=	Flow rate, exit	lb./sec.
$\dot{w}_s$	=	Flow rate, supply	lb./sec.
Y	=	Front lip droop	in.
g	=	Gravitational constant	ft./sec^2
θ	=	Initial jet angle, measured from vertical	degrees
ρ_s	=	Density of supply air	slugs/ft.^{3}
$\rho_{S.L.}$	=	Air density sea level standard	slugs/ft.^{3}
α	=	Angle of attack	Compatible units
ΔP_f	=	Fan pressure rise	psf

2. INTRODUCTION

Hiller Aircraft Corp., under this program, has investigated two GEM concepts (diffuser-recirculation and diffuser-plenum) which have potential for achieving efficient, high-speed transportation. As originally conceived, (Ref. 1) both of these concepts operate in part as open throat wind tunnels where the sealed peripheral gap represents the tunnel "test section". The diffuser-recirculation concept may be thought of as a "return-type" tunnel, i.e., no working fluid loss and fan pressure rise equals pressure losses in the circuit. The diffuser-plenum concept may be thought of as a "non-return-type" tunnel. Both concepts are shown in Fig. 1.

The diffuser-recirculation concept is the ultimate in hovering efficiency (zero power) in the ideal case. This assumes zero friction and working fluid loss. Friction losses are unavoidable, but with efficient duct and diffuser design the resultant hovering performance is superior to conventional systems.

The diffuser-plenum concept does not conserve its basic jet energy, but its mass flow requirements are considerably lower than in the recirculating concept because the air supply seals the peripheral gap twice, as influx and as efflux. (In Ref. 1 it is shown to be theoretically possible to reduce its mass flow to one-third that of the conventional plenum-annular nozzle ($C_c = 1$) or the diffuser-recirculation concept.) This concept also has the advantage of an unbalanced reaction in the forward direction, which provides a propulsive force as a free byproduct of the lift-producing system. This combination results in slightly superior

performance than that obtained with the diffuser-recirculation concept.

2.1 Description of Concepts

The hovering performance expressions, which are summarized in Fig. 2, were derived for the diffuser-recirculation concept, the diffuser-plenum concept, and the conventional plenum concept, and originally presented in Reference 1. The derivations are given in the Appendix of Reference 1. These expressions describe the required fan pressure rise and mass flux parameter for hovering flight at the design point in terms of the planform loading (L/A_p), the associated loss coefficients, and other pertinent variables. It will be noted that the mass flux parameter is, in actuality, the quantity of flow per unit of sealed gap area. The Air Horsepower parameter, which properly compares the systems, is the product of the fan pressure rise and mass flux parameter.

2.1.1 Diffuser-Recirculation Concept

In the analysis of this concept, the entire gap or diffuser inlet is assumed to be exactly filled by the horizontal jet, i.e., the static pressure across the gap is equal to ambient pressure. The jet is then diffused between the ground surface and lower surface of the GEM to convert its kinetic energy (dynamic pressure) to potential energy (static pressure), Fig. 1. This static pressure is applied over the base area to produce the lift force. Air from the pressurized zone is then recirculated by a small pressure boost with the fan to overcome the friction losses and the slight residual velocity head loss due to the finite expansion ratio of the diffuser. (The assumption that residual velocity is a complete

loss may be overly conservative.)

This analysis showed that the concept approached the ultimate in lift effectiveness in the ideal case (no pressure rise required once circulation is established) by virtue of the fact that the jet energy is conserved. Moreover, the mass flux required equals that of the conventional plenum chamber configuration in the ideal case. (In general, the ideal case is defined as one in which there are no friction losses, the escaping-jet-outlet-gap is flowing full ($C_c = 1$), and an infinite diffuser expansion ratio exists.)

In this analysis, it was assumed for simplicity that continuity is maintained throughout the system without efflux or influx. However, in a practical application of this concept, it is likely that make-up air will be required. This air could be supplied by an auxiliary fan installed to introduce air directly into the pressurized zone from the ambient. Another variation would supply the make-up air with an ejector pump.

2.1.2 Diffuser-Plenum Concept

Examination of the expressions (Fig. 2) derived for this concept reveals that the mass flux parameter is 1/2 that required for the conventional plenum concept when the peripheral gap is flowing full (contraction coefficient equals 1). The required fan pressure rise has been increased approximately by the factor of one minus the sum of the loss coefficients $(1 - K_L)$ or to the same value as the conventional plenum concept. Further examination of the expression in Fig. 2 indicates that if means are employed to reduce the outlet gap contraction coefficient to 0.5 in both concepts, the mass flux parameters of the diffuser-plenum concept are

reduced to 1/3, and the conventional plenum chamber is reduced to 1/2 of that which results from the peripheral gap of the conventional plenum concept flowing full ($C_c = 1$).

In addition to the advantage of a reduced mass flux, a horizontal propulsive thrust is obtained from the unbalanced portion of the escaping jet that opposes the diffuser inlet. This thrust is a free by-product of the lift-producing system. Referring to the expressions of Fig. 2 in the ideal case ($C_c = 1$), and with uniform ground clearance, the thrust is equal to twice the planform loading multiplied by the unbalanced area. As may be seen by examination of the expression in Fig. 2, the effect of the contraction coefficient is to decrease the horizontal thrust while the loss coefficient effect is nil. The reduction in mass flux, production of free forward thrust, and utilization of the high velocity air directly from the fan without prior diffusion and contraction give this concept the potential for improved performance over existing systems.

Fig. 3 presents graphically the hovering performance expressions of Fig. 2. The upper plot shows the required fan pressure rise, the middle plot gives the mass flux parameter, and the lower one indicates the air horsepower per unit sealed gap area. These parameters are plotted versus the planform loading.

The shaded areas indicate the probable regimes of the specified cycles. The curved arrows represent the regimes of the annular nozzle configuration. The data points indicate the results of the work which formed the basis for this ONR program.

3. DISCUSSION

Hiller's pre-contract work provided adequate documentation of the hovering performance of the original concepts considering the state-of-the-knowledge of the stability characteristics at the beginning of the program. Consequently, the major effort under this contract has been directed toward investigation and documentation of the stability characteristics of the two concepts in hover and forward flight, and the attainment of the required positive stability characteristics. More complete hovering performance was obtained as a by-product of the stability investigation.

An experimental study was conducted using two-dimensional models with both free-floating and fixed ground boards (Figs. 4 through 7), and three-dimensional GEM models powered by model airplane engines. The most sophisticated model (DP-3) is shown in Figs. 8 through 11. Appropriate mathematical analyses were made in support of the experimental program.

3.1 Concept Modifications

Four concept modifications were evaluated in this study. They are listed below with their specific contributions to the stability of the system and are illustrated in Fig. 9.

1. Forward Lip Droop

   Forward lip droop prevents the diffuser inlet from completely closing when the ground clearance goes to zero. This insures uninterrupted flow to the plenum chamber.

2. Initial Jet Angle

The initial jet angle controls the jet's lift reaction which contributes to positive stability, and also controls, to a large extent, the amount of reverse flow.

3. Ventilation of the Diffuser Inlet

The ventilation of the diffuser inlet greatly reduces the negative base pressure generated by Bernoulli's effect when the diffuser inlet drops below the height equal to the initial jet thickness.

4. Exit Gap Geometry

A trailing flap applied to the exit gap of the diffuser plenum configuration produces a very stable element at that point, and eliminates unstable coupling between the diffuser inlet and exit gap.

3.2 Diffuser Plenum Concept

The initial emphasis was placed on the achievement of suitable stability characteristics with the diffuser plenum (DP) concept because of its potential in forward flight.

3.2.1 Two-Dimensional (2-D) Program

3.2.1.1 Experimental Apparatus and Procedures

The two-dimensional or component model used in these tests

was supplied with air by V1710 Allison superchargers as required to maintain a base pressure (diffuser exit pressure) of 20.8 psf. This value was maintained throughout the test program. Fig. 4a shows the basic component model. The model was tested in an inverted attitude to permit qualitative stability observations with a floating ground board. The forward lip shown installed in this figure gives an initial jet angle (θ) of 90°. Fig. 4 shows the model installed on the air supply duct. The test technician is adjusting the forward lip droop with the "$\theta = 61^{\circ}$" forward lip installed. Fig. 5 shows the model and the manometer panel with data recording camera at the far right.

A standard sharp-edged orifice was used as the primary flow meter in the supply duct upstream of the model. The necessary pressure, temperature and area measurements were made to determine accurately the flow rate of air supplied to the model. The total supply pressure (P_{ts}), which represents the required fan total discharge pressure, was measured upstream of the jet nozzle (at floor level in Fig. 4) in the 12-inch-diameter supply duct. The total exit pressure (P_{te}) was measured downstream of the sharp-edged outlet gap of the model. A total pressure probe (P_{tr}) was installed forward of the model to indicate the presence of reversed flow from the inlet. Fig. 12 locates these points of measurement. In the first 2-D test series only model base static pressures were determined; in the second 2-D series both ground plane and model base static pressures were measured. The static pressure tap locations are shown in Fig. 12.

All pressures were simultaneously recorded photographically.

A typical photo is shown in Fig. 13. The pressure distribution data was reduced to useable form by projecting the photographed data directly on graph paper of the proper scale. The image was then traced on the graph paper for further analysis, and pressure-area calculations were made for the determination of pitching moment and generated lift. These tracings are presented in Appendix 2.

The model exit gap was calibrated as a flow meter under actual test conditions so that mass flow lost either by reversed flow at the diffuser inlet or by venting could be determined. The calibration is tabulated below:

Rear Ground Clearance $\frac{h_r}{l}$	Exit Area A_{gr}, ft.^{2}	C_d
0.0336	.0953	.465
0.0461	.131	.615
0.0568	.161	.625
0.0685	.199	.659
0.0798	.226	.679
0.0906	.257	.679

$$\text{where } C_d = \frac{\dot{w}_{e\ actual}}{\dot{w}_{e\ theo}}$$

$$\dot{w}_{e\ actual} = \dot{w}_s$$

$$\dot{w}_{e\ theo} = g\rho_e A_{gr} V_e$$

$$V_e = \sqrt{\frac{2}{\rho_e}}\sqrt{P_{te}}$$

This tabulation shows an unusual characteristic in that the flow coef-

ficient drops to an abnormal value at $\frac{h_r}{\ell}$ of 0.0336. A study of the static pressure distribution at this test condition reveals that such a coefficient can be attributed to the highly turbulent flow which exists in the plenum chamber.

Fig. 14 presents, for convenience, the relationships between rear gap clearance and ground clearance at the various test conditions. This figure also permits correlation to be made between the discharge coefficients and $\frac{h}{\ell}$, the front ground clearance.

The primary nozzle exit dimensions (diffuser inlet dimensions at the design condition) were 0.75 in. (G) by 18.3 in. The 0.75 dimension represents the side wall area, and the 18.3 dimension the ground board area. Since the former dimension was much less than the 18.3 inch dimension, side wall effects were negligible. One side wall was constructed of Formica and the other of Plexiglas to reduce side wall friction further. The model base was constructed of aluminum and finished with 400 grit, wet-or-dry paper; the ground board was constructed of unfinished plywood. The rigid ground board shown in Fig. 4 was used in quantitative fixed ground board tests. A lightweight, loosely fitting, floating ground board was used in the tests conducted for a qualitative appraisal of the stability characteristics.

The rear gap (h_r, A_{gr}) was set to give the minimum reverse or pumping flow at each basic test condition (Y/ℓ, θ, vented or unvented) with the diffuser inlet height ($\frac{h+Y}{\ell}$) equal to the initial jet thickness (G/ℓ). This flow condition was monitored by the P_{tr} probe and flow visualization techniques. This value of h_r was used in each pitch case, and

is the starting point for each heave case.

3.2.1.2 Experimental Program (2-D)

The initial series of two-dimensional tests, using a free-floating ground board, were largely qualitative in nature. This series indicated that strong negative stability (pitch and heave) characteristics existed at the diffuser inlet. In an attempt to overcome this problem, the effects of venting the diffuser inlet to atmospheric pressure and of manipulating forward lip geometry were evaluated. With the ground board fixed, model base surface pressure distributions were obtained for various front lip geometries, with and without ventilation of the diffuser inlet, along with the other data mentioned in previous paragraph 3.2.1.1.

This test series indicated that manipulation of the forward lip geometry (that is θ and Y, see Fig. 12) and venting of the diffuser inlet tended qualitatively to result in desirable stability characteristics. However, detailed analysis of the model base pressure distributions failed to support this observation. It is believed that this contradiction was due to the lack of detailed knowledge of the primary jet contribution. The qualitative observations made in this test series gave sufficient encouragement to warrant the construction of a small three-dimensional model using the diffuser-plenum concept and incorporating the geometry evolved from the two-dimensional tests. The results of model (DP-3) tests are discussed in detail in paragraph 3.2.2.

The second test series added considerably to the knowledge of the concept. The notable difference between this series and the

previous series was that this series measured both the model base and ground plane static pressures, whereas the previous measured only the model base pressures. The ground plane static pressures include the effect of the primary jet. In this series two different modes of operation were studied: in the first, the ground plane was adjusted to simulate heave above and below the basic h and h_r described in paragraph 3.2.1.1 (Heave Case), and in the second, the exit gap area (A_{gr}) was maintained at a constant value (i.e., the ground plane was pitched about the exit flap of the diffuser-plenum concept - Pitch Case). This latter case is also applicable to the diffuser-recirculation case. The data will be discussed from the viewpoint of the diffuser-recirculation concept in paragraph 3.3.

3.2.1.3 Data Presentation Philosophy (2-D)

The 2-D data analysis philosophy is as follows: The diffuser system was considered as the means of sealing the peripheral gap around and beneath a GEM of any base area; the component model is a two-dimensional slice of this edge seal. The diffuser-plenum model's exit gap represents the total exit area of a three-dimensional configuration, which may have this exit area distributed over 3 sides of the vehicle depending on the detail design.

In the test program the air power input to this edge seal was varied (and measured) as required to achieve a constant diffuser static exit pressure (i.e., base pressure) of approximately 20 psf (4 inches of water) over the range of ground clearance tested with the various geometrical variations.

All of the 2-D data presented is plotted against the ground clearance h/ℓ measured at the forward lip (see Fig. 12). In addition, selected data is plotted against the diffuser inlet ground clearance $\frac{(h+Y)}{\ell}$ to demonstrate the general dependence of the specific data on this parameter. All data is presented as a function of the forward lip droop, (Y/ℓ) and initial jet angle, θ. Also included as reference for each basic data parameter (pitching moment, diffuser efficiency, etc.) is a similar curve of the basic data parameter for the unmodified concept (i.e., $\theta = 90^\circ$, $Y/\ell = 0$, unvented diffuser).

The relationship between the dimensionless ground clearance (h/ℓ) and the dimensionless forward lip droop (Y/ℓ), for $\frac{h+Y}{\ell} = \frac{G}{\ell}$ (the design point), is tabulated below:

Y/ℓ	h/ℓ for $\frac{(h+Y)}{\ell} = \frac{G}{\ell}$
0	.0341
.0114	.0227
.0170	.0171

It will be noticed that the various data will tend to become optimum at these appropriate values of ground clearance.

The pitching moment is taken about the apparent diffuser exit. The apparent diffuser exit is defined as that point along the diffuser where the static pressure equals 95 percent of the exit static or base pressure. This point was established at the test condition requiring the greatest diffusion length, and was maintained constant throughout the data reduction. To non-dimensionalize the pitching moment, it is referred

to the diffuser length (ℓ), which is the distance from the apparent diffuser exit to the point representing the forward edge of the diffuser inlet vent, and L is the lift force generated by the diffuser. The sense of the moment is conventional: positive, nose up. (Refer to Fig. 12).

3.2.1.4 Discussion of Results (2-D)

3.2.1.4.1 Diffuser Pitching Moment

The non-dimensionalized form of the pitching moment, which, in effect, is the center-of-pressure location forward of the reference point expressed as a fraction of the diffuser length, ℓ, is presented for the heave case in Fig. 15 and for the pitch case in Fig. 22. Notice in the heave case, with $\theta = 90^{\circ}$, that the effect of venting becomes apparent at low ground clearances. Forward lip droop has no apparent significance at $\theta = 90^{\circ}$ or at the other values of θ. Further examination of Fig. 15 indicates improved stability due to decrease in jet angle. These results are contrary to the qualitative observations which indicated that leading edge droop equal to a minimum of 40 percent of the initial jet thickness was required to achieve positive stability throughout the entire operating regime. The same general trends are seen to hold for the pitch case (Fig. 22).

3.2.1.4.2 Diffuser Lift Effectiveness (and Heave Stability)

The diffuser lift effectiveness curves describe two characteristics. First, the lifting efficiency of the diffuser is expressed as a ratio of its generated lift to the lift which would be produced if the base pressure (diffuser exit static pressure) were applied to the entire

diffuser area. Second, it describes the heave stability of the diffuser section where the denominator of the effective ratio, $(\frac{L}{p_b \lambda_p})$ can be considered the required lift, since the base pressure (p_b) is held constant. The heave case is presented in Fig. 16 and the pitch case in Fig. 23. Study of these figures will show venting effects similar to those seen on the pitching moment characteristics discussed previously for $\theta = 90^{\circ}$. The effect of θ is not the same as on the pitching moment characteristic. The general effect of droop is repeated from the pitching moment case.

3.2.1.4.3 Diffuser Efficiency

The diffuser efficiency is presented as the ratio of exit total pressure to the supply total pressure. This ratio defines the energy remaining in the jet after being diffused to create the base pressure and then reaccelerated out the rear gap. This data is presented in Figs. 17 and 18 for the heave case and in 24 for the pitch case. In the heave case the diffuser efficiency is plotted against the diffuser inlet ground clearance $(h+Y)/\ell$ (Fig. 18) as well as the ground clearance h/ℓ (Fig. 17). These duplicate plots demonstrate the dependence of the system characteristics on the diffuser inlet ground clearance. It will be noted from the curves describing the heave case that venting causes the curves to peak more sharply and also reverses the effect of droop, Y/ℓ, i.e., efficiency decreases with increasing droop when vented, while it increases with increasing droop when unvented. There is no significant effect due to θ in the heave case.

The same does not hold true for the pitch case, Fig. 24, where an appreciable increase in diffuser efficiency with decreasing θ is shown. Venting in the pitch case results in an appreciable decrease in diffuser efficiency at the higher values of droop for $\theta = 90^\circ$. The trend with droop at $\theta = 61^\circ$ and 32° is not strongly defined.

3.2.1.4.4 Flow Available for Forward Propulsion

The flow available for forward propulsion is presented in Fig. 19 for the heave case, and in Fig. 25 for the pitch case. This data is presented as the ratio of the flow rate through the calibrated exit gap of the model to the flow rate supplied to model. These curves, in effect, describe the divergence of the particular configuration from the idealized original concept and design point. In this concept ambient pressure was assumed to exist at the diffuser inlet, and consequently, no reverse or pumping flow occurred. This parameter has significantly different characteristics between the heave and pitch case. Properly combining this factor with the diffuser efficiency factor defines the maximum horizontal integrated propulsive thrust available to the diffuser-plenum concept.

3.2.1.4.5 Diffuser Pressure Rise

The diffuser pressure rise is presented in Fig. 20 for the heave case and in Fig. 26 for the pitch case as the ratio of the diffuser exit static pressure (base pressure) to total supply pressure. This parameter completes the description of the flow system. It will be noted that these curves have the same general characteristics as the diffuser

efficiency curves.

3.2.1.4.6 Hover Performance

The hovering performance is presented in terms of the air horsepower (at sea level standard) per unit sealed gap area corrected to a constant value of diffuser exit static pressure (base pressure). This was obtained as follows:

$$\frac{HP_{S.L.}}{A_g} = \frac{HP}{A_g}\sqrt{\frac{\sigma_t}{\sigma_{S.L.}}}\left(\frac{h}{P_b}\right)^{3/2}$$

$$= \frac{w_s P_{ts}}{\rho_{S.L.} A_g}\sqrt{\left(\frac{T_s}{T_{S.L.}}\right)\left(\frac{P_{S.L.}}{P_o}\right)}\ \frac{5.2}{550}\ \left(\frac{h}{P_t}\right)^{3/2}$$

This data is presented in Fig. 21 for the heave case and in Fig. 27 for the pitch case. As might be anticipated, there is a small loss in performance chargeable to venting the diffuser inlet. In the heave case the loss chargeable to droop is much more severe. Interestingly enough, in the pitch case there is essentially no loss chargeable to droop. It will be noticed that with $\theta = 90^\circ$ and the diffuser inlet vented, the minimum power occurs when h/ℓ is such as to give a diffuser inlet ground clearance equal to G/ℓ. However, decrease of θ to 32° decreases the power further for minimum power. As θ decreases to 61° h/ℓ tends to exceed G/ℓ. The minimum power in the pitch case decreases as $\frac{h+Y}{\ell}$ exceeds $\frac{G}{\ell}$

3.2.1.4.7 Effect of Initial Jet Angle on Diffuser Inlet Flow

With $\theta = 90^\circ$ it was possible to achieve negligible reverse or pumping flow. At $\theta = 61^\circ$ or 32°, it was not possible to achieve this zero secondary flow condition due to splitting of the jet when it strikes the

ground plane. However, at $\theta = 90^{\circ}$, 51° or 32°, the minimum reversed or pumping flow occurred at the same rear gap setting (h_r, A_{gr}). This was found to be true whether the diffuser inlet was vented or not.

3.2.2 Three-Dimensional (3-D) Model Tests

As mentioned in paragraph 3.2.1.2, the results of the initial 2-D test series, which indicated that a stable configuration could be achieved by appropriate geometrical adjustments, gave sufficient encouragement to warrant construction of a small 3-dimensional model of the diffuser plenum concept incorporating the geometric changes evolved in the 2-D tests. This model incorporated a trapezoidal planform to achieve maximum utilization of the available free by-product propulsion, but preserved the model length to achieve efficient diffusion and model span for maximum roll stability. The planform can be seen in Figure 8. The characteristic dimensions of the model are given in Fig. 9.

Successful free flight tests with this model confirmed the findings of the 2-D tests. In the initial tests before the diffuser inlet vent was installed this model showed stability characteristics somewhat similar to those observed in the initial 2-D tests with a floating ground board. (The original stability characteristics and the specific problem areas are discussed in paragraph 3.2.1.2). The addition of diffuser inlet venting to the system in combination with the existing forward lip droop greatly improved the stability. However, in order to achieve positive stability characteristics in the 3-D case throughout the operating regime, it was necessary to modify the rear gap from the original sharp edged configuration to one incorporating a trailing flap. The resulting rear gap geometry

is shown in Fig. 8. Fig. 9 shows a longitudinal section through the model. The concept modifications can be easily identified. The flat, trailing flap gave strong positive stability at the rear gap, which eliminated the undesirable coupling between the diffuser inlet and sharp edged rear gap. The re-entrant orifices at the side-rear were used to reclaim a portion of the ground clearance lost by means of the flat, trailing surface (jet thickness equals ground clearance (exit gas) in the case of an orifice formed by such a flat, trailing flap).

Fig. 2C shows a series of photos of the GEM model approaching and passing the viewer on a tether, moving at a velocity of approximately 14 feet per second. Forward thrust force supplied as a free by-product of the lift system is discussed in paragraph 3.2.2.4. The gross weight of the model at the time of the tests was 13.2 pounds; the installed horsepower approximately 0.3; the operating altitude approximately 3/5" (3% of h/D). No instability was noted in either roll or heave.

Following the qualitative free flight tests, this model was completely evaluated in the static (hover) case. Complete ground plane pressure surveys were made over a range of rear gap ground clearances and angles of attack. The flow rate of air supplied to the model was also determined. The supply pressure immediately upstream of the primary jet nozzle was monitored closely during the tests to insure that its value represented that which existed with the original power plant installation. Previous tests with the model power plant had indicated that an essentially flat fan characteristic existed in the model operating range. The test setup is shown in Figs. 10 and 11. The model is

inverted beneath the plexiglas ground plane.

3.2.2.1 Static Performance (3-D)

The ground-plane pressures, along with the air flow rate and supply pressure data, have been reduced to give curves which describe the static performance and stability of the model. The static performance presented as the air horsepower per unit lift (specific horsepower) can be found in Fig. 29, plotted against a ground clearance parameter (one quarter of the ratio of total scaled peripheral gap area to planform area) or an effective $\frac{h}{D}$ ratio. The data in this plot is corrected to the design planform loading of 2.5 psf, but not to sea level standard conditions. Cross-plotted on this figure are lines of constant rear gap ground clearance (h_r). A large increase in the specific horsepower occurs at a given value of the effective ground clearance parameter when the rear gap ground clearance increases from 1/4 to 3/8 inch ($\frac{h}{l}$ = .0083 to .0125). This is particularly noticeable at angles of attack greater than approximately 0.50 degrees. To explain this characteristic, consider that to achieve an increase in rear gap at a constant value of the effective ground clearance parameter, it is necessary to reduce the angle of attack. This, in turn, increases the diffuser area ratio and, simultaneously, the diffuser included angle. The increase in area ratio tends to create a situation of overexpansion in the diffuser. This condition, plus the increase in diffuser angle, results in separation in the diffuser and understandable losses. The design value of the ground clearance parameter for this model is 0.02;

the operating rear gap clearance is approximately .1", and the operating trim angle of attack is approximately 0.75 degrees.

3.2.2.2 Pitch Stability

The pitch stability characteristics in hover are presented in Fig. 30. This characteristic is presented as a non-dimensional pitching moment versus the angle of attack for each test, rear gap clearance of 1/8", 1/4", 3/8" and 1/2". These curves quantitatively support the demonstrated pitch stability of the 3-D model in free flight. Comparison of the curves will show that there is no definable trend for the variation of trim angle with rear gap clearance. The trim angle ranges between zero and plus one degree. This lack of correlation can be attributed to two factors: 1) data spread inherent in obtaining pitching moment from pressure distribution, and (2) general insensitivity of trim angle to rear gap clearance. It is believed that the lack of correlation between the slopes of these curved ($\frac{dM}{d\alpha}$) can be similarly explained. The sense of this pitching moment is conventional, i.e., positive-nose up, taken about the center of gravity.

3.2.2.3 Heave Stability (3-D)

The heave stability of this model is presented in Fig. 31 in terms of generated lift divided by required lift, or model gross weight, versus rear gap clearance. This information is presented for various test angles of attack. It is seen from this plot that, in general, heave stability exists at all ground clearances and at angles of attack from 0° through 2.86° with a neutral to negative stability area below a rear gap height of 1/4" at an angle of attack (α) equal to 2.86 degrees. It is

It is believed that additional data at α = 2.86 degrees would indicate positive heave stability characteristics down to zero gap clearance. The data also indicates that if a pitch-down occurs below zero degree angle of attack, a loss in ground clearance will result. This characteristic was not observed in the free flight tests of the model.

3.2.2.4 Inherent Integrated Propulsion (3-D)

In this static evaluation of the DP-3 GEM model it was found difficult to measure accurately its inherent unbalanced horizontal reaction (the free by-product propulsive thrust) due to the small magnitude of this force. Measured values were 1.0-1.5 pounds. This force may be estimated from the other known data, if it is assumed that the air escaping through the side gaps of the vehicle leaves at right angles to the side, and that the thrust coefficient is unity.

Classically

$$F = \frac{\dot{W}}{g} V = \rho C_c A_{gr} V^2$$

where A_{gr} is the total rearward projected sealed are of the side and rear gaps and V is the velocity resulting from a driving pressure equal, on the average, to the model planform loading, $V = \frac{2}{\rho} \frac{L}{A_p}$. Substituting this expression into the previous expression

$$\text{gives } F = 2(A_{gr}) \left(\frac{L}{A_p}\right)$$

At the operating point the estimated forward propulsive thrust is approximately 0.42 lb. Comparing this value to one of approximately 1.3 lb. obtained from the tests, it can be surmised that the air escaping through

the side gaps does so at an angle which is favorable for forward propulsion, i.e., one which is considerably more rearward than perpendicular to the GEM side.

3.2.2.5 Preliminary Over-Water Tests (3-D)

Upon completion of the static evaluation of the DP-3 GEM, the original power plant was re-installed to permit a quick, preliminary insight into the over-water characteristics of this GEM concept. Fig. 32 shows the model in stable over-water operation. These initial tests indicated that there was insufficient power installed for the vehicle to accelerate itself beyond hump speed. When the model was accelerated above hump speed by means of a self-releasing "tow-line", it was found that the integrated propulsion was adequate to cause the model to overtake the tow line (resulting in release) and to continue in "planing" operation. It is to be emphasized that stable operation resulted both below and above hump speed.

3.2.2.6 Hover Performance Comparison (3-D)

Fig. 33 (similar to Fig. 2) shows a comparison of the original predicted performance for the diffuser-plenum concept with performance data for the stabilized 3-D model. The 3-D data point represents the operating point of the model. For clarity, this data is scaled to and plotted at a planform loading of 100 psf. It will be noted that considerable variance is indicated. This can be attributed to several causes; model scale, 3-d dimensional flow in the diffuser, and the stability fixes. Recall, however, that this plot does not

include the performance benefits accrued from the "free" horizontal propulsive thrust. An additional item of explanation defining the air horsepower parameter ordinate is that it is related to total sealed peripheral gap area in square feet.

3.2.3 Exit Gap Geometry

Considerable effort was extended to describe mathematically the lift and characteristics of a trailing flap applied to the exit gap of the diffuser-plenum concept. The analysis was made assuming conservation of mass and energy, one-dimensional, inviscid, incompressible flow with $C_c = 1$, and considering one foot of exit flap width. Two general cases were examined: that of a straight flap, and that of an elliptical flap.

3.2.3.1 Straight Flap

The results of the straight flap analysis, derived in Appendix I are shown in Fig. 34. This figure defines the lift coefficient for variations of the trailing flap slope, characterized by dimension b, as a function of the ground clearance h. Further analysis of the straight flap characteristics equation, from which Fig. 34 was drawn, was made to determine the design configuration. This is the configuration which would give the maximum rate of change of lift with variations in ground clearance, m*,

---

* $m = \frac{\partial}{\partial h} \left(\frac{L}{q_a a}\right)$

as a function of that ground clearance and the flap slope. This was accomplished by the simultaneous solution of the partial derivatives, with respect to h and b of the straight flap equation set equal to 0. This analysis indicated that dimension b should equal the ground clearance h in order to achieve this maximum m. At this condition, m was found to equal minus one quarter of the reciprocal of the ground clearance. The locus of the points of the maximum m is shown in Fig. 34, and occurs at a constant value of the non-dimensionalized lift coefficient equal to 0.5.

Although the characteristics equation for the straight flap was sufficiently simple so that the above mentioned locus could be determined entirely from mathematical considerations, a graphical presentation of this locus is given in Fig. 35 to aid in the understanding of the solution. From Fig. 35 the relationship of h and b at the points of maximum m was easily determined and is presented in Fig. 36. The relationship thus determined was that b should equal h to achieve this maximum value of m, which is equal to $\frac{.25}{h}$. Thus, for any desired operating ground clearance, the design flap dimensions and the rate-of-change-of-lift with h can be determined.

Pitch effects on the straight flap were investigated, as described in Appendix 1. The net effect of pitching on the operation of an initially stable system is one of stabilization. An examination of the equation (10a) in Appendix 1 and the accompanying sketch shows that pitch changes cause a change in the flap slope, effectively represented by b (up to about 15°). A nose up or positive pitch produces an increase in

by a nose down or negative pitch produces a decrease in b. Reference to Fig. 36 shows that an increase in b increases the lift due to the flap, while a decrease in b has an opposite effect. Both these effects tend to return the complete system to the equilibrium attitude.

3.2.3.2 Elliptical Flap

The results of the elliptical flap analysis, derived in the appendix, are shown in Fig. 37, which describes the lift coefficient for various eccentricities as a function of ground clearance h. Since the elliptical flap characteristics equation, from which Fig. 37 was drawn, was of a complex nature, the determination of the configuration for maximum m by ordinary mathematical means proved to be beyond the scope of the study. The resulting expressions are shown in Appendix 1. Consequently, it was necessary to revert to the graphical method described previously for the straight flap. The curves of Fig. 38 show the relationship between h, b, and m. The curve through the maximum points of the curves of Fig. 38 describes the maximum rate of lift change with ground clearance. From the analysis of Fig. 35 this maximum rate of lift change was found to equal $-(\frac{.296}{h})$. This curve has been cross plotted in Fig. 39. Figure 39 can be considered a "design" relationship, i.e., for a specified design ground clearance h the curve specifies the value of b which will cause maximum m to occur at the design ground clearance. It can be seen that for b values greater than 0.50 the curve of h as a function of b is essentially a straight line. Below 0.50 the relationship between h and b, as determined from the curve of Fig. 38, deviates at an increasing rate from that which would satisfy the same limit as the

straight flap case, i.e., pass through the origin. It is apparent that in both cases, straight and elliptical, the solution should become equivalent as b approaches zero.

Pitch effects on the elliptic flap were also investigated, as described in Appendix 1. As in the case of the straight flap, the net effect of pitching on an initially stable system is one of stabilization. Examination of equation (43), Appendix 1, shows that small pitch changes effectively cause a change in the eccentricity ratio of the ellipse, characterized by dimension b. Reference to Fig. 38 shows that an increase in b increases the lift coefficient, while a decrease in b has an opposite effect. Both these effects tend to return the complete system to the equilibrium attitude.

A brief investigation revealed that there are at least two other methods of integrating equation (15), Appendix 1, but the limitations of this program did not allow an extensive study of the results so obtained. Cursory examination, however, indicated that the elliptic flap characteristic curves obtained from these other solutions would be identical to those obtained by the solution derived in the Appendix, equation (40), for values of b greater than approximately 0.50 even though the basic expressions differed.

It should be pointed out that for both the straight and elliptical flaps the characteristic equations and their derivatives with respect to h cease to have meaning at h = 0 and b = 0, at least in their presented forms. At this point the expressions become functions of indeterminate ratios. The values of the expressions could possibly be found for h and b = 0 by application of L'Hôpital's rule, but this step again was beyond the scope of this program.

3.3 Diffuser-Recirculation Concept

The 2-D diffuser-recirculation model is shown in Figs. 6 and 7. This model consisted of a diametric slice of the concept configuration with a reduced (shortened in 2-D) base area. The purpose of this model was to evaluate the coupling between the opposing diffusers, to determine the amount of make-up air required and also the effect of excess air on the stability of the system. It was not possible to carry this study as far as had been intended due to time limitations, and consequently, only qualitative observations are available.

It was noted that "excess cycle air" tended to improve the stability of the system, and that unstable coupling did exist between the opposed diffuser inlet. Sufficient time did not exist to evaluate the geometrical variables that were successful in the diffuser-plenum case to determine their effect on coupling. It would be expected that these same stability components would have similar results in this case.

The data presented for the diffuser-plenum concept pitch case (Figs. 22 through 27) can be appropriately corrected and applied to the diffuser-recirculation concept, since the basic edge seals are identical. Reference to Fig. 26 which presents the flow available for recirculation, indicates that make-up (or excess cycle air) is required, and also that this requirement, the make-up air fraction $(1 - \frac{\dot{w}_e}{\dot{w}_s})$, increases only slightly with decreasing θ. The flatness of the curve indicates that this requirement is essentially constant. This documented need for make-up air supports the qualitative observation that "excess cycle air" improved system stability.

It is believed that the addition of this air to the cycle will not affect the validity of the other parameters, since this addition occurs external to the edge seal. Consequently, all the pitch case data is applicable as presented. Only the hovering performance need be modified. The following equation corrects this parameter:

$$\left.\frac{HP_{S.L.}}{W_g}\right|_{I-R} = \left.\frac{HP_{S.L.}}{W_g}\right|_{L-P} \left(1 + \frac{h_r}{h}\right) \left(1 - \frac{P_{te}}{P_{ts}}\right) + \left(1 - \frac{Q_e}{Q_s}\right)$$

where the term $(1 + \frac{h_r}{h})$ corrects the sealed fan area, the term $(1 - \frac{P_{te}}{P_{ts}})$, which is defined by Fig. 24, corrects for the pressure loss of the system, and the term $(1 - \frac{Q_e}{Q_s})$ corrects for the make-up air required. Further correction must be made for inefficiencies of the return ducting.

4. CONCLUSIONS

4.1 Simple geometrical modifications to the original concepts were devised to overcome the inherent instabilities. These instabilities resulted from a strong destabilizing force at the diffuser inlet due to Bernoulli effect which occurred when the diffuser inlet ground clearance decreased below the design value. The geometrical modifications required to overcome the destabilizing force consisted of venting the diffuser inlet to atmospheric pressure, extending the forward lip below the diffuser inlet, and orienting the primary jet outlet to provide a positive jet contribution to the stability of the system.

4.2 To achieve positive stability characteristics for the diffuser-plenum 3-D model, it was necessary to modify the rear exit geometry to incorporate a trailing surface. This modification provides a positive stability contribution at that location, and eliminates the undesirable coupling which previously occurred between the neutrally stable, sharp-edged exit geometry and the diffuser inlet. Mathematical analyses of this exit geometry were made to map it's stability characteristics.

4.3 The magnitude of the inherent integrated propulsion in the 3-D diffuser-plenum model was found to be on the order of twice that predicted by the previous performance estimates. This increase can be attributed primarily to the escaping jet leaving the vehicle at an angle more favorable to propulsion than had been originally assumed. Also, in the original performance estimate, no accounting was made for the rearward component of the residual velocity existing in the base area.

4.4 On the basis of the work completed, the Miller diffuser-recirculation concept warrants more extensive investigation than was possible within the scope of this program. Future research should include more detailed investigations on the effect of excess air on coupling between the opposing diffuser inlets.

5. REFERENCES

1. Gates, M. F., and Sargent, E. R.: "Development of a Unique GEM Concept with Potential for Achieving Efficient Forward Flight", Hiller Aircraft Corp., Advanced Research Division Report No. 248, October, 1959.

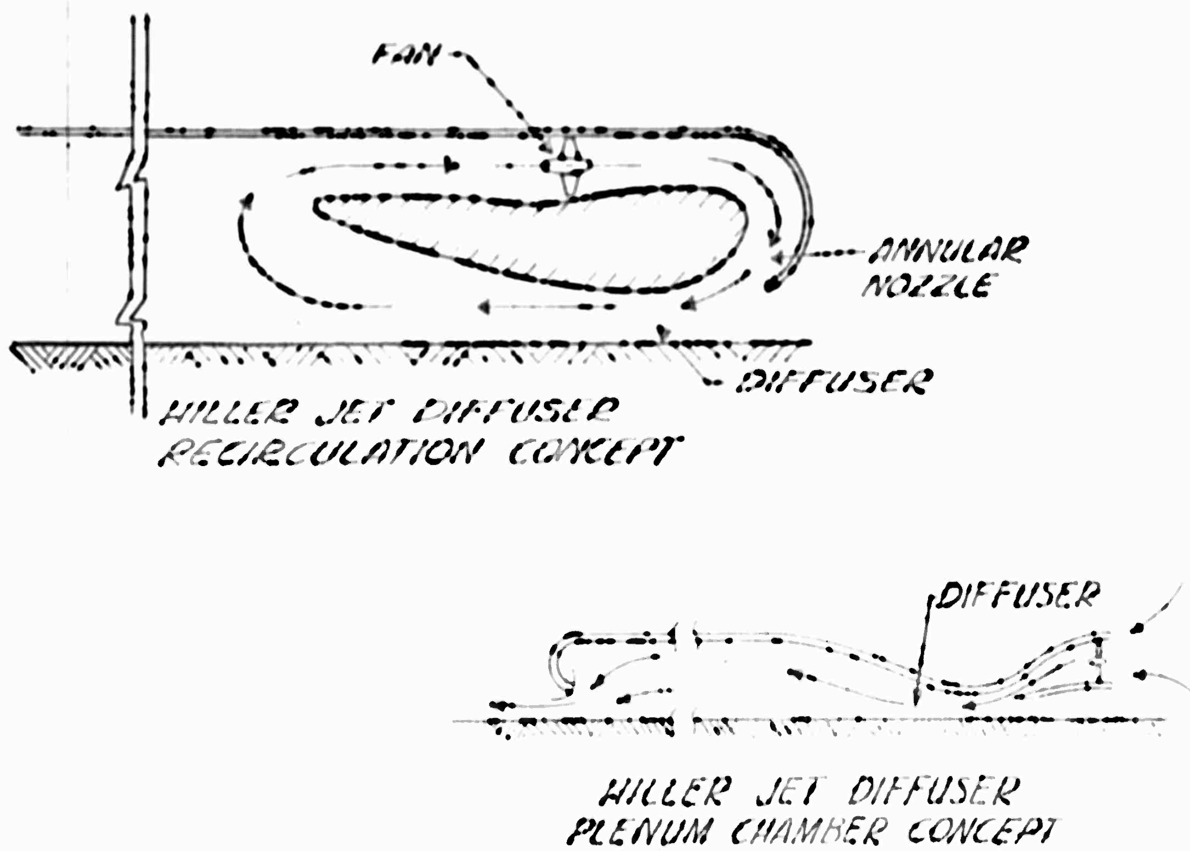

FIGURE 1; HILLER DIFFUSER CONCEPT

	Fan Pressure Rise ΔP_f	Mass Flux Parameter $\frac{W}{g\rho}\cdot\frac{1}{A_1}$	Air Horse Power Parameter $HP\cdot\frac{1}{A_3}$
	$\dfrac{K_L \frac{L}{A_P}}{\left[1-K_D-\left(\frac{A_3}{A_2}\right)^2\right]}$	$\left\{\dfrac{\frac{2}{\rho}\frac{L}{A_P}}{1-K_D-\left(\frac{A_3}{A_2}\right)^2}\right\}^{1/2}$	$\Delta P_f\left(\frac{W}{g\rho}\cdot\frac{1}{A_3}\right)\frac{1}{550}$
 $\frac{F}{A_1}=\dfrac{2\frac{L}{A_P}C_c[1-K_D]}{1-K_D-\left(\frac{A_3}{A_2}\right)^2}$	$\dfrac{\frac{L}{A_P}}{\left[1-K_D-\left(\frac{A_3}{A_2}\right)^2\right]}$	$\dfrac{\left\{\dfrac{\frac{2}{\rho}\frac{L}{A_P}}{1-K_D-\left(\frac{A_3}{A_2}\right)^2}\right\}^{1/2}}{\frac{A_1}{A_3}+\frac{1}{C_c[1-K_D]^{1/2}}}$	
	$\frac{L}{A_{P_L}}\left[1+(K_3+K_4)C_c^2\left(\frac{A_3}{A_1}\right)^2\right]$	$C_c\left(\frac{2}{\rho}\frac{L}{A_P}\right)^{1/2}$	

Figure 2 Summary Tabulation of Performance Expressions

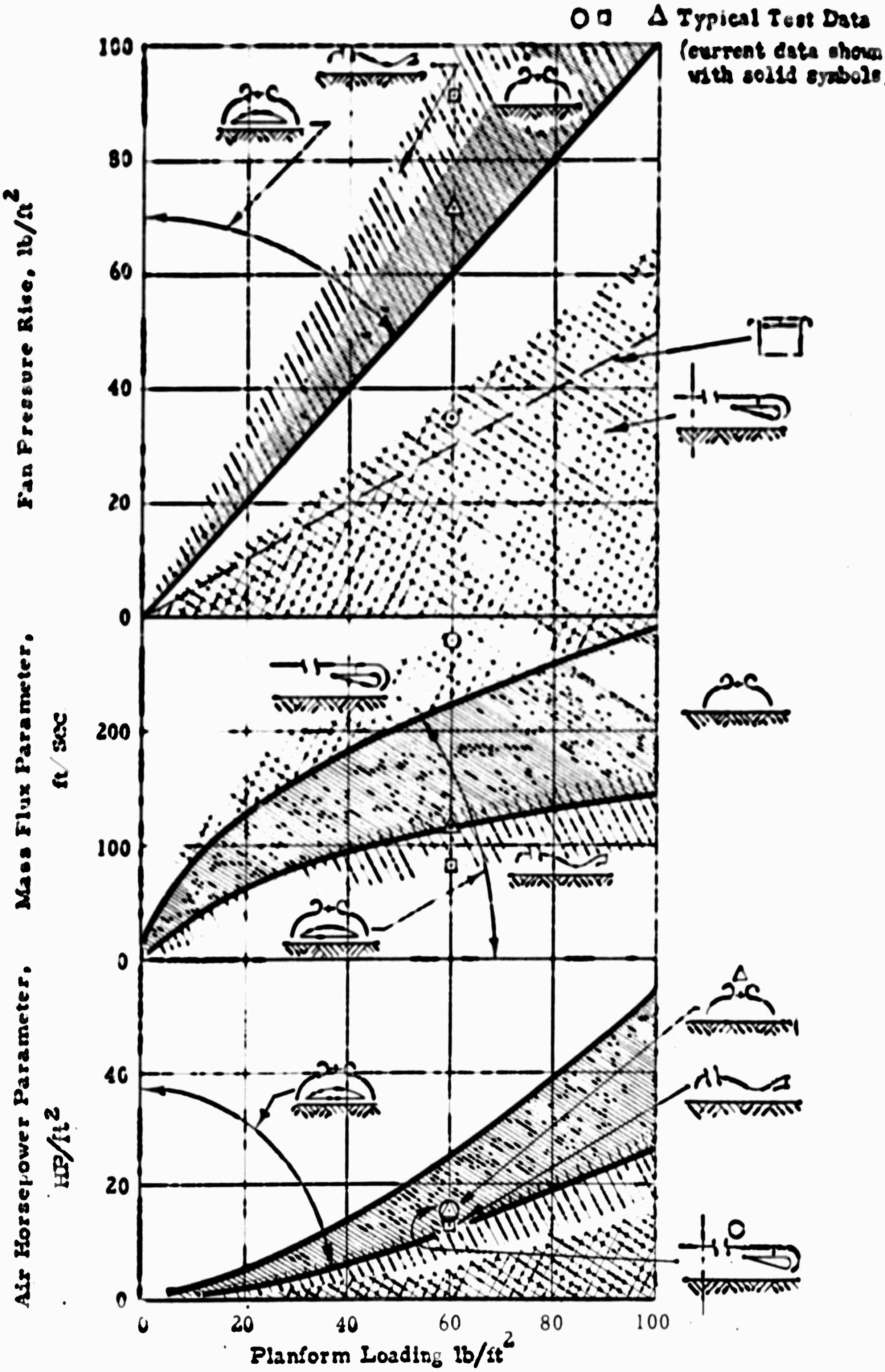

FIGURE 3: GEM HOVER PERFORMANCE

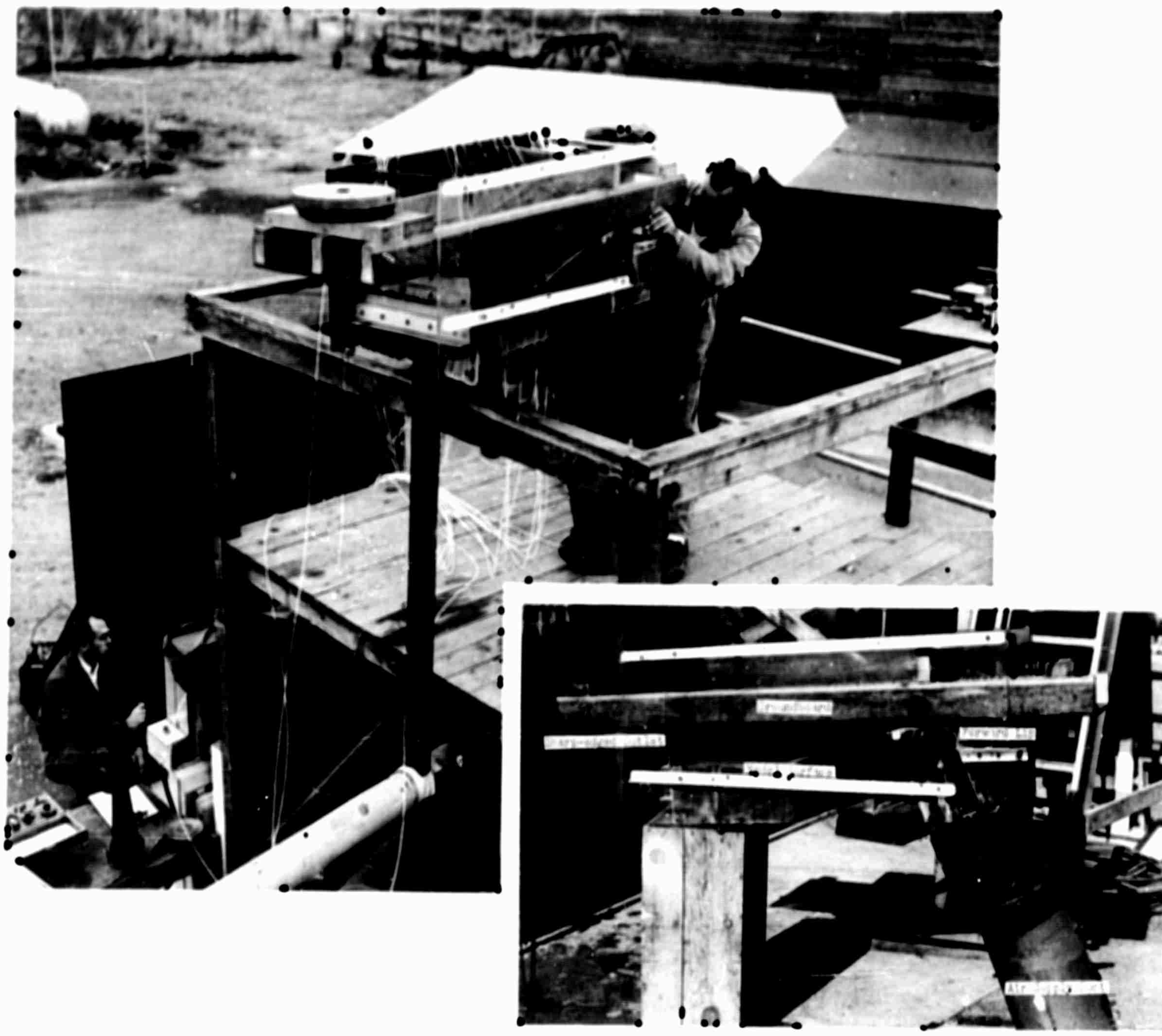

FIGURE 4: TWO-DIMENSIONAL DIFFUSER PLENUM MODEL

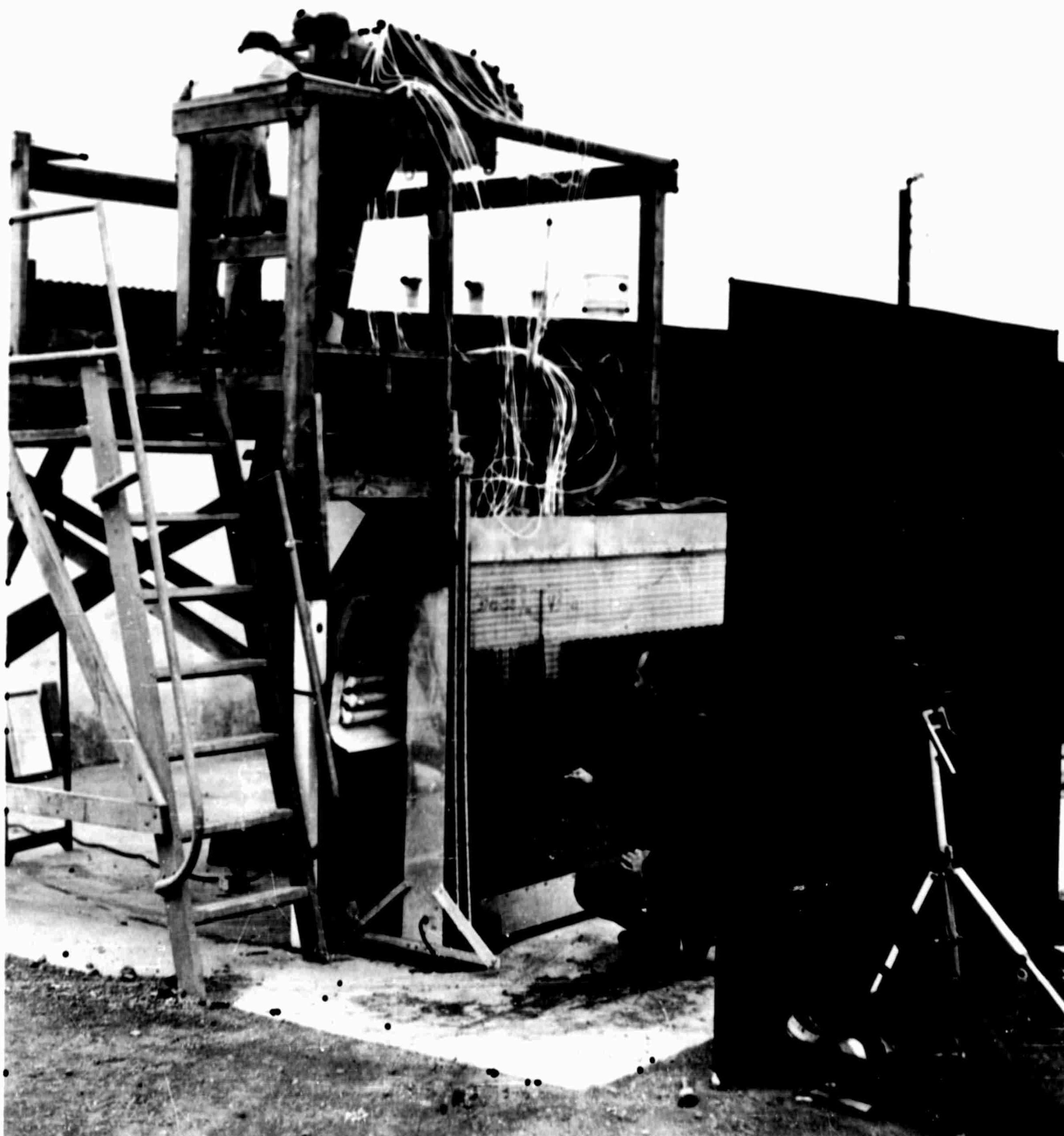

FIGURE 5: TWO-DIMENSIONAL DIFFUSER PLENUM MODEL TEST SET-UP

1/2 front view with plexiglas side plate

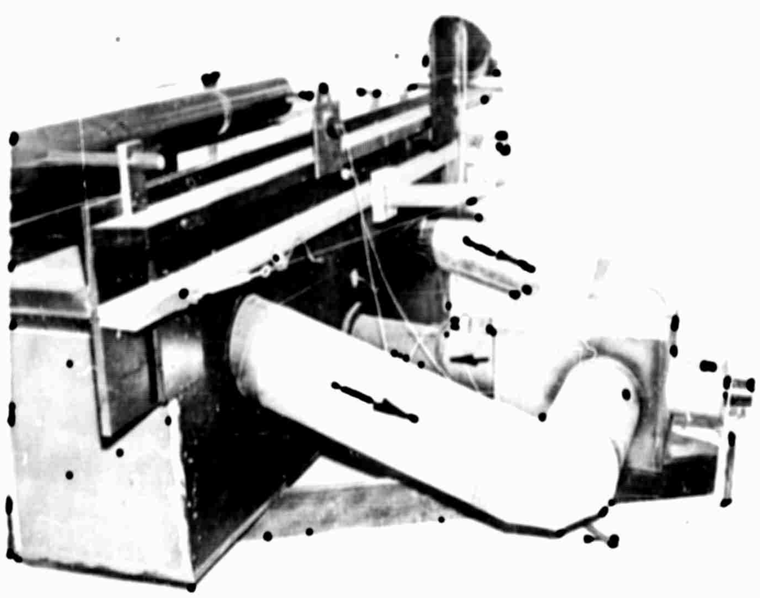

rear view - showing recirculation system and
fan for "make-up" air.

FIGURE 6: DIFFUSER-RECIRCULATION TWO-DIMENSIONAL MODEL.

FIGURE 7: TWO-DIMENSIONAL DIFFUSER RECIRCULATION MODEL

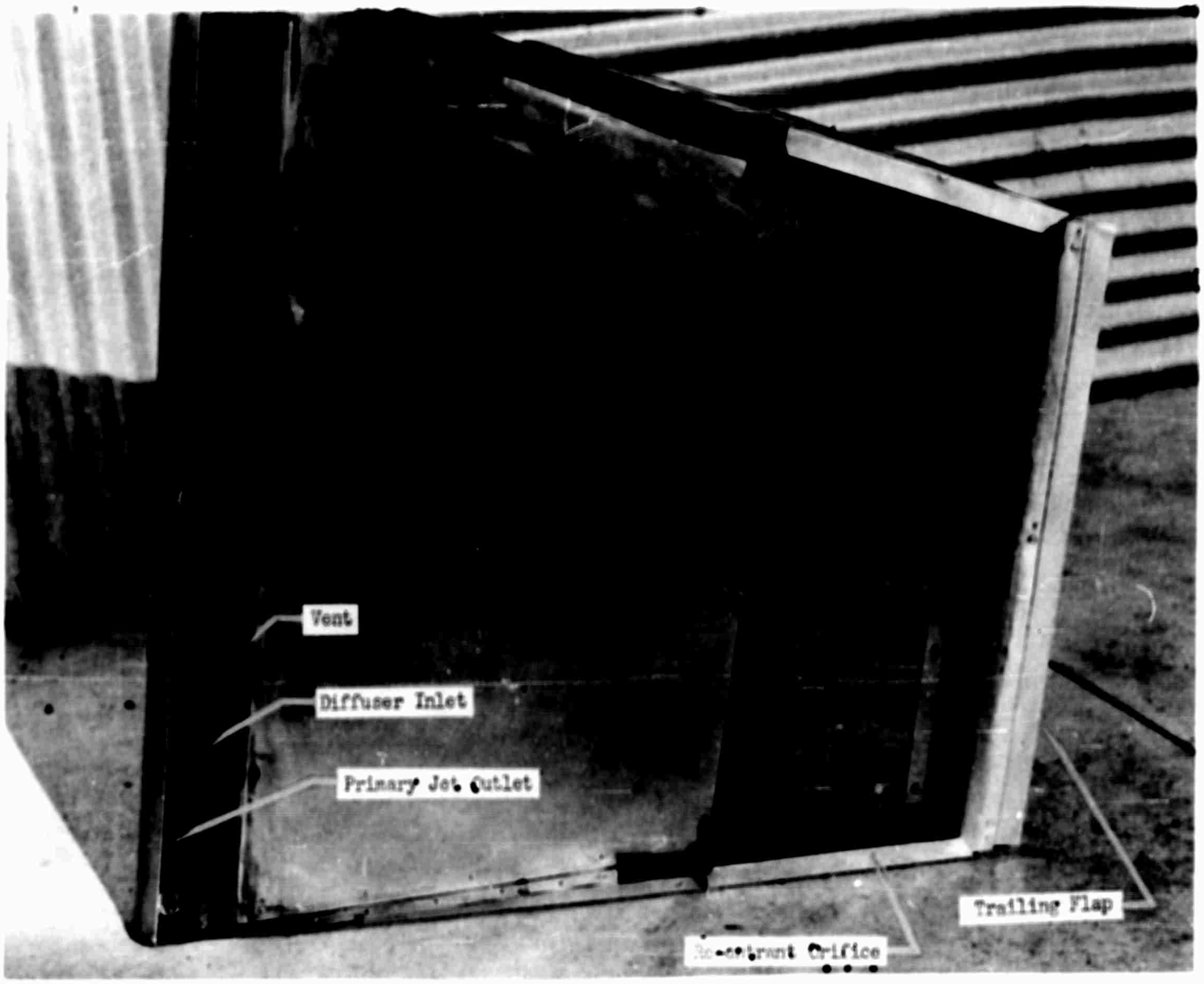

FIGURE 8: BOTTOM SURFACE OF DP-3 GEM

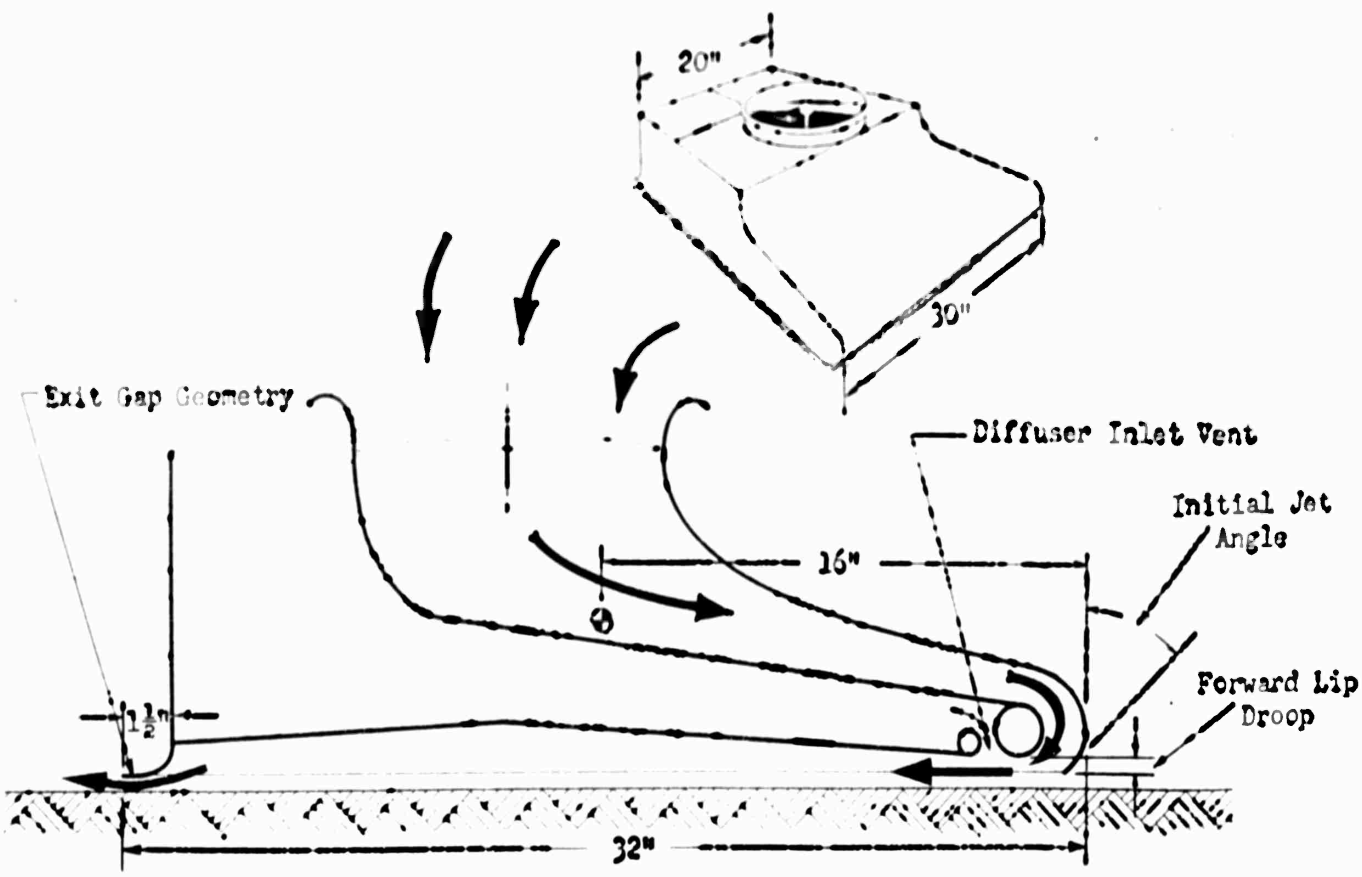

FIGURE 9: LONGITUDINAL SECTION THROUGH DP-3 GEM

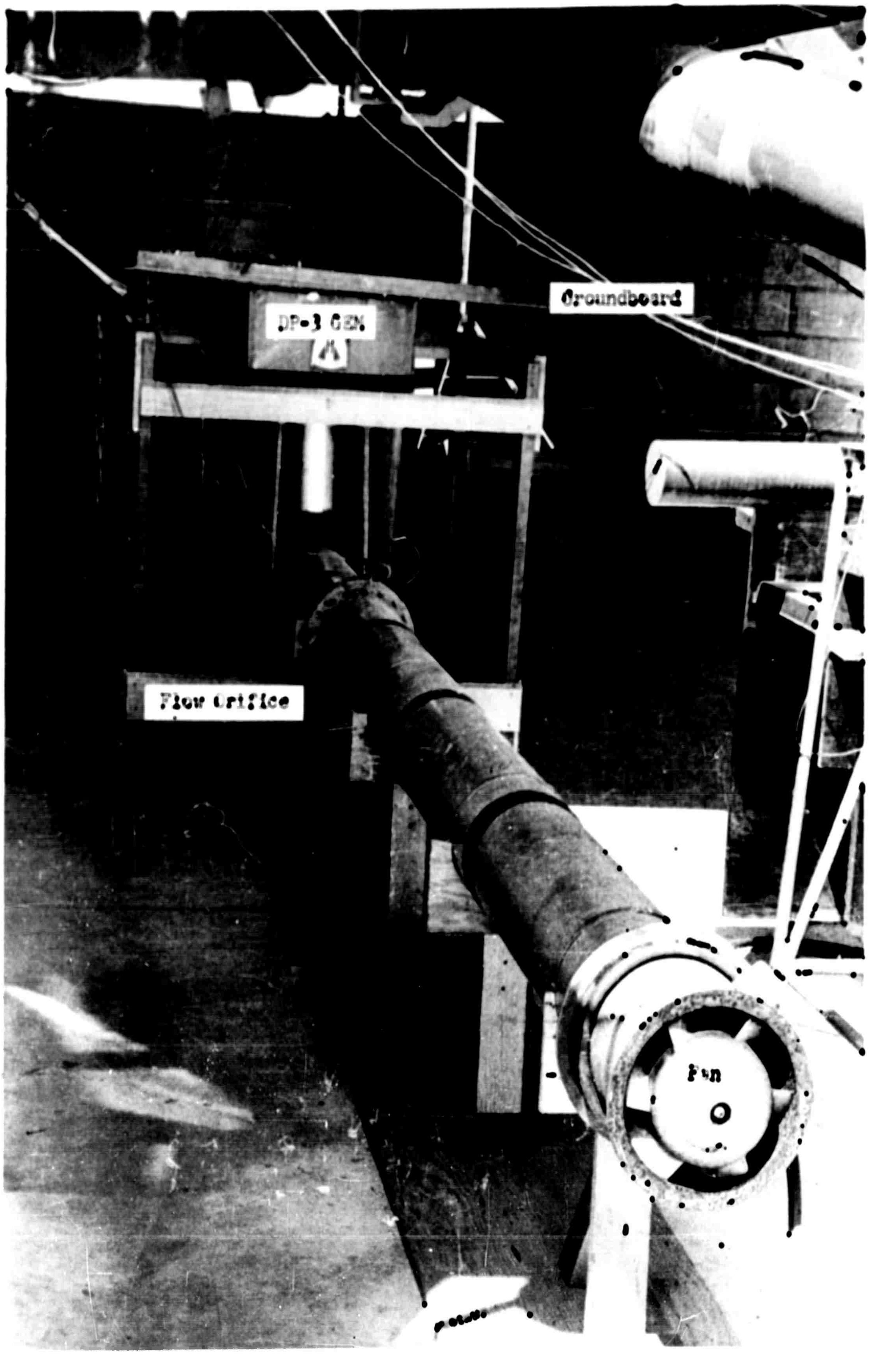

FIGURE 10: STATIC TEST DP-3 GEM WITH AIR SUPPLY SYSTEM

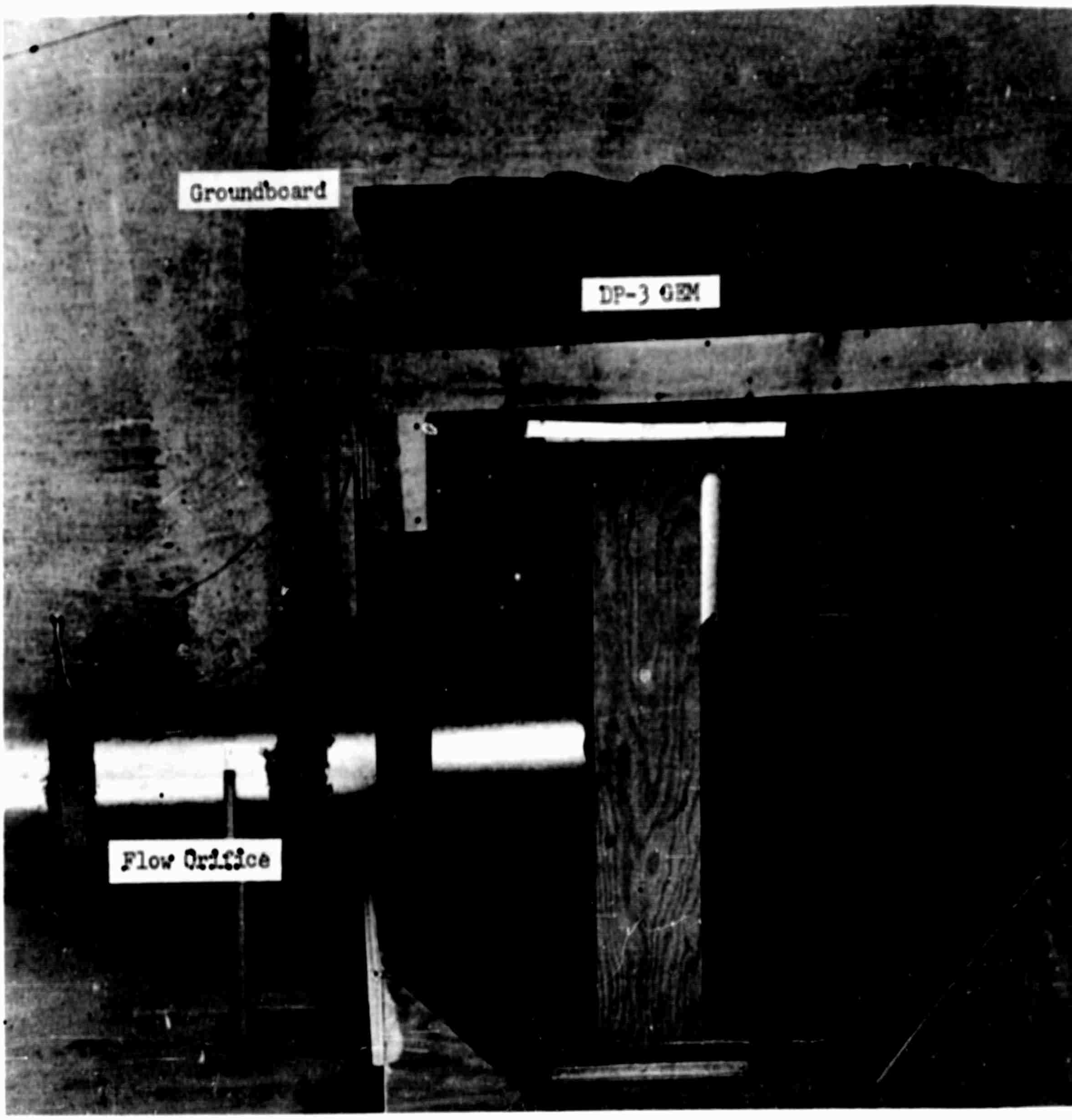

FIGURE 11: STATIC TEST DP-3 GEM-GROUND BOARD-MODEL
ARRANGEMENT AND FLOW MEASURING ORIFICE

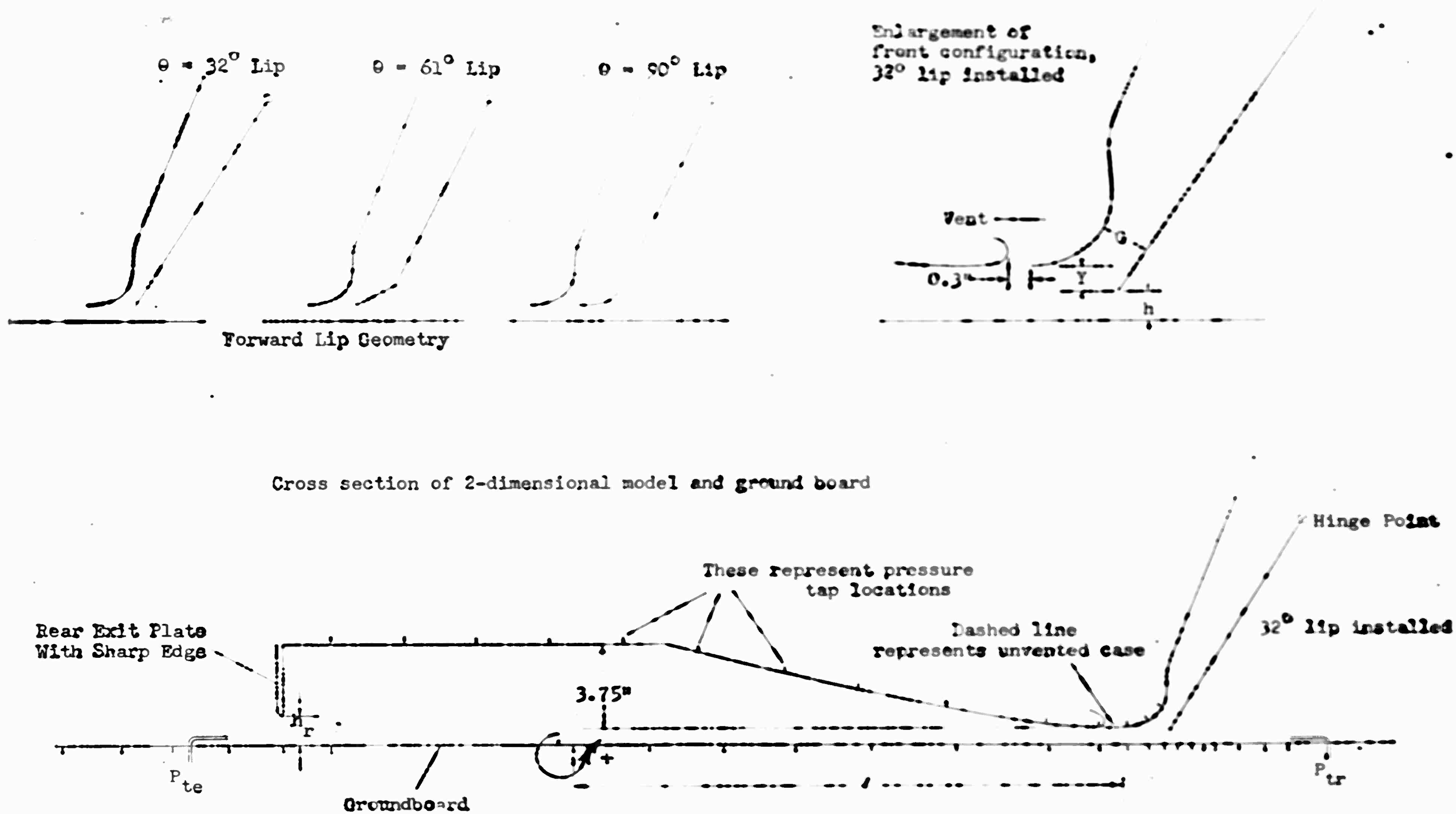

FIGURE 12: 2-DIMENSIONAL MODEL DETAILS

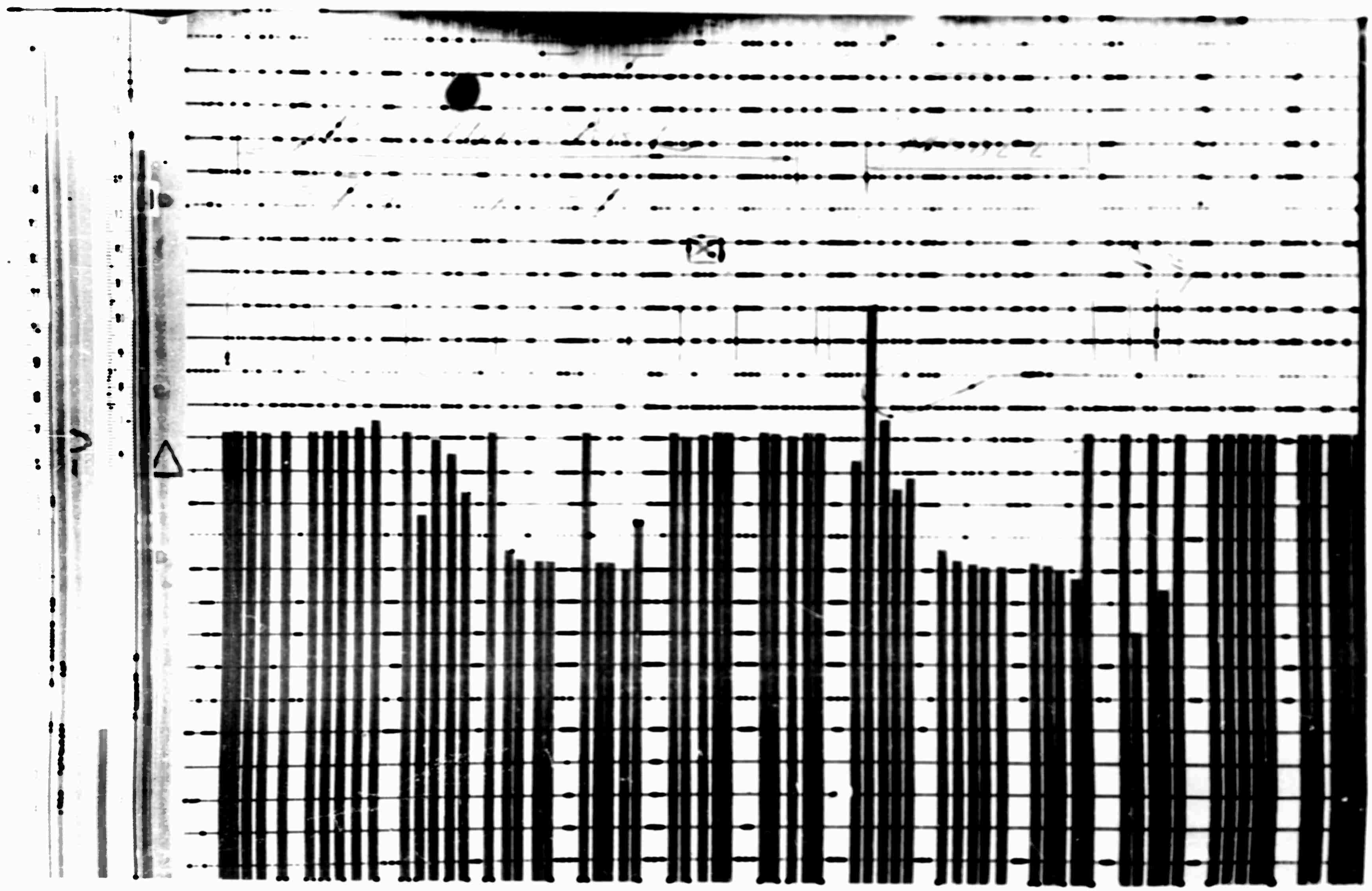

FIGURE 13: TYPICAL PHOTOGRAPHIC DATA RECORD

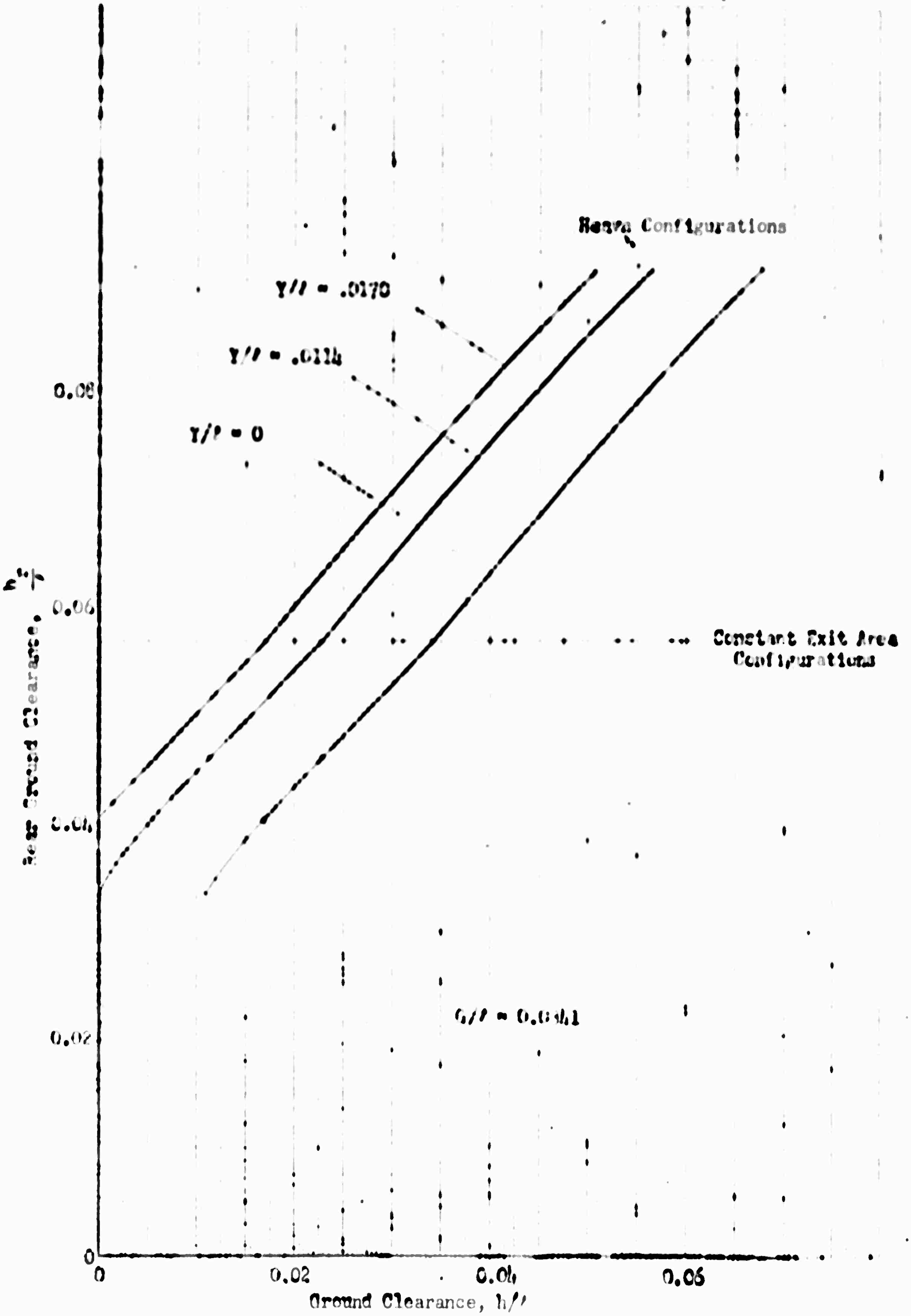

FIGURE 14: REAR GROUND CLEARANCE AS A FUNCTION OF FRONT GROUND CLEARANCE

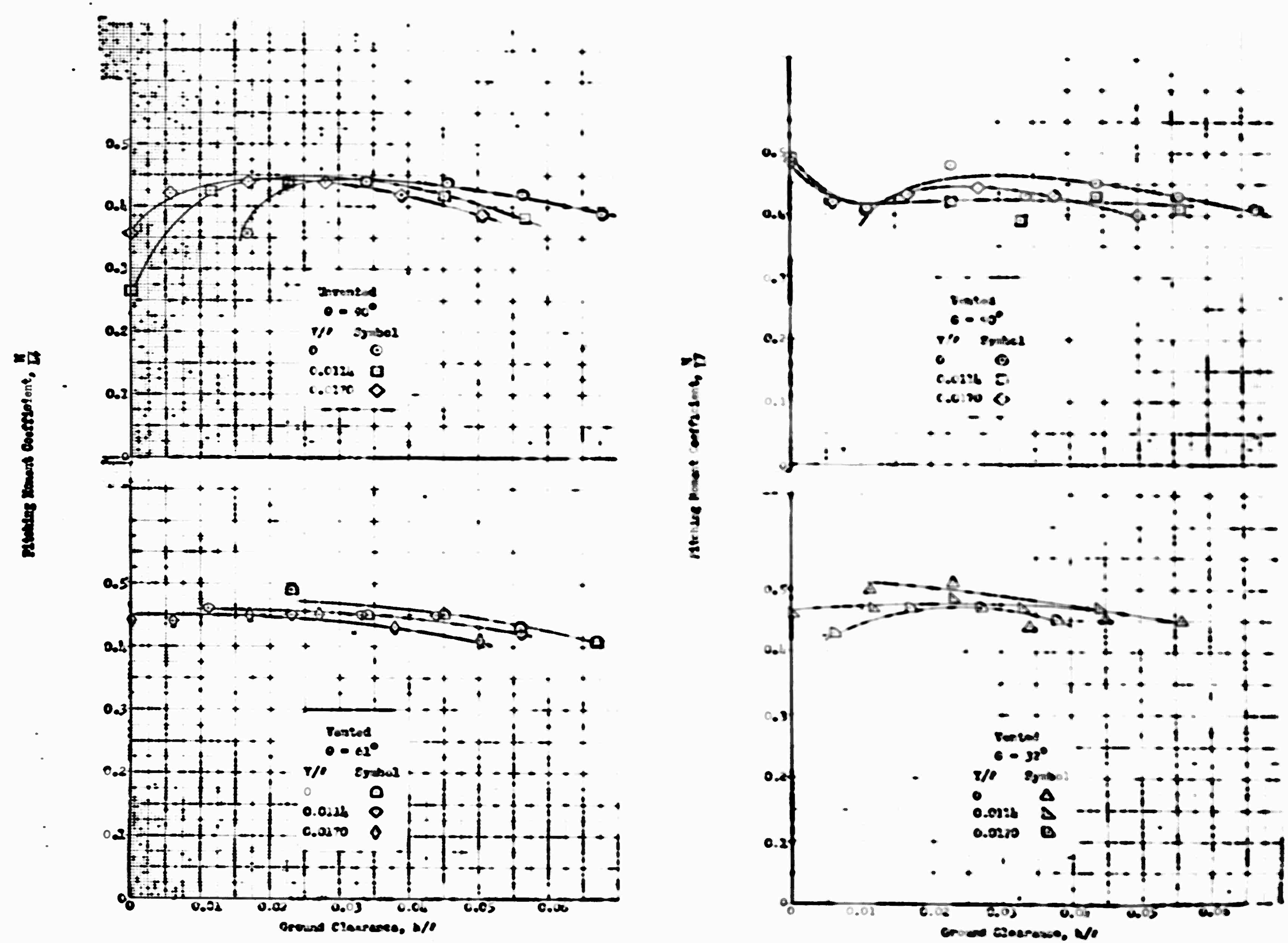

FIGURE 15: [illegible] PITCHING MOMENT CHARACTERISTICS IN [illegible]

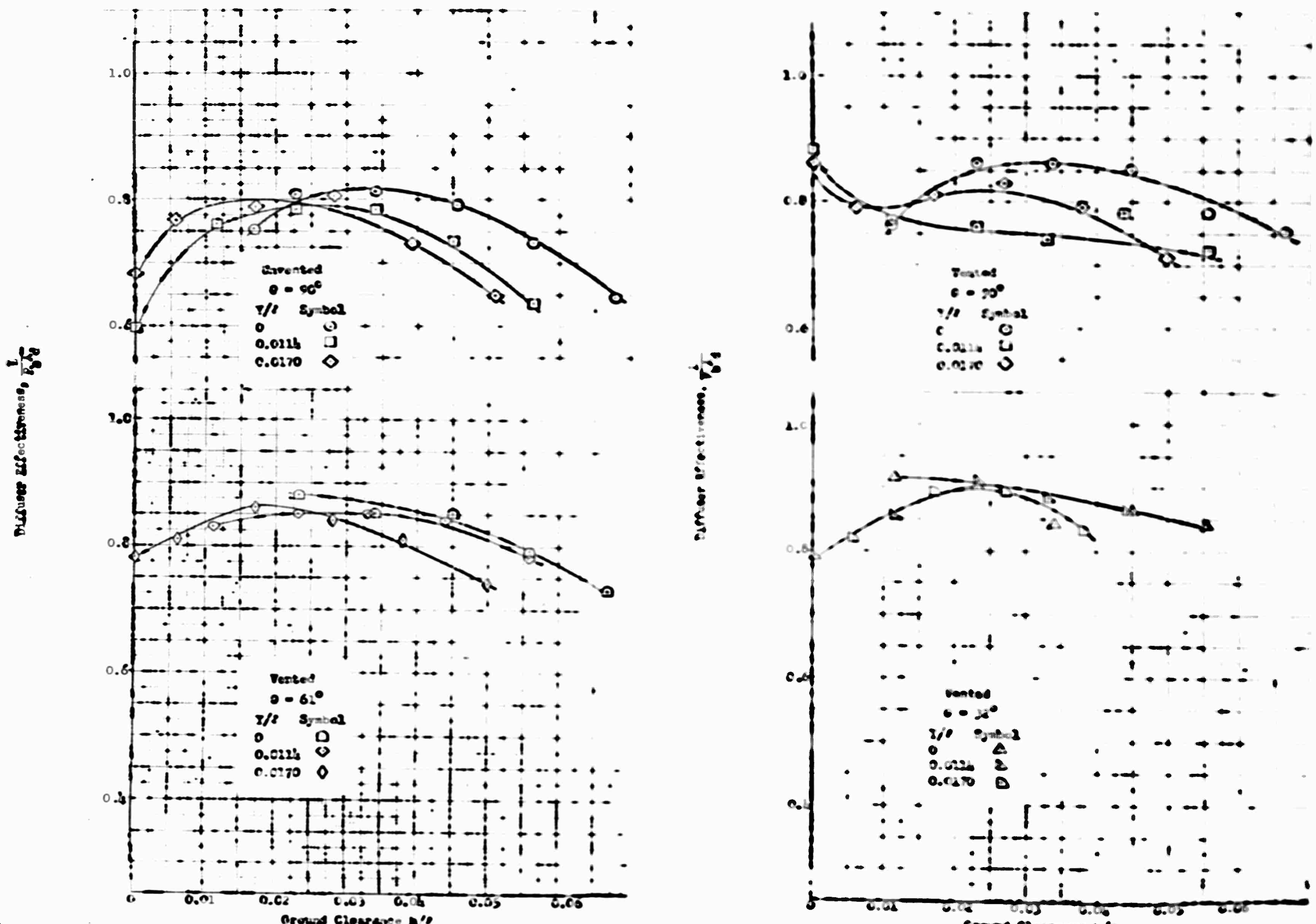

FIGURE 36: LIFT EFFECTIVENESS OF DIFFUSER IN [illegible]

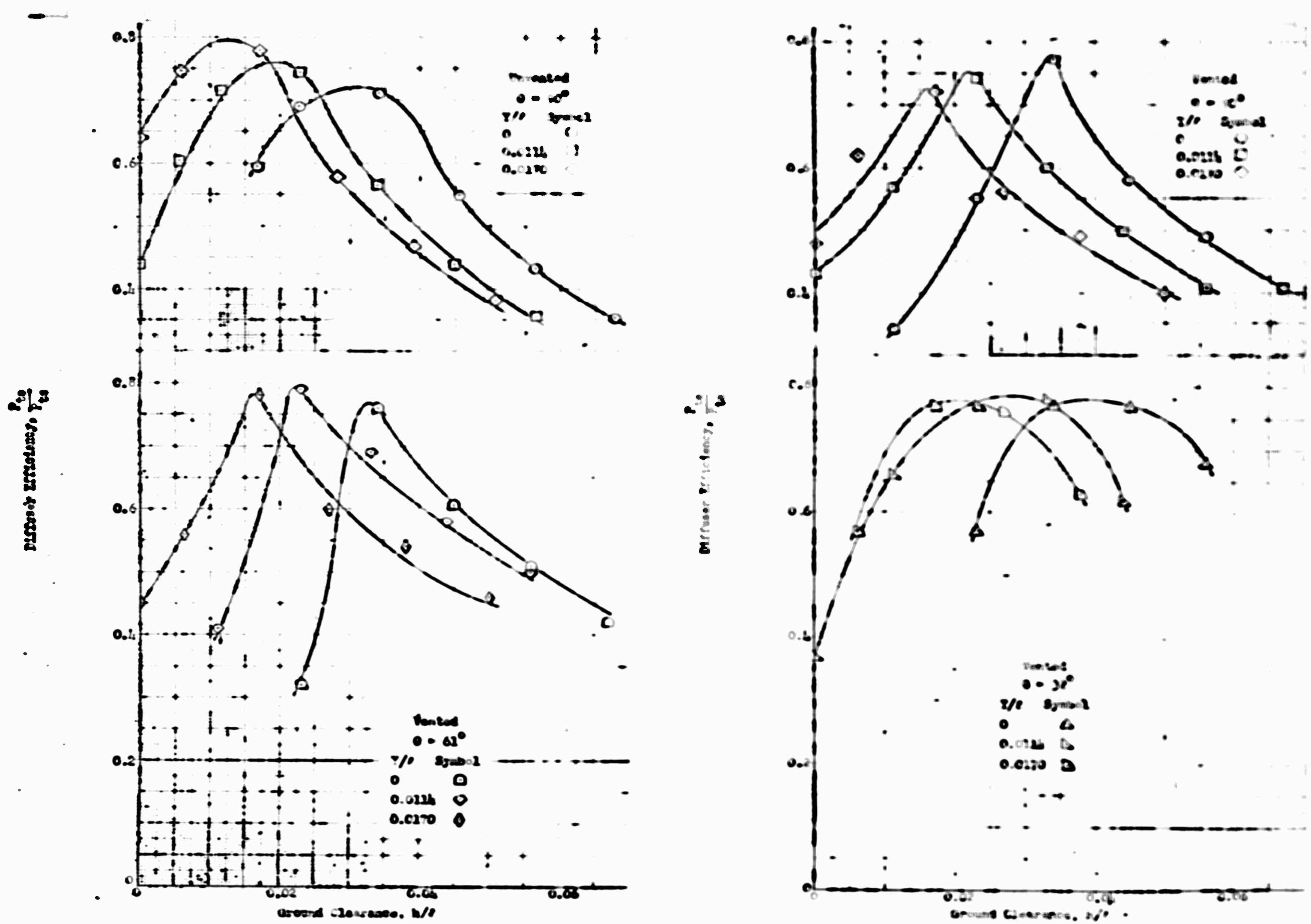

FIGURE 17: DIFFUSER EFFICIENCY IN HEAVE

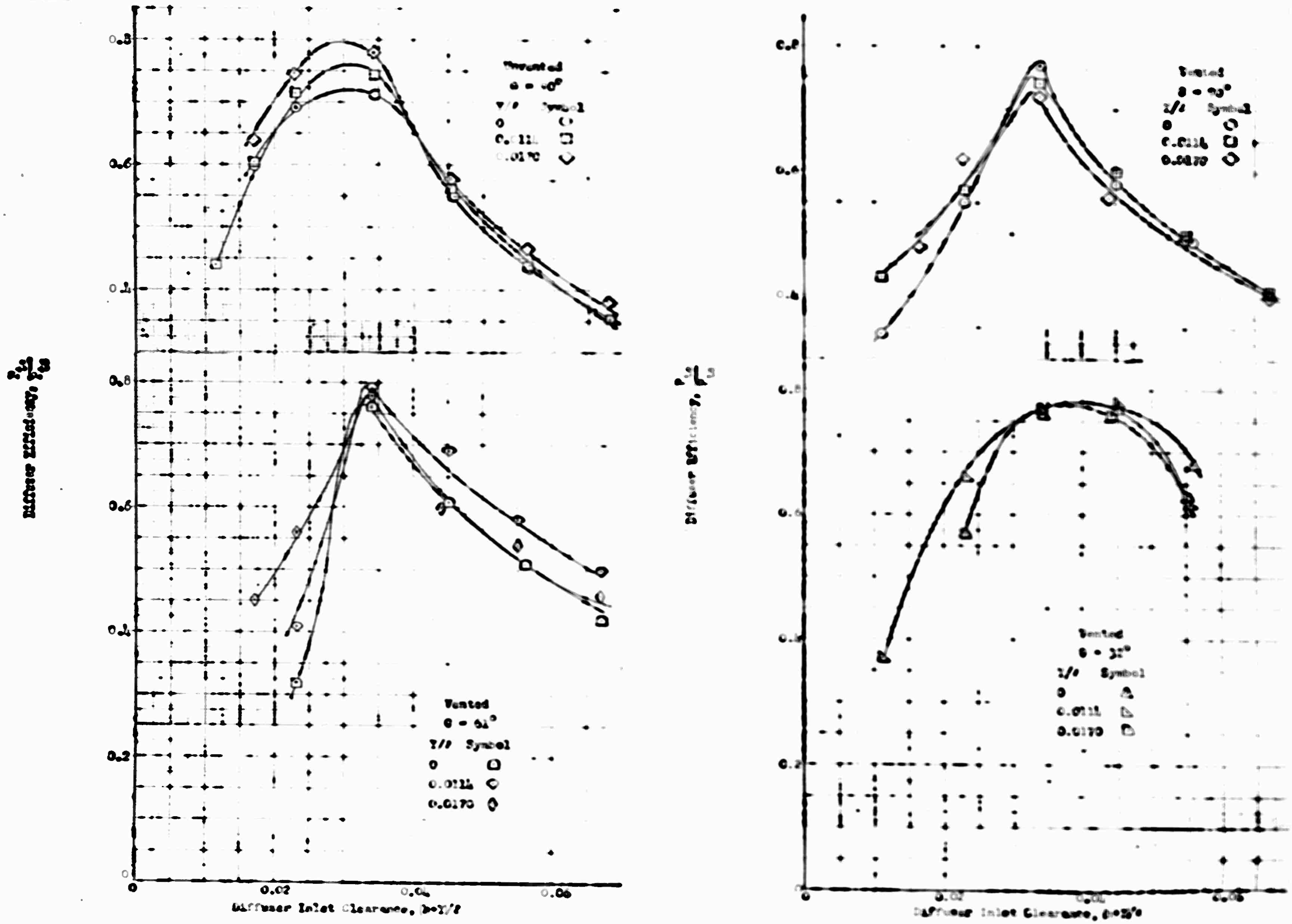

FIGURE 13: DIFFUSER EFFICIENCY IN VANES

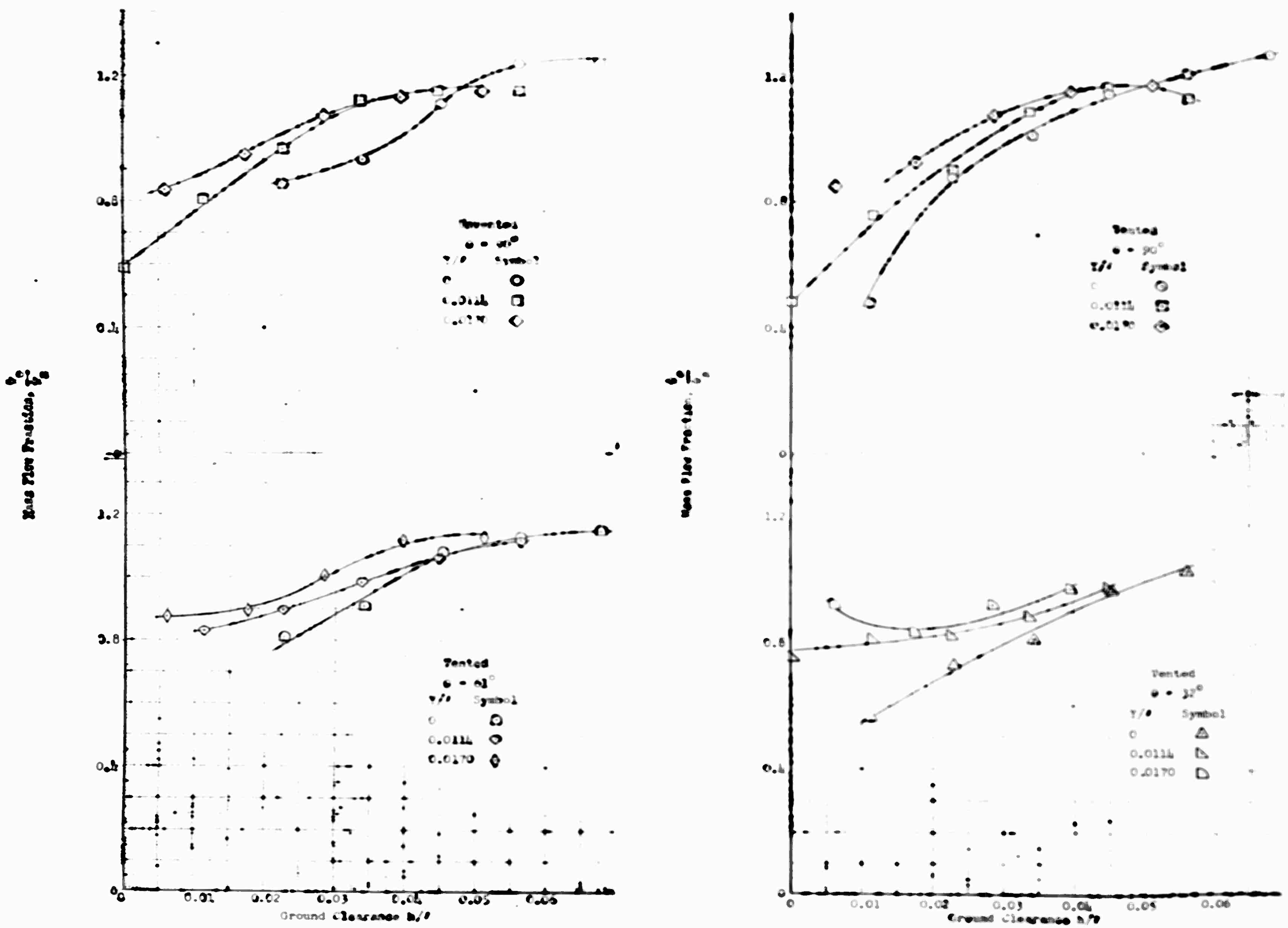

FIGURE 39: FLOW AVAILABLE TO WEAVE FOR FORWARD PROPULSION

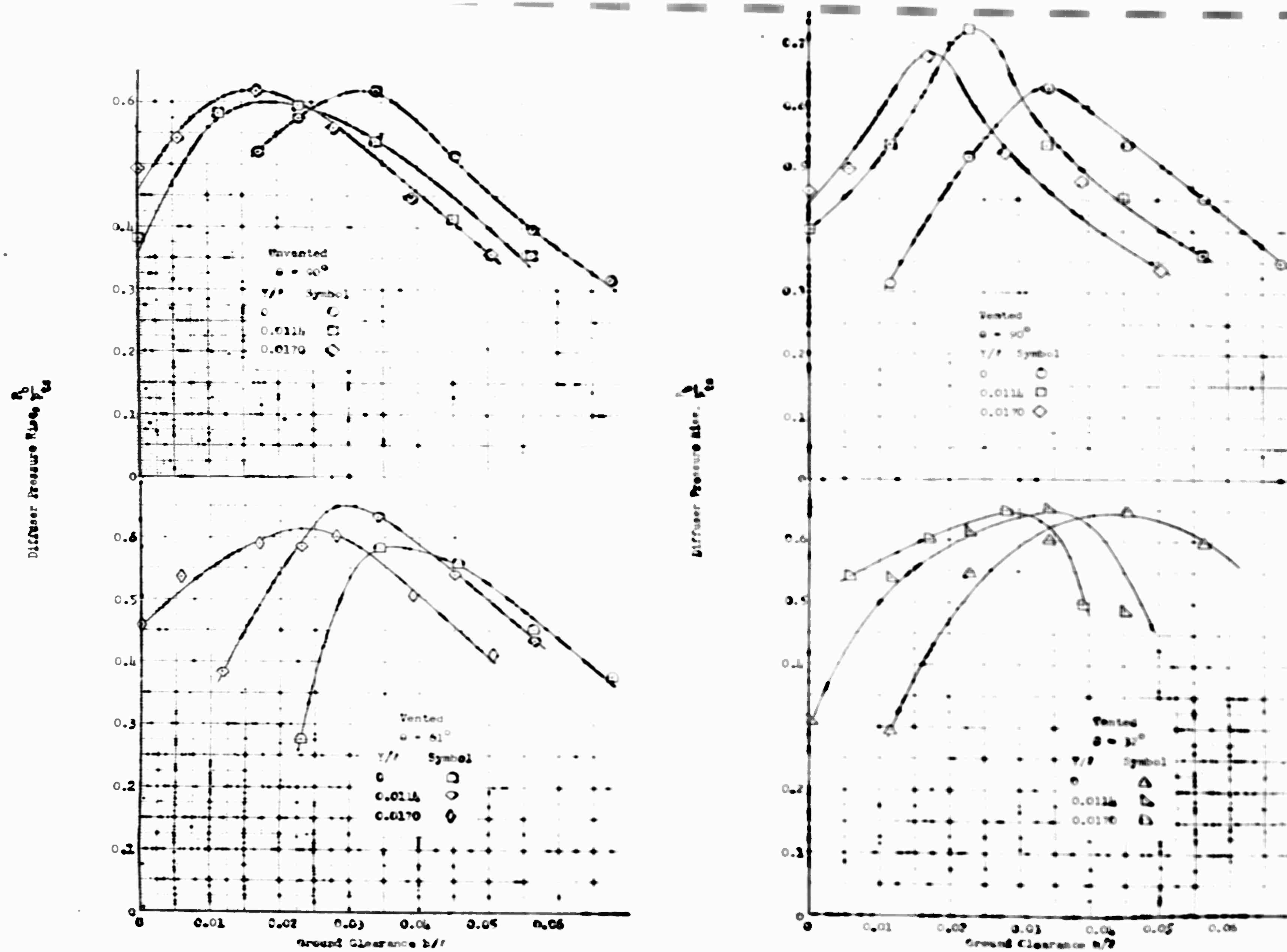

FIGURE 20. DIFFUSER PRESSURE RISE IN [illegible]

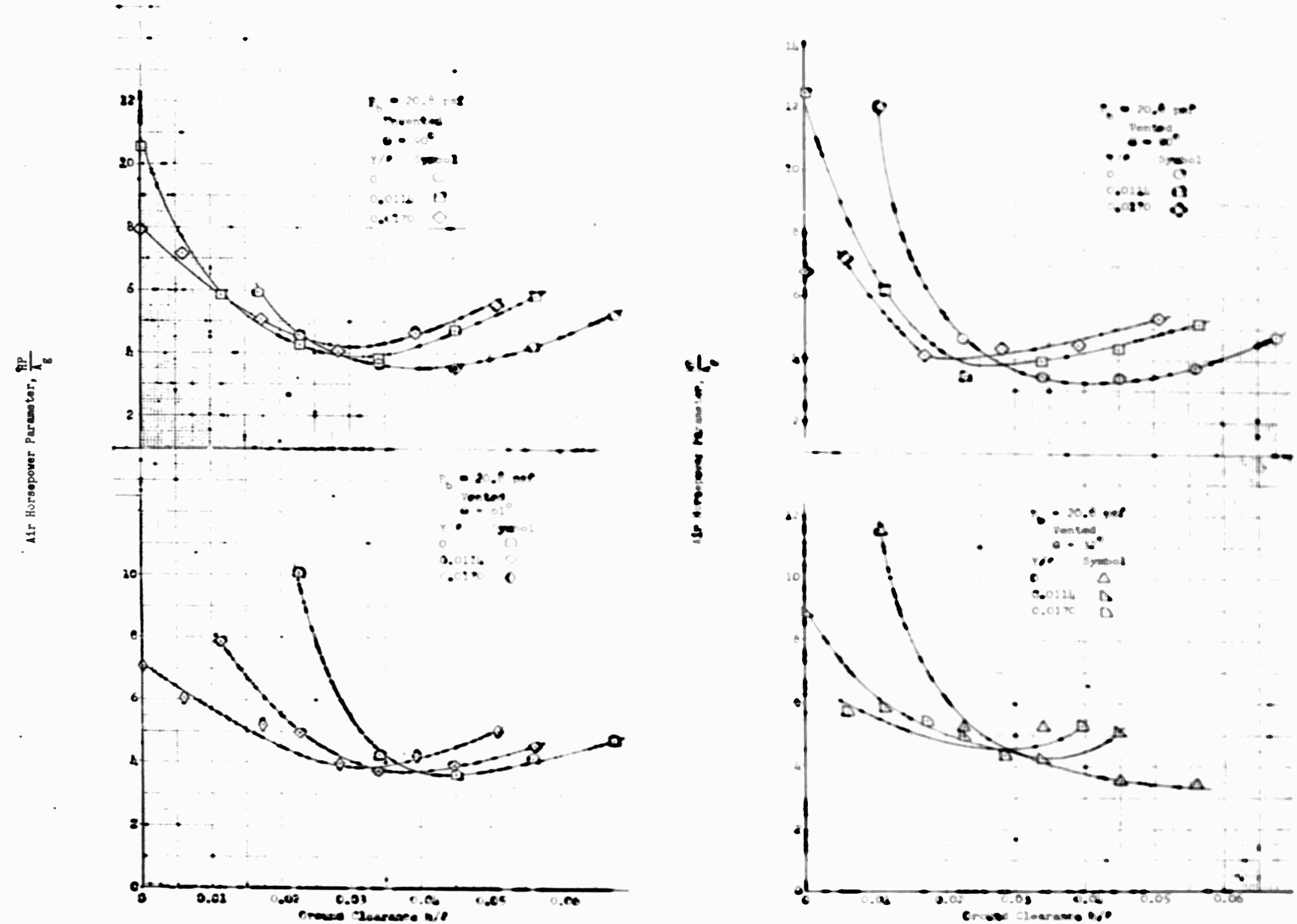

FIGURE 21: HOVERING PERFORMANCE IN [illegible]

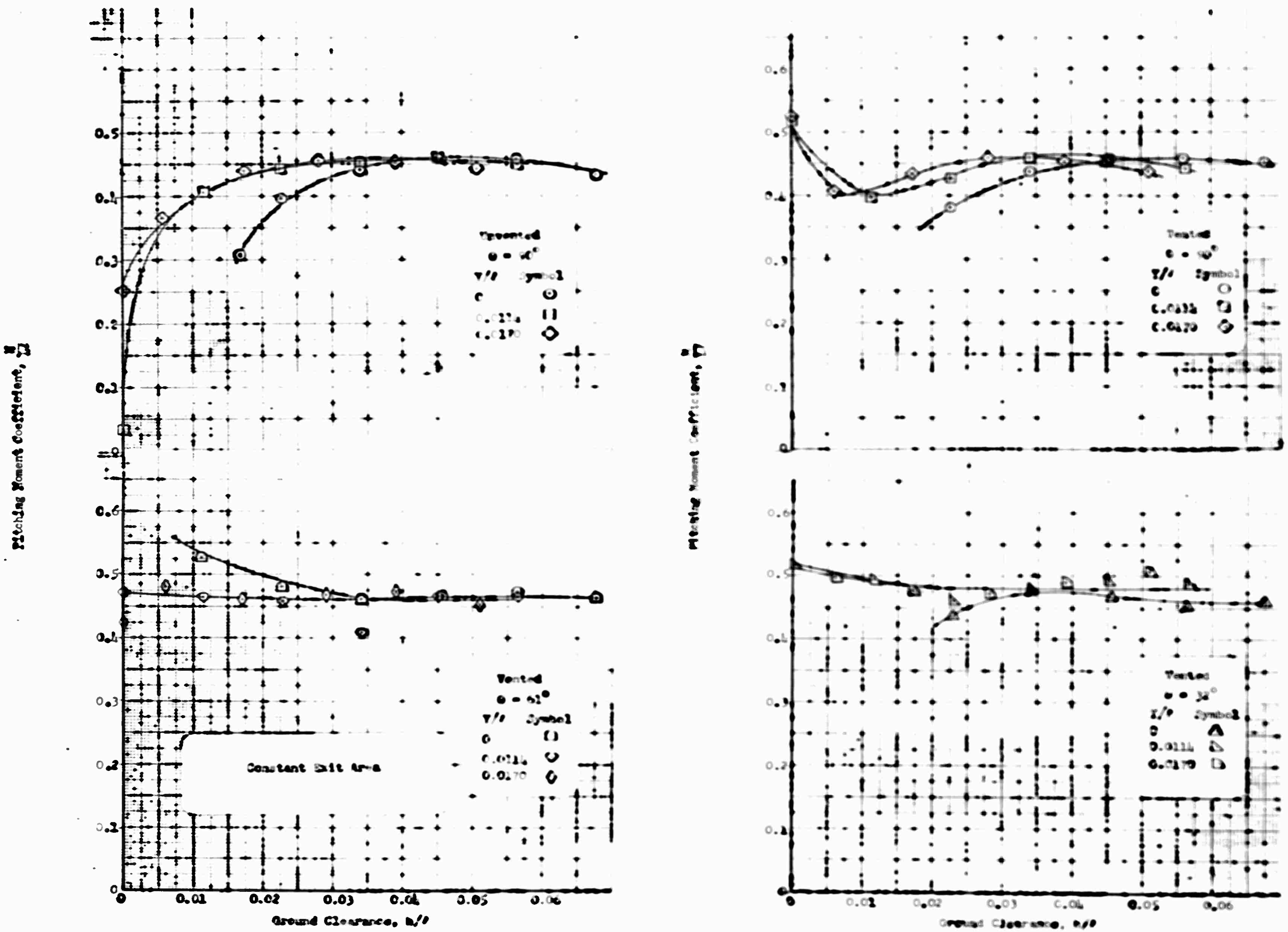

FIGURE 22. DIFFUSER PITCHING MOMENT CHARACTERISTICS IN PITCH ABOUT EXIT FLAP

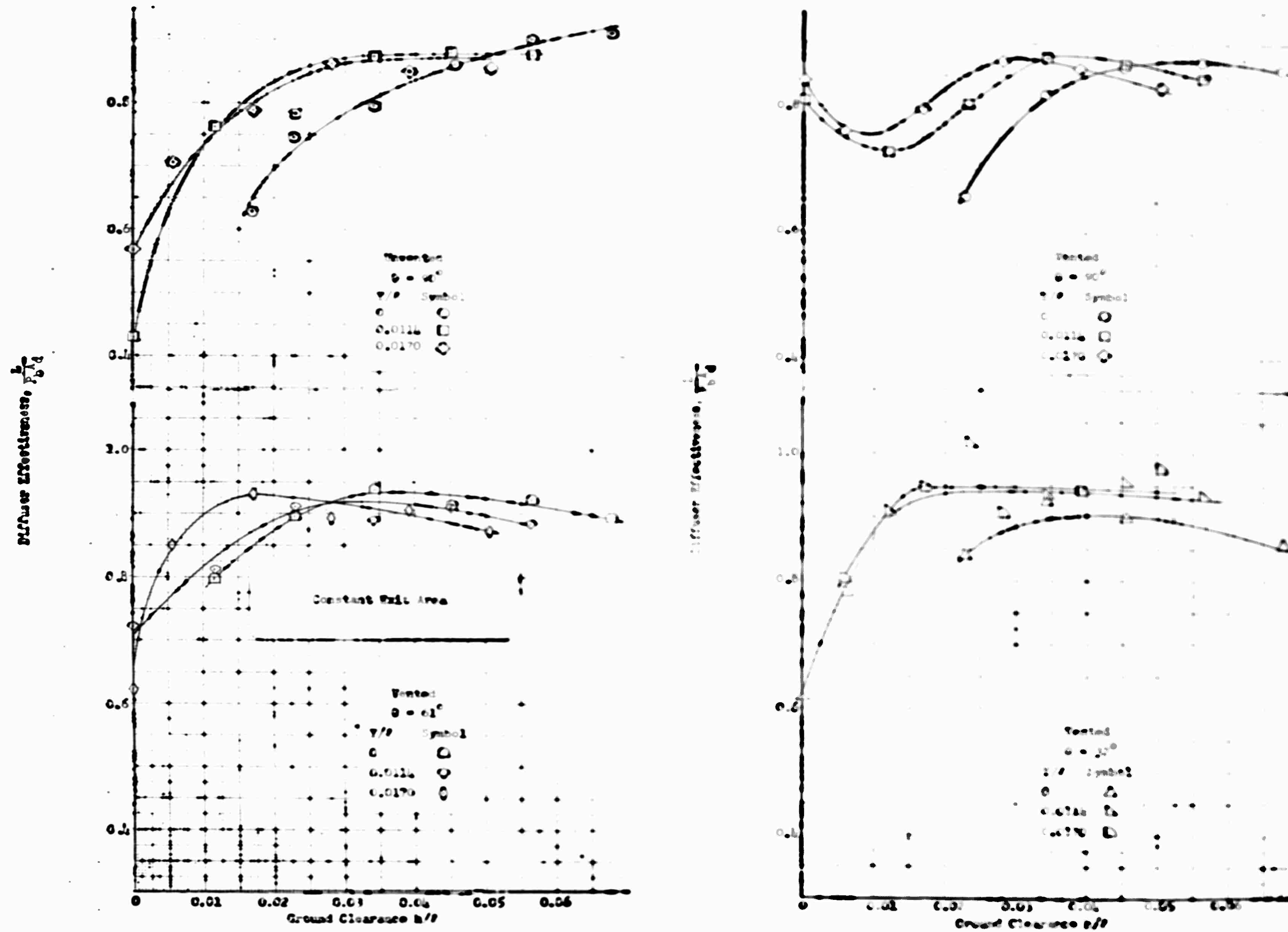

FIGURE 23: LIFT EFFECTIVENESS OF DIFFUSER TO PITCH ABOUT EXIT FLAP

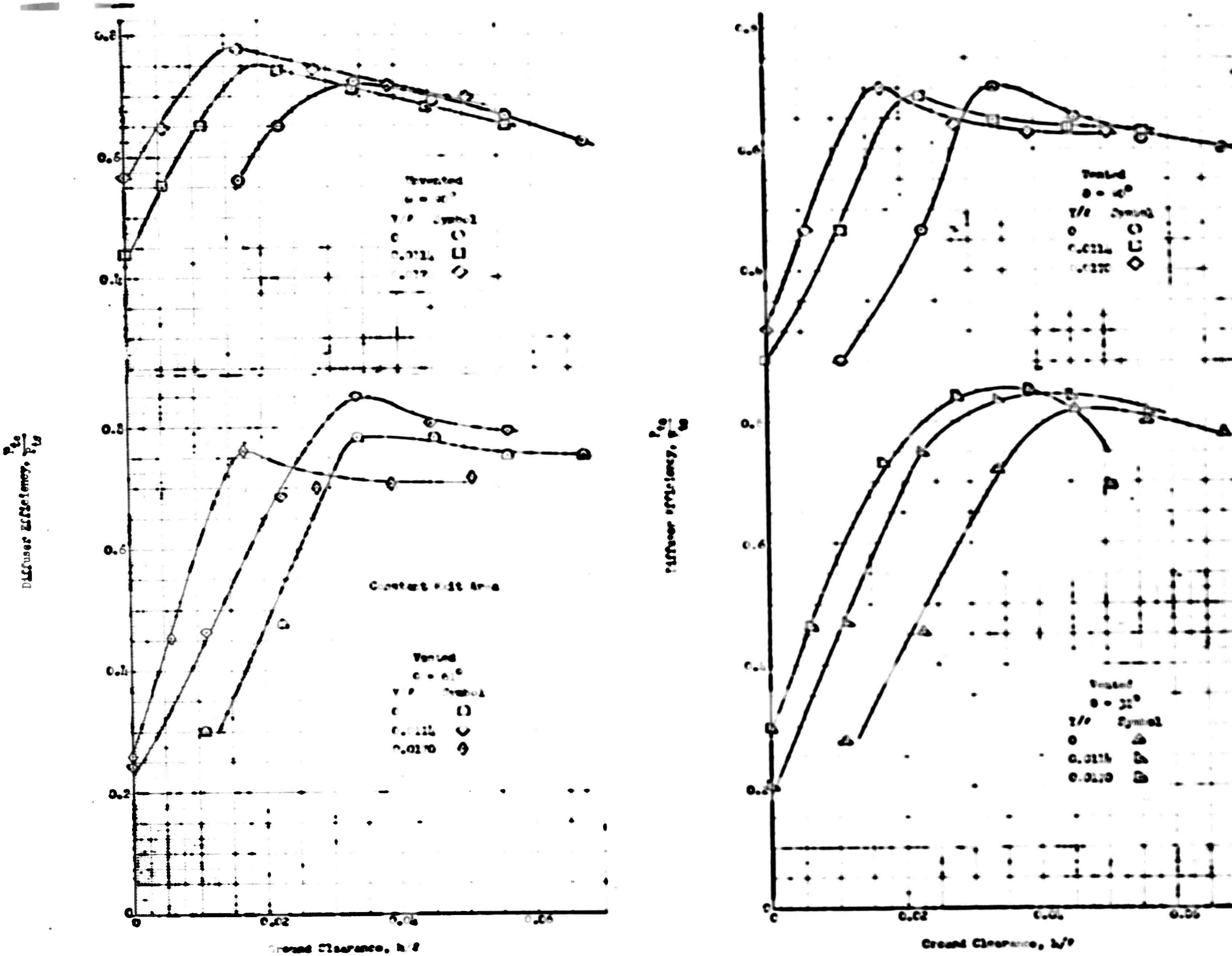

FIGURE 2[illegible]: DIFFUSER EFFICIENCY IN [illegible] EXIT FLAP

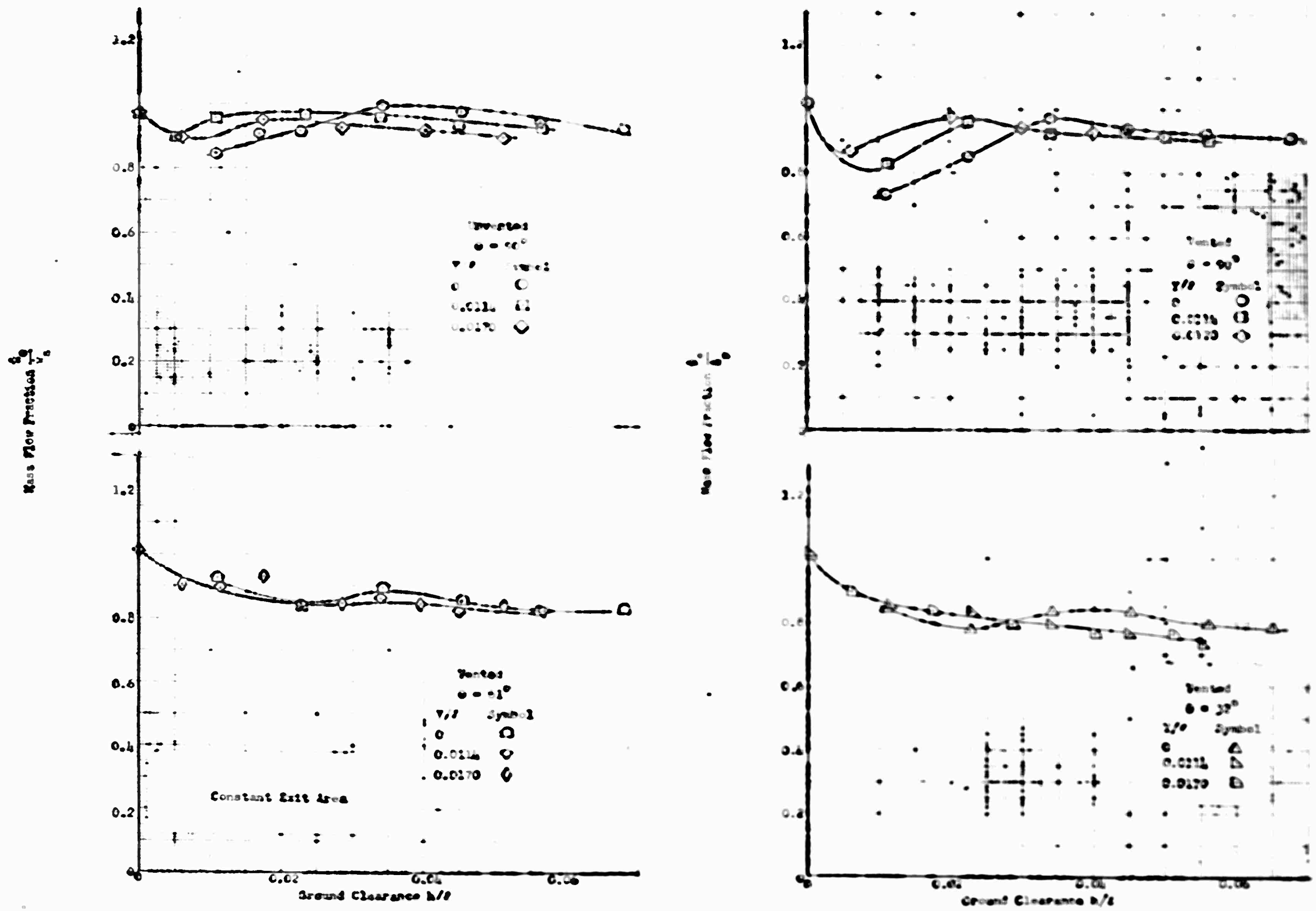

FIGURE 25: FLOW AVAILABLE IN PITCH FOR RECIRCULATION OR FORWARD PROPULSION

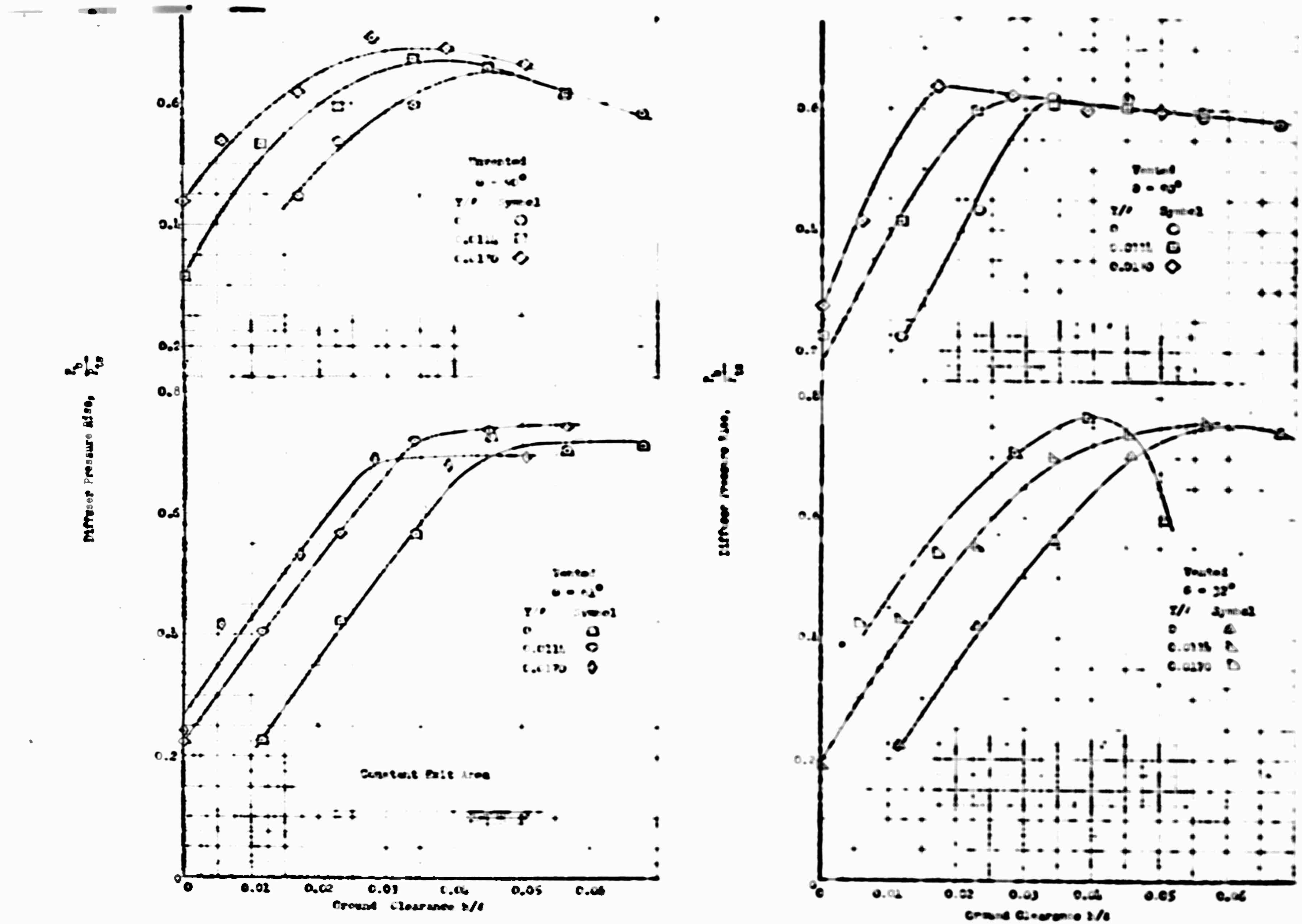

FIGURE [illegible]: DIFFUSER PRESSURE RISE IN PITCH ABOUT EXIT FLAP

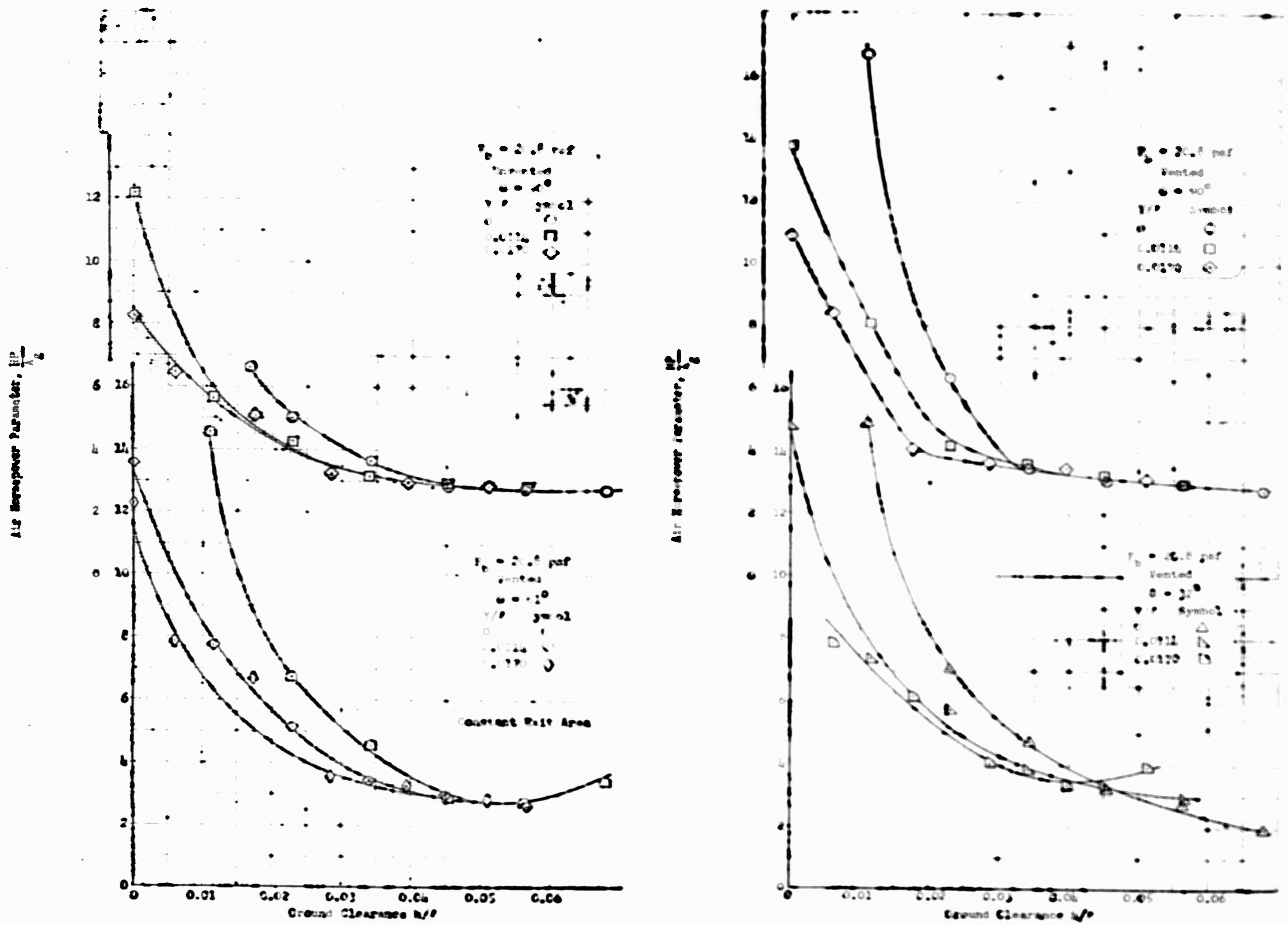

FIGURE 27: HOVERING PERFORMANCE IN PITCH ABOUT EXIT FLAP

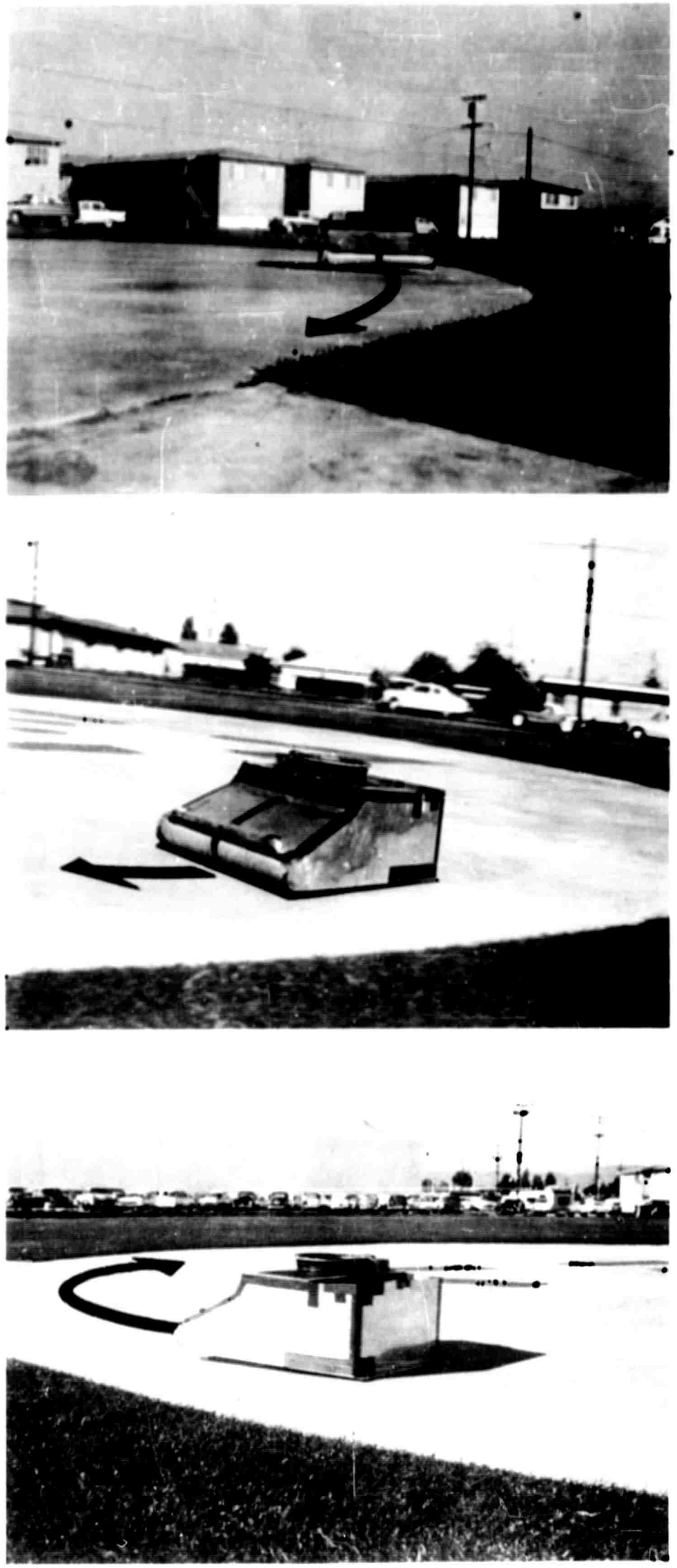

FIGURE 28: THE DP-3 GEM THREE-DIMENSIONAL MODEL IN OPERATION ON TETHER

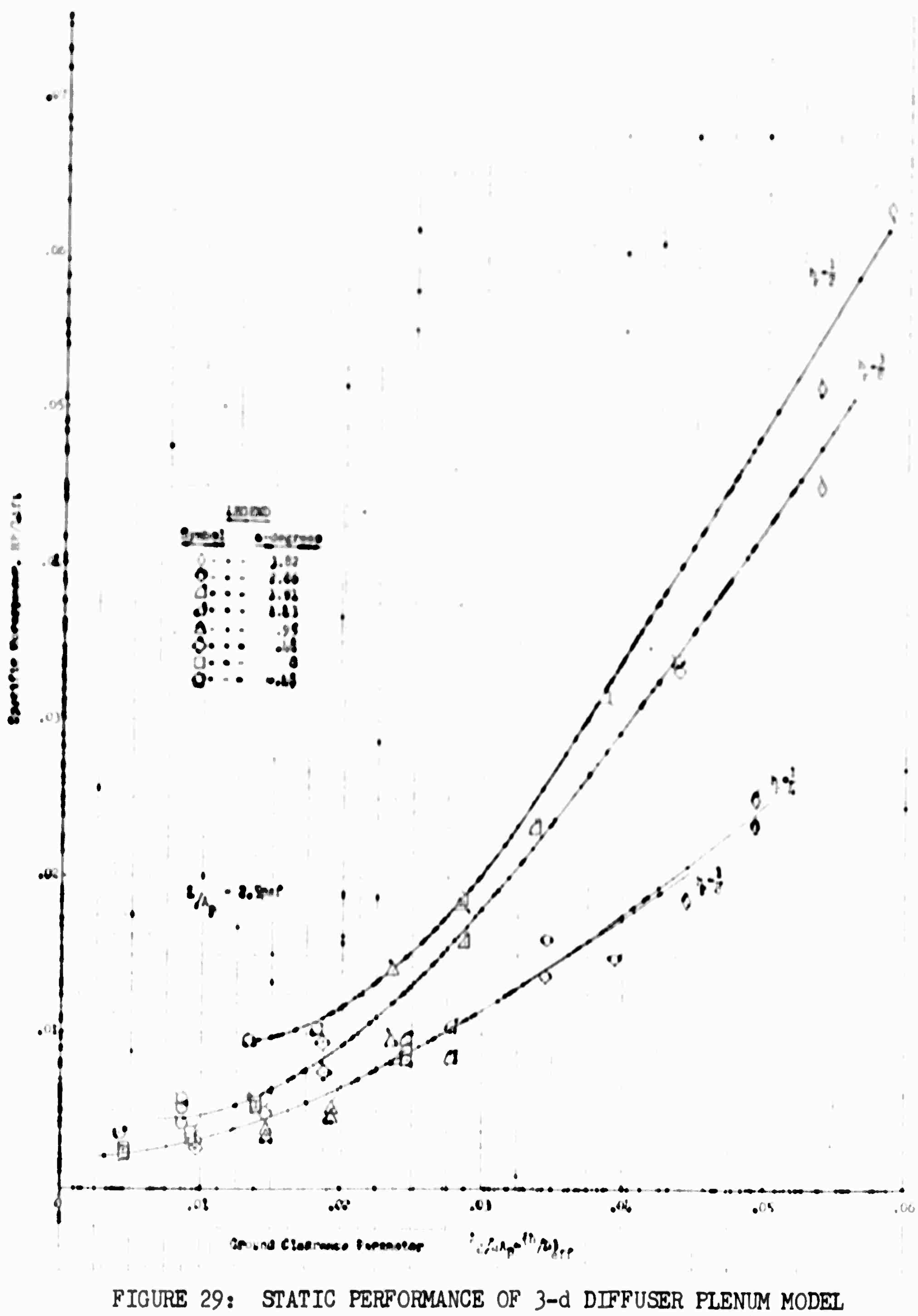

FIGURE 29: STATIC PERFORMANCE OF 3-d DIFFUSER PLENUM MODEL

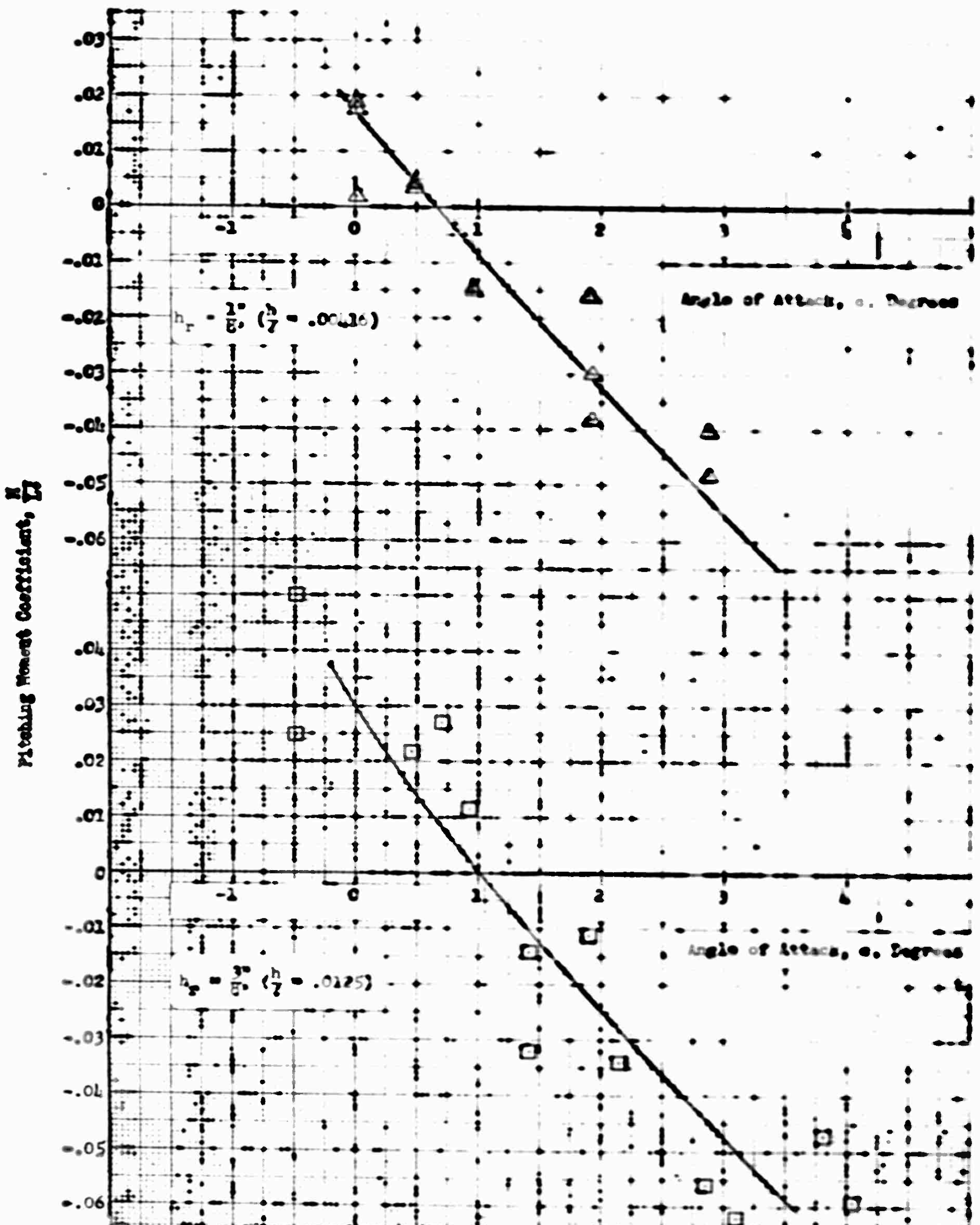

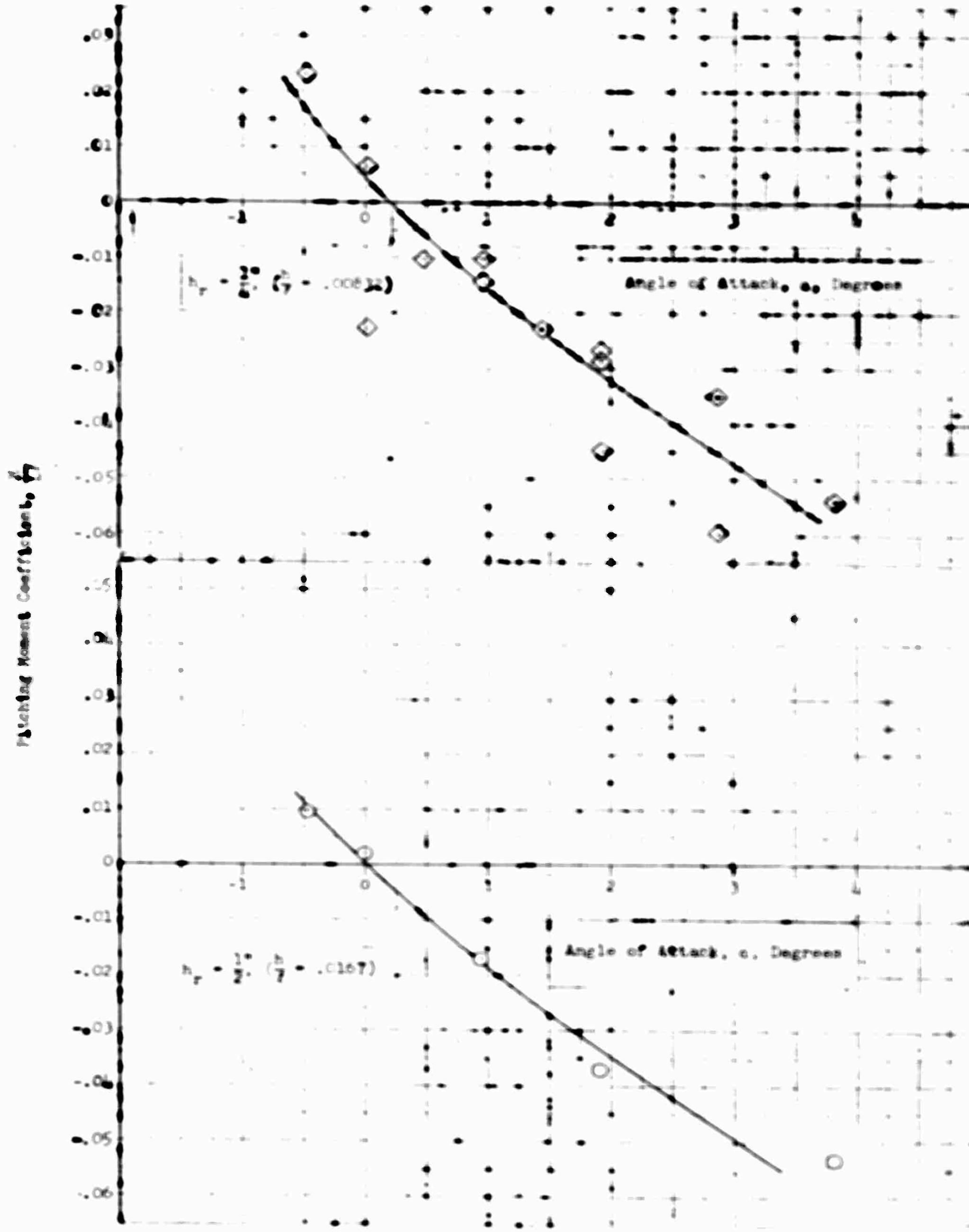

FIGURE 30: PITCH STABILITY CHARACTERISTICS DP-3 GEM

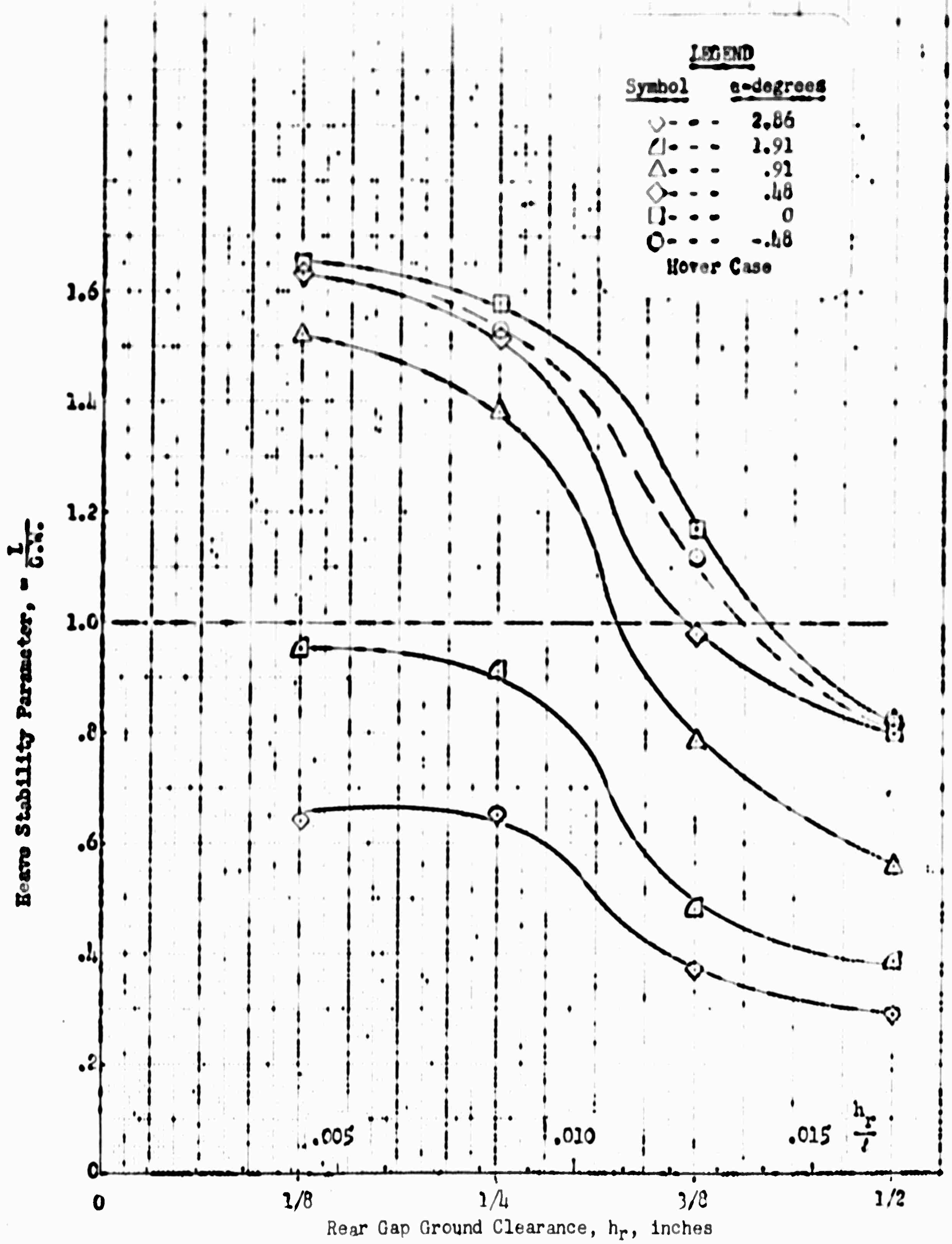

FIGURE 31: HEAVE STABILITY CHARACTERISTICS DP-3 GEM

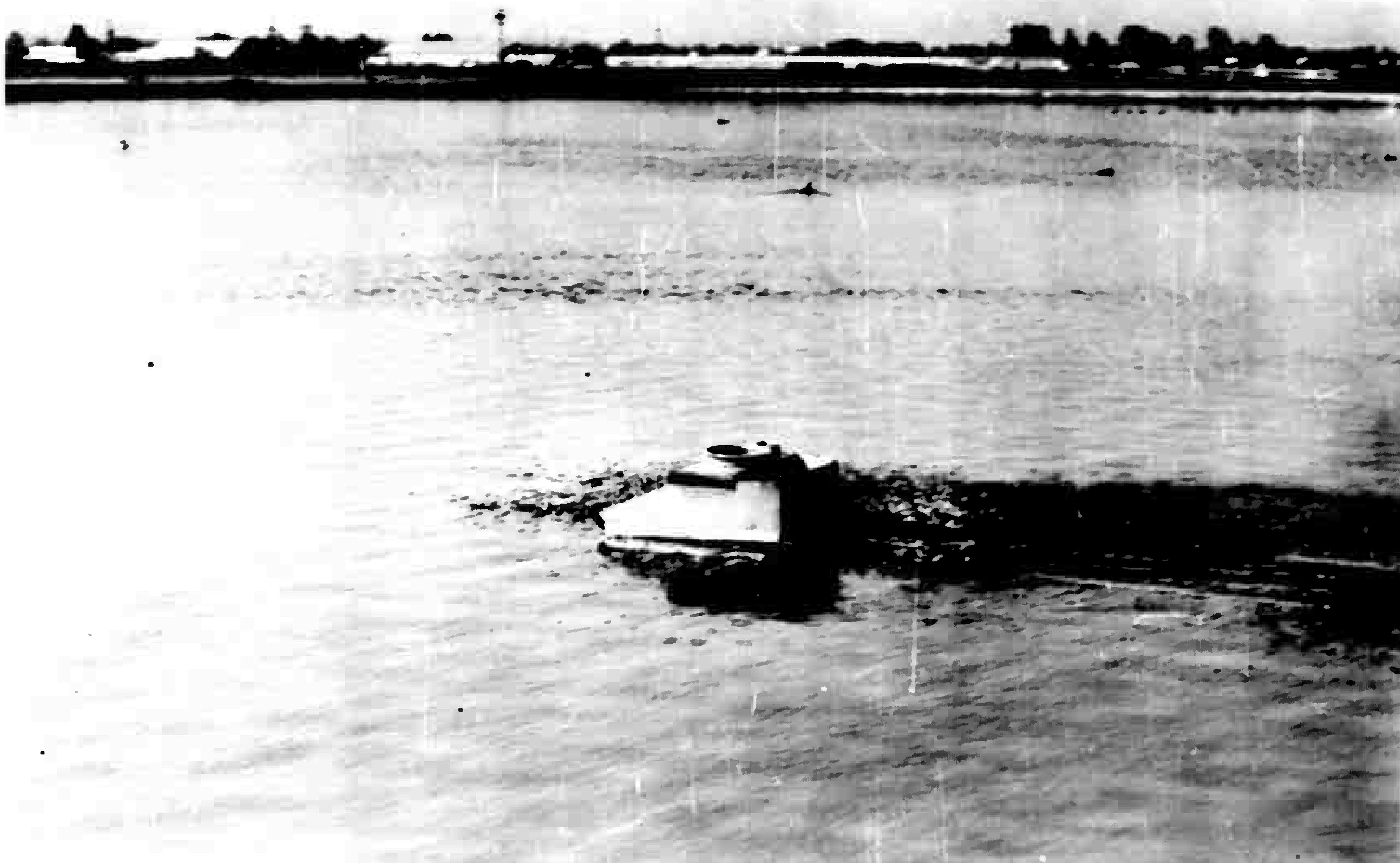

FIGURE 32: DP-3 GEM STABLE OVER-WATER OPERATION

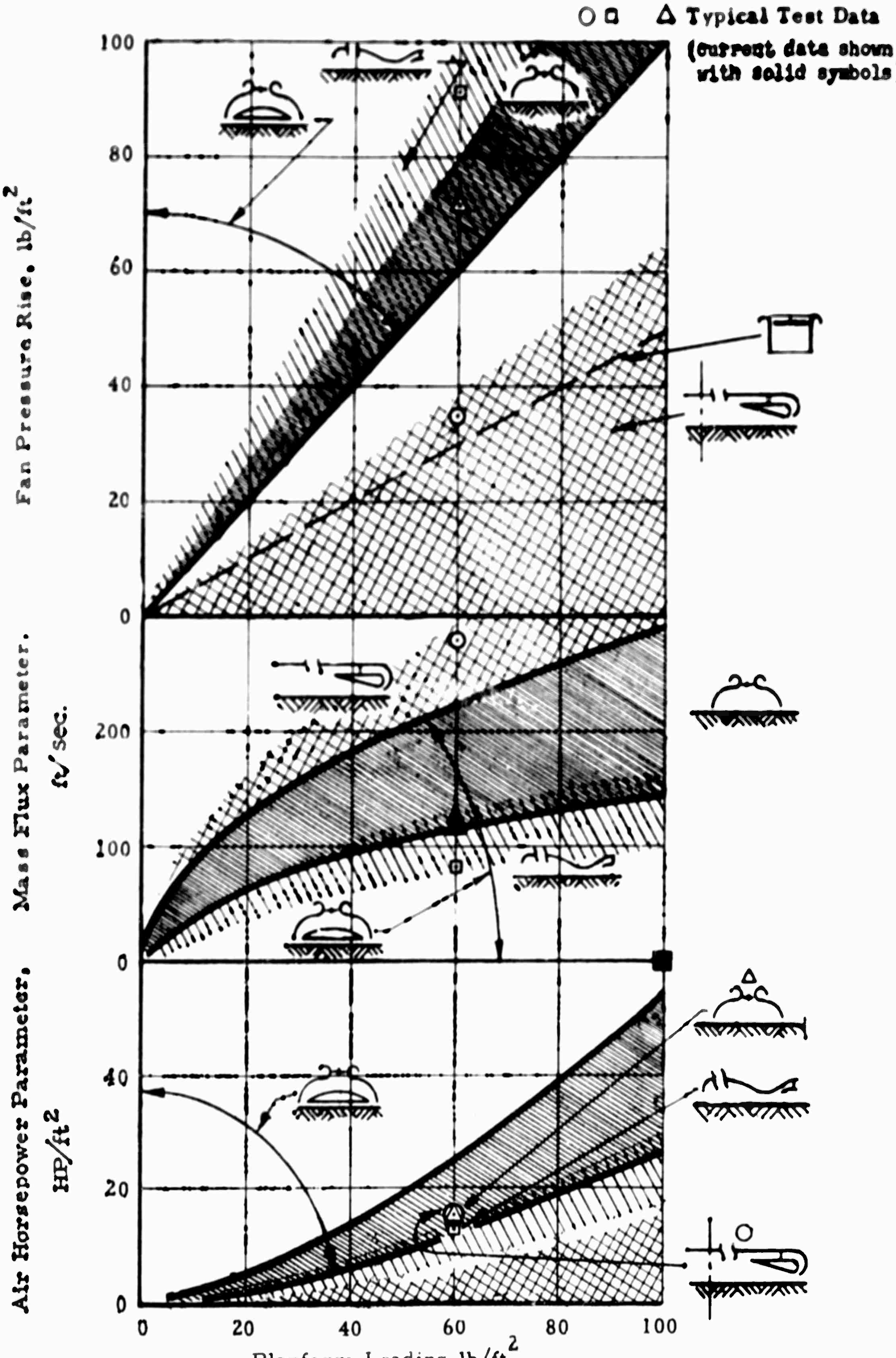

FIGURE 33: GEM HOVER PERFORMANCE

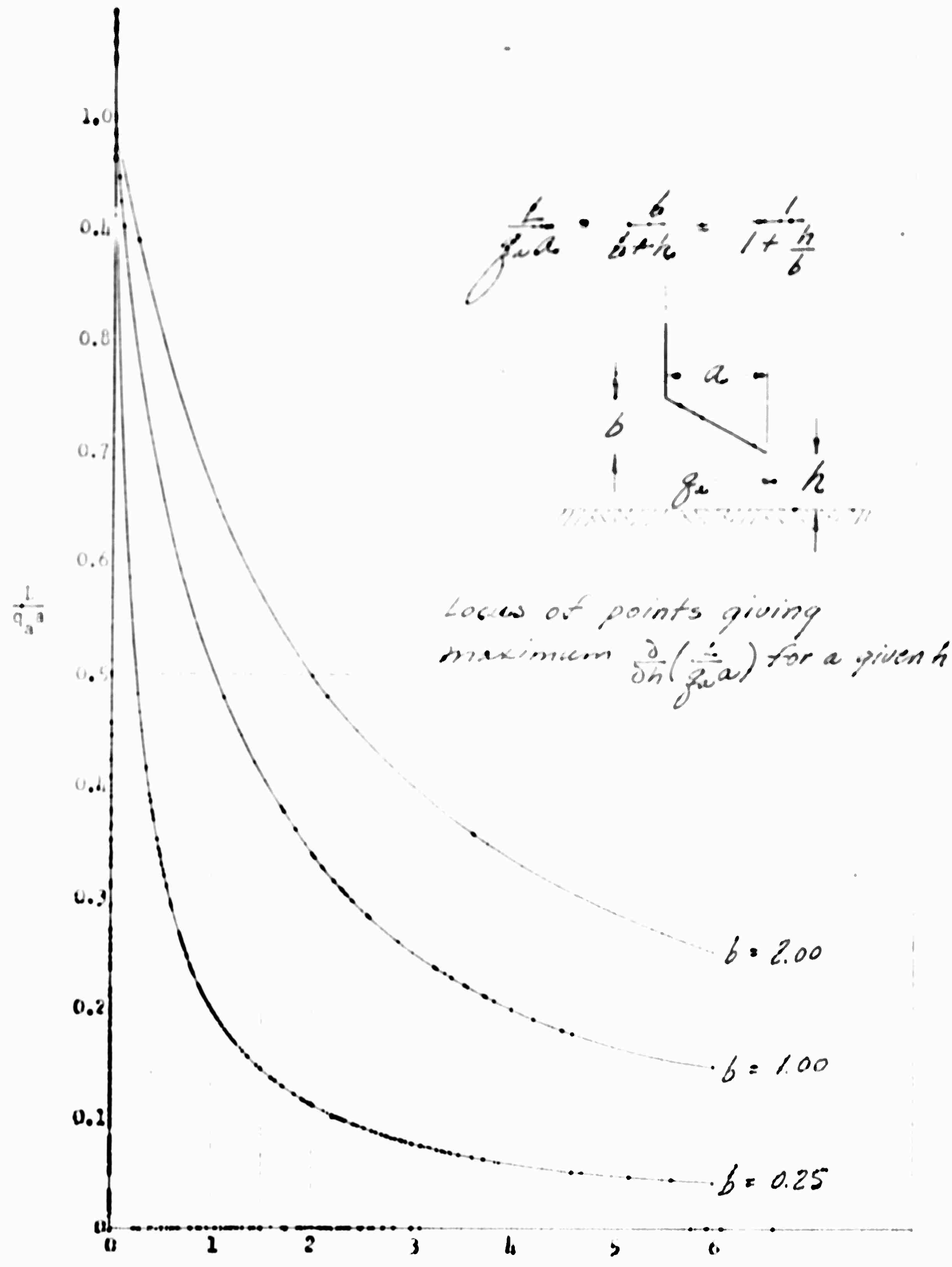

FIGURE 34: STRAIGHT FLAP CHARACTERISTICS

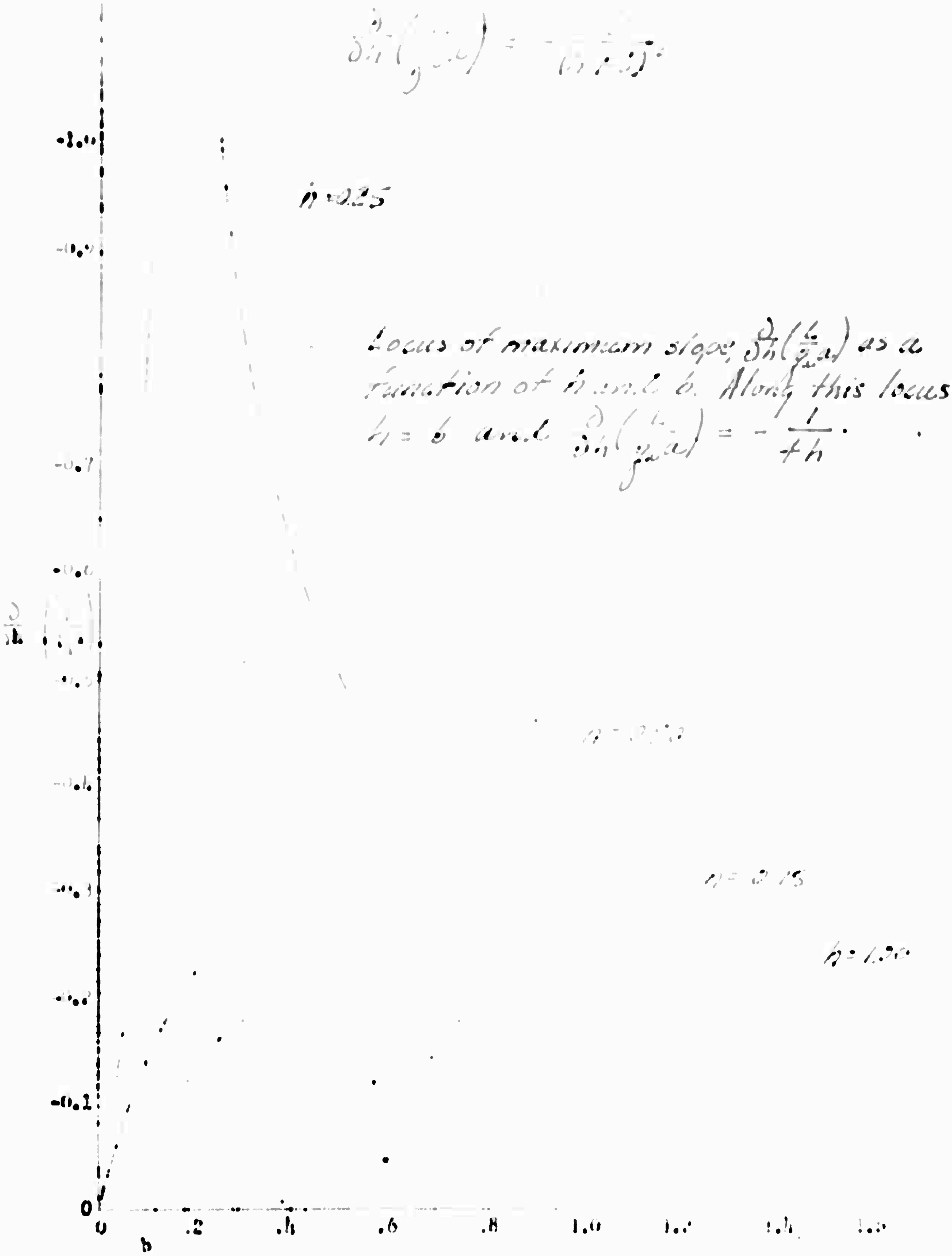

FIGURE 35: RATE OF CHANGE OF $\frac{L}{q_a a}$ WITH h FOR STRAIGHT FLAP

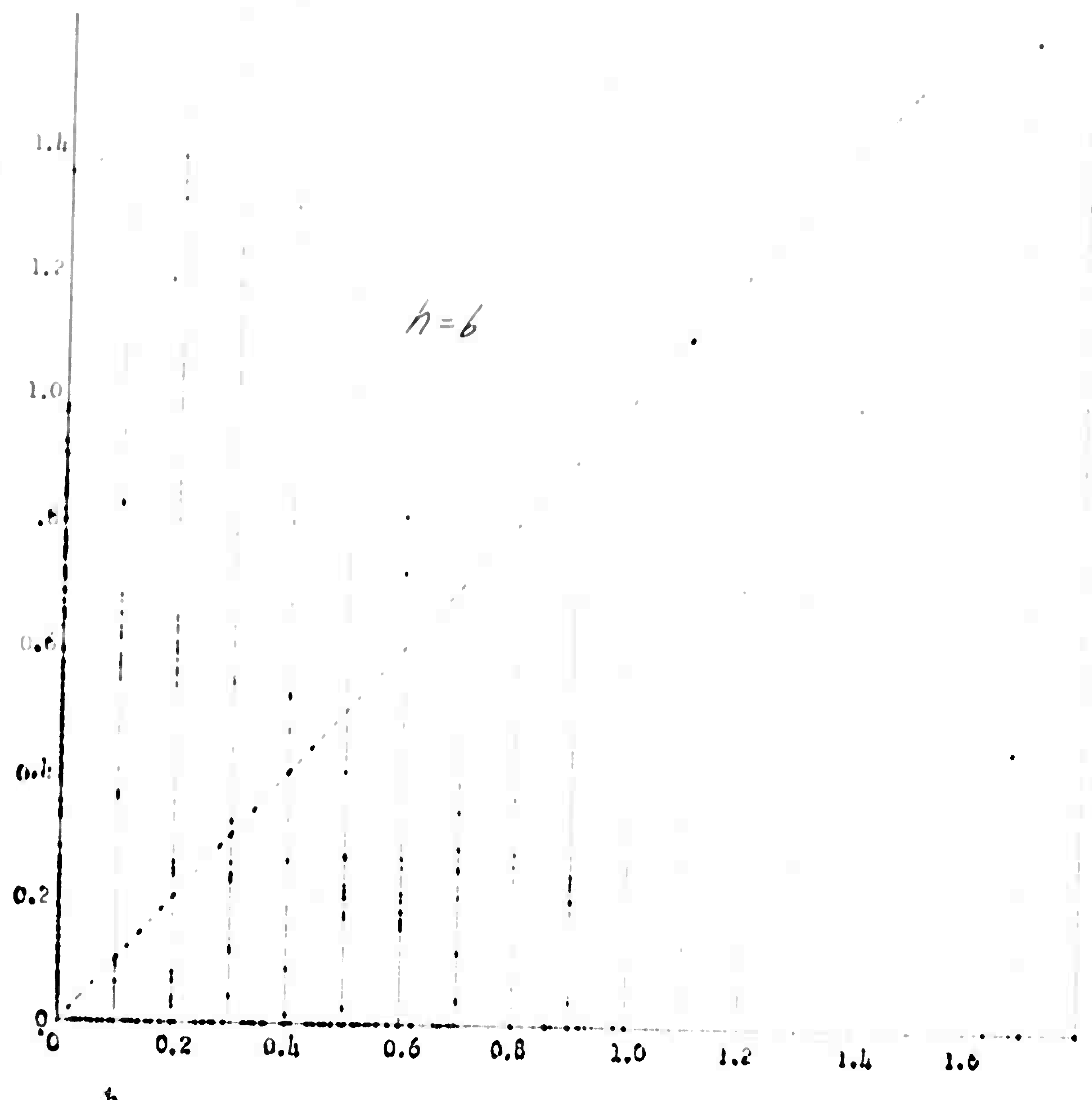

FIGURE 36: STRAIGHT FLAP: $h = f(b)$ FOR MAXIMUM RATE OF CHANGE OF $\frac{L}{q_a a}$ WITH h

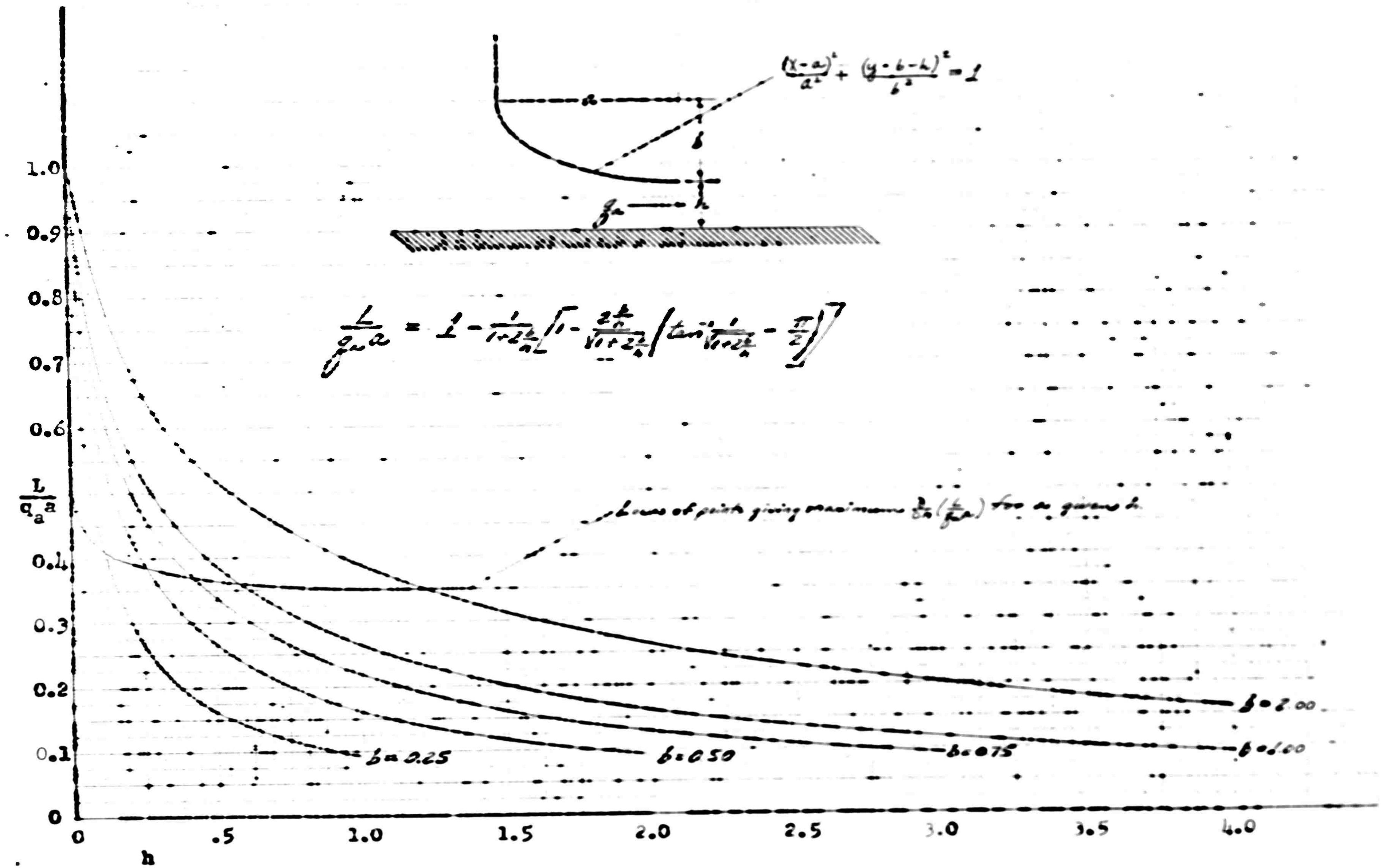

FIGURE 37: ELLIPTICAL FLAP CHARACTERISTICS

$$\frac{\partial}{\partial h}\left(\frac{L}{q_a a}\right) = \frac{-1}{1+2\frac{b}{h}}\left\{\frac{b}{h^2(h+b)(1+2\frac{b}{h})} + \left[\tan^{-1}\frac{1}{\sqrt{1+2\frac{b}{h}}} - \frac{\pi}{2}\right]\left[\frac{2b}{h^2\sqrt{1+2\frac{b}{h}}} - \frac{2b^2}{h^3(1+2\frac{b}{h})^{3/2}}\right]\right\}$$

$$+\left\{1 + \frac{2\frac{b}{h}}{\sqrt{1+2\frac{b}{h}}}\left[\tan^{-1}\frac{1}{\sqrt{1+2\frac{b}{h}}} - \frac{\pi}{2}\right]\right\}\left\{\frac{-2b}{h^2(1+2\frac{b}{h})^2}\right\}$$

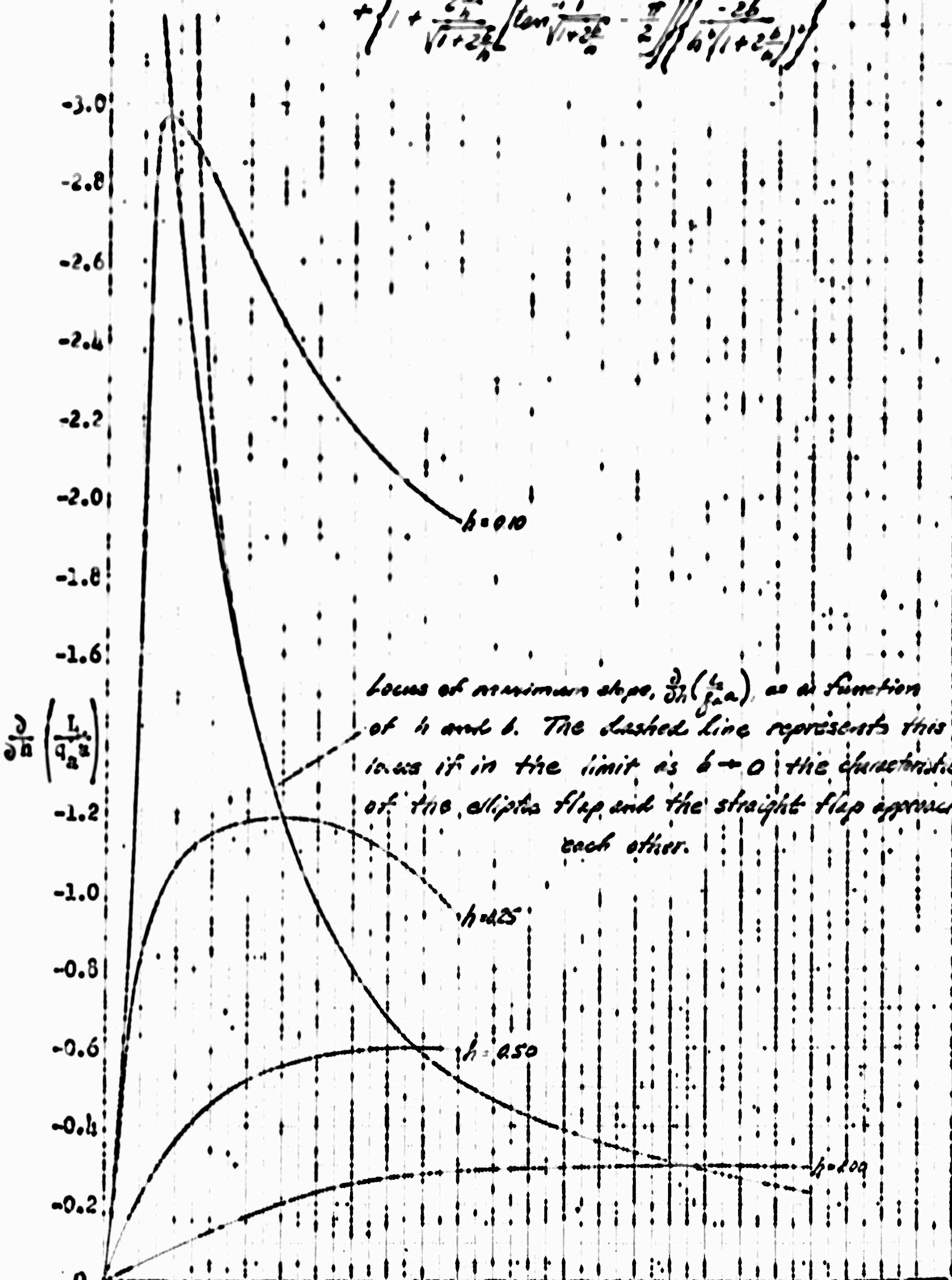

FIGURE 38: RATE OF CHANGE OF $\frac{L}{q_a a}$ WITH h FOR ELLIPTIC FLAP

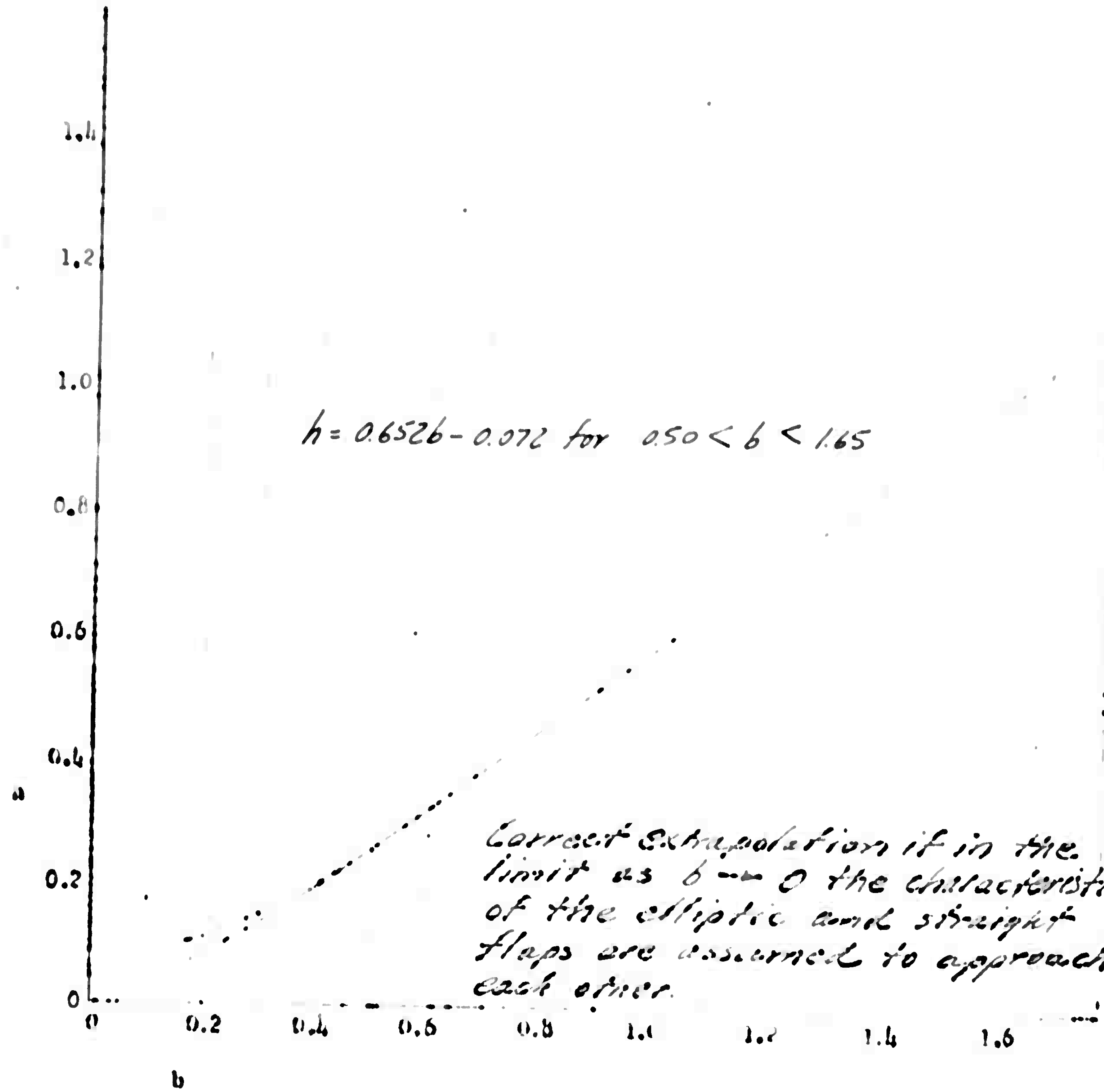

FIGURE 39: ELLIPTIC FLAP: h = f(b) FOR MAXIMUM RATE OF CHANGE OF $\frac{L}{q_a a}$ WITH h

APPENDIX I

EXIT GEOMETRY ANALYSIS DERIVATIONS

CASE 1: STRAIGHT FLAP

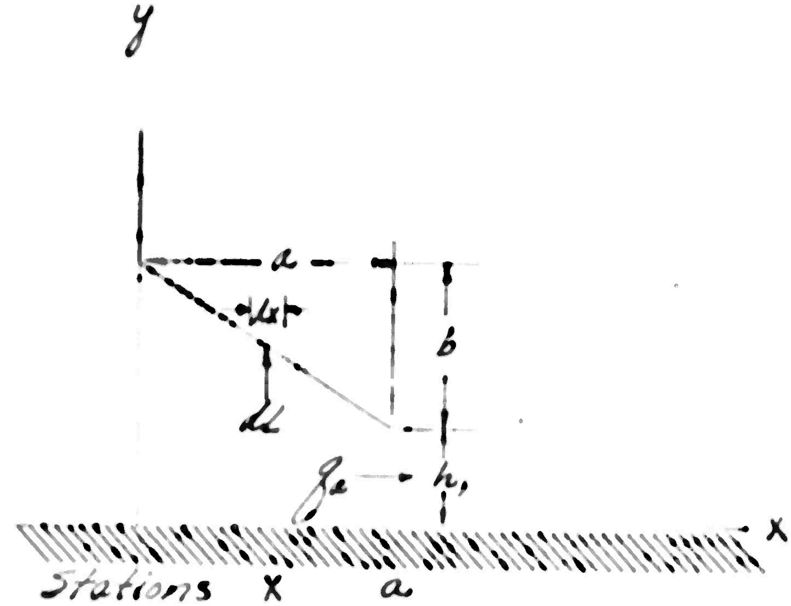

For an elemental dimension along x

$$dL = (P_x - P_a)\,dx \qquad (1)$$

or, integrating

$$L = \int_0^a (P_x - P_a)\,dx \qquad (2)$$

Since $P_x = P_a + q_a - q_x$, (2) becomes

$$L = \int_0^a (q_a - q_x)\,dx \qquad (3)$$

Since P_a is constant, q_a is also constant, and (3) becomes

$$L = q_a a - \int_0^a q_x\,dx \qquad (4)$$

From continuity $q_x = q_a \dfrac{A_a^2}{A_x^2}$ and (4) ... written as

$$L = q_w a - q_w A_a^2 \int_0^a \frac{dx}{A_x^2} \qquad (5)$$

From the sketch, $A_x = y = h_1 + b - \frac{b}{a}x$ (6)

so (5) becomes

$$L = q_w a - q_w A_a^2 \int_0^a \frac{dx}{\left(h_1 + b - \frac{b}{a}x\right)^2} \qquad (7)$$

Integrating (7) and substituting the limits gives

$$L = q_w a - q_w A_a^2 \left[\frac{1}{\frac{b}{a}(h_1+b-b)} - \frac{1}{\frac{b}{a}(h_1+b)}\right] \qquad (8)$$

Simplifying (8)

$$L = q_w a - q_w \frac{a A_a^2}{b} \left[\frac{h_1 + b - A_a}{A_a(h_1+b)}\right] \qquad (9)$$

Noting that $A_a = h_1$, (9) reduces to

$$\frac{L}{q_w a} = \frac{b}{h_1 + b} = \frac{1}{1 + \frac{h_1}{b}} \qquad (10)$$

PITCH EFFECTS

STRAIGHT FLAP

Note the change of position of the straight flap outlet with respect to the X-y plane.

Assume that the dimension "h_1" remains constant.

Since $\frac{b}{a}$ is likely to be a small ratio, for small angles of rotation $\Delta\alpha$, the fractional change of length "a" due to this rotation can be taken as negligibly small.

Under these conditions, then, the straight flap characteristics equation becomes

$$\frac{L}{g_a a} = 1 - \frac{h_1}{h_1 + b'} \quad \text{where } b' = b + a\Delta\alpha \qquad (10a)$$

CASE 2: ELLIPTIC FLAP

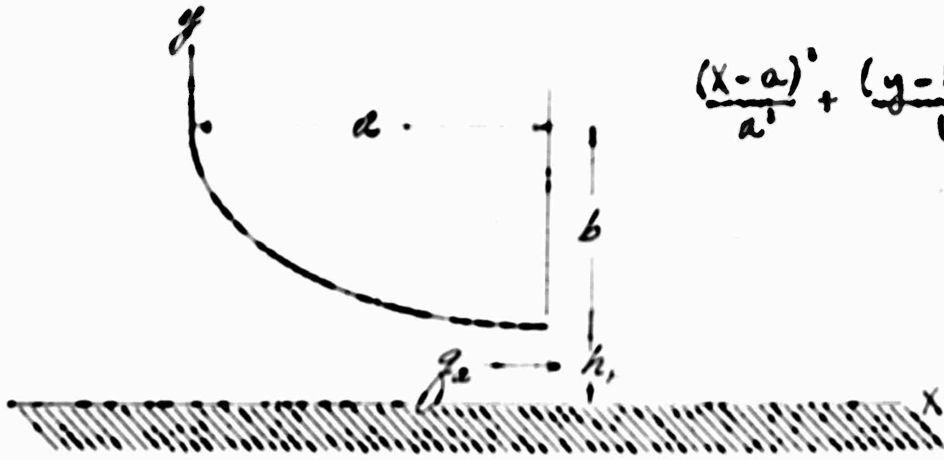

$$\frac{(x-a)^2}{a^2}+\frac{(y-b-h)^2}{b^2}=1$$

For this case we can start with a form similar to equation (5) of the straight flap case:

$$L = q_a a - q_a h_1^2 \int_0^a \frac{dx}{A_x^2} \qquad (11)$$

As in the former case, $A_x = y$. Solving for y from the equation of the ellipse above we get

$$y = b + h_1 \pm \sqrt{b^2 - \frac{b^2}{a^2}(x-a)^2} \qquad (12)$$

The controlling boundary condition on $L/q_a a$ is that $0 < \frac{L}{q_\omega a} \leq 1$. This follows from the fact that the velocity existing at the outlet is greater than that existing anywhere upstream and the static pressure

at the outlet equals ambient pressure. This can result in only a positive static pressure difference in the direction of lift. Also since q_a is the total pressure (gage) of the system, it is not possible to generate a lift pressure greater than q_a. Under this boundary condition we can thus choose either root of (12) such that the boundary condition is satisfied. In this case the root of y involving the negative radical satisfies the condition, the other does not.

Substituting (12) into (11) gives

$$L = q_a a - q_a h_1^2 \int_0^a \frac{dx}{\left(b+h_1 - \frac{b}{a}\sqrt{a^2-(x-a)^2}\right)^2} \quad (13)$$

To simplify integration, make the following substitutions:

$$\text{Let } z = x - a \qquad \text{When } x = a,\ z = 0$$
$$dz = dx \qquad x = 0,\ z = -a \quad (14)$$

Using (14) in (13) gives

$$L = q_a a - q_a h_1^2 \int_{-a}^{0} \frac{dz}{\left(b+h_1 - \frac{b}{a}\sqrt{a^2 - z^2}\right)^2} \quad (15)$$

Now let

$$z = a\cos\theta \qquad \text{When } z = 0,\ \theta = \pi/2$$
$$dz = -a\sin\theta\, d\theta \qquad z = -a,\ \theta = \pi \quad (16)$$

Using equations (16) in (15) and simplifying gives

$$\frac{L}{\rho_a a} = 1 + \left(\frac{h}{a}\right)^2 \int_{\pi}^{\pi/2} \frac{\sin\theta \, d\theta}{\left(\frac{h}{b} + 1 - \sin\theta\right)^2} \qquad (17)$$

Use partial fractions to simplify the integrand:

Let $\frac{h}{b} + 1 - \sin\theta = y$ (18)

so $\sin\theta = \frac{h}{b} + 1 - y$

Then

$$\frac{\sin\theta}{\left(\frac{h}{b} + 1 - \sin\theta\right)^2} = \frac{1}{y^2} \frac{1}{\left(\frac{1}{\frac{h}{b}+1-y}\right)} = \frac{A}{y^2} + \frac{B}{y} + \frac{C}{\left(\frac{1}{\frac{h}{b}+1-y}\right)} \qquad (19)$$

From the 2 right hand members of (19) we get

$$\frac{h}{b} + 1 - y = A + By + y^2\left(\frac{h}{b} + 1 - y\right) \qquad (20)$$

From (20)

$$A = \frac{h}{b} + 1, \quad B = -1, \quad C = 0 \qquad (21)$$

Thus by partial fractions (17) takes the following form, where $A = \frac{h}{b} + 1$ for convenience:

$$\frac{L}{\rho_a a} = 1 + \left(\frac{h}{b}\right)^2 \left[A \int_{\pi}^{\pi/2} \frac{d\theta}{(A - \sin\theta)^2} - \int_{\pi}^{\pi/2} \frac{d\theta}{(A - \sin\theta)} \right] \qquad (22)$$

These integrals can be reduced in the following manner:

Let
$$I_1 = \int \frac{d\theta}{(A - \sin\theta)^2} \tag{23}$$

$$I_2 = \int \frac{d\theta}{(A - \sin\theta)} \tag{24}$$

$$P = \frac{\cos\theta}{A - \sin\theta} \tag{25}$$

Differentiate P with respect to θ to get

$$\frac{dP}{d\theta} = \frac{(A - \sin\theta)(-\sin\theta) - (\cos\theta)(-\cos\theta)}{(A - \sin\theta)^2} \tag{26}$$

$$= \frac{1 - A\sin\theta}{(A - \sin\theta)^2} \tag{27}$$

$$= \frac{1 - A^2 + A(A - \sin\theta)}{(A - \sin\theta)^2} \tag{28}$$

$$= \frac{1 - A^2}{(A - \sin\theta)^2} + \frac{A}{A - \sin\theta} \tag{29}$$

Integrating (29) gives

$$P = (1 - A^2)\, I_1 + A\, I_2 \tag{30}$$

Solving (30) for I_1 gives

$$I_1 = \frac{1}{1 - A^2}\left[P - A I_2\right] \tag{31}$$

Substituting (31) into (22) gives

$$\frac{L}{q_0 a} = 1 + \left(\frac{h}{a}\right)^2 \left[\frac{A}{1-A^2}\left(P - A I_2\right) - I_2\right] \tag{32}$$

$$= 1 + \left(\frac{h}{a}\right)^2 \left[\frac{A}{1-A^2} P - \left(\frac{A^2}{1-A^2} + 1\right) I_2\right] \tag{33}$$

$$= 1 + \left(\frac{h}{a}\right)^2 \left[\frac{A}{1-A^2} P - \frac{1}{1-A^2} I_2\right] \tag{34}$$

$$= 1 + \frac{\left(h/a\right)^2}{1-A^2} \left[A P - I_2\right] \tag{35}$$

Now I_2 is a standard form which integrates to

$$I_2 = \frac{2}{\sqrt{A^2-1}} \tan^{-1}\left[\frac{A \tan\theta/2 - 1}{\sqrt{A^2-1}}\right]_{\pi}^{\pi/2} \tag{36}$$

$$= \frac{2}{\sqrt{A^2-1}} \left[\tan^{-1}\left(\frac{A-1}{\sqrt{A^2-1}}\right) - \frac{\pi}{2}\right] \tag{37}$$

Apply the limits of integration to AP

$$\left.\frac{A \cos\theta}{A - \sin\theta}\right]_{\pi}^{\pi/2} = 0 - \frac{A(-1)}{A-0} = 1 \tag{38}$$

Using (37) and (38) in (35) gives

$$\frac{L}{g_a a} = 1 + \frac{(h_1/b)^2}{1-A^2}\left\{1 - \frac{2}{\sqrt{A^2-1}}\left[\tan^{-1}\left(\frac{h_1/b}{\sqrt{A^2-1}}\right) - \frac{\pi}{2}\right]\right\} \qquad (39)$$

Substituting $\frac{h_1}{b}+1 = A$ in (39) gives, upon simplification

$$\frac{L}{g_a a} = 1 - \frac{1}{1+2\frac{b}{h_1}}\left[1 - \frac{2\frac{b}{h_1}}{\sqrt{1+2\frac{b}{h_1}}}\left(\tan^{-1}\frac{1}{\sqrt{1+2\frac{b}{h_1}}} - \frac{\pi}{2}\right)\right] \qquad (40)$$

In order to determine the design configuration for the elliptic flap, the partial derivatives with respect to h_r and b of equation (40) were taken and set equal to zero. This resulted in the following two expressions:

$$\frac{\partial}{\partial h}\left(\frac{L}{q_\infty a}\right) = \frac{-1}{1+2\frac{b}{h_r}}\left\{\frac{b^2}{h_r^2(h_r+b)(1+2\frac{b}{h_r})}\right.$$

$$+\left[\tan^{-1}\frac{1}{\sqrt{1+2\frac{b}{h_r}}}-\frac{\pi}{2}\right]\left[\frac{2b}{h_r^2\sqrt{1+2\frac{b}{h_r}}}-\frac{2b^2}{h_r^3(1+2\frac{b}{h_r})^{3/2}}\right]$$

$$\left.+\left\{1+\frac{2b}{h_r\sqrt{1+2\frac{b}{h_r}}}\left[\tan^{-1}\frac{1}{\sqrt{1+2\frac{b}{h_r}}}-\frac{\pi}{2}\right]\right\}\left\{\frac{-2b}{h_r^2(1+2\frac{b}{h_r})^2}\right\}\right\}$$

$$= 0 \qquad (41)$$

$$\frac{\partial}{\partial b}\left(\frac{L}{q_\infty a}\right) = \frac{-1}{1+2\frac{b}{h_r}}\left\{\frac{b}{h_r\sqrt{1+2\frac{b}{h_r}}}\left(\frac{-1}{h_r+b}\right)\left(\frac{1}{\sqrt{1+2\frac{b}{h_r}}}\right)\right.$$

$$+\left[\tan^{-1}\frac{1}{\sqrt{1+2\frac{b}{h_r}}}-\frac{\pi}{2}\right]\left[\frac{2}{h_r\sqrt{1+2\frac{b}{h_r}}}-\frac{2b}{h_r^2(1+2\frac{b}{h_r})^{3/2}}\right]$$

$$\left.+\left\{1-\frac{2b}{h_r\sqrt{1+2\frac{b}{h_r}}}\left[\tan^{-1}\frac{1}{\sqrt{1+2\frac{b}{h_r}}}-\frac{\pi}{2}\right]\right\}\left\{\frac{2}{h_r(1+2\frac{b}{h_r})^2}\right\}\right\}$$

$$= 0 \qquad (42)$$

Examination of these two simultaneous equations in h and b reveals that any ordinary algebraic solution of these equations for a relationship between h and b would be extremely difficult, if not impossible. Thus it was decided that the quickest method of determining this relationship, commensurate with the scope of this program, was the graphical method described in the text.

PITCH EFFECTS

ELLIPTIC FLAP

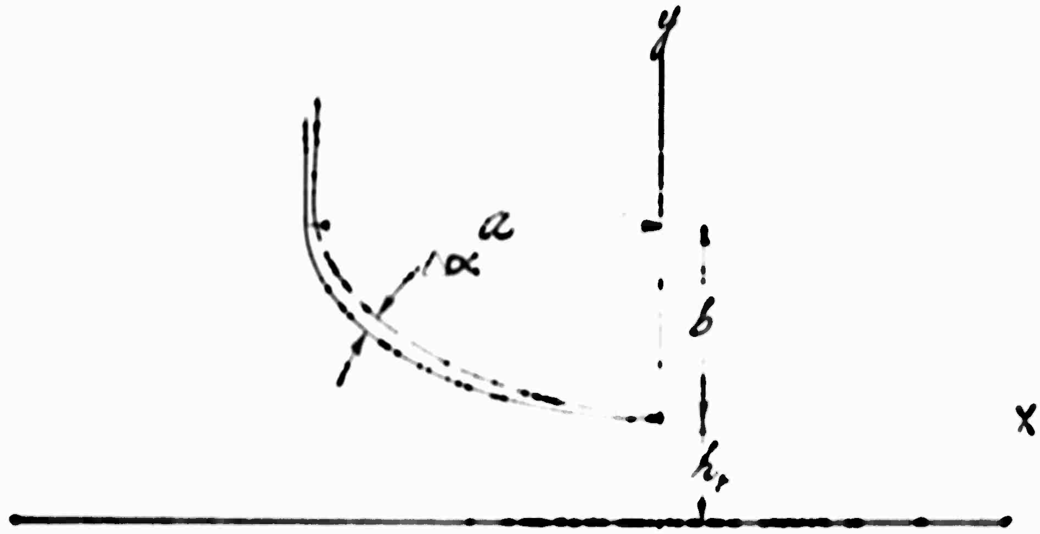

Note the change of position of the elliptic outlet with respect to the x-y plane.

Assume that "h_r" remains constant:

As for the straight flap, assume that for small pitch angles $\Delta\alpha$, dimension "a" remains essentially constant.

Applying the equations of rotation of axes about a fixed origin to the elliptic flap derivation gives an equation similar in form to (17):

$$\frac{L}{q_u a} = 1 + h_r^2 \int_{\frac{\pi}{2}}^{0} \frac{\cos\theta \, d\theta}{\left[h_r + b + (a\sin\theta)\Delta\alpha - b\cos\theta\right]^2} \quad (43)$$

Since the solution of (43) is an extremely complicated expression, the effect of pitching is more easily seen from an examination of (43). Immediately it can be seen that pitching essentially produces a change in dimension b. This is evident since $a \sin \theta$ is always positive within the limits of investigation and therefore $b' [= b + (a \sin \theta) \Delta\alpha]$, would tend to be greater or less than b depending upon whether $\Delta\alpha$ was positive or negative.

APPENDIX II

GROUND PLANE PRESSURE DISTRIBUTION

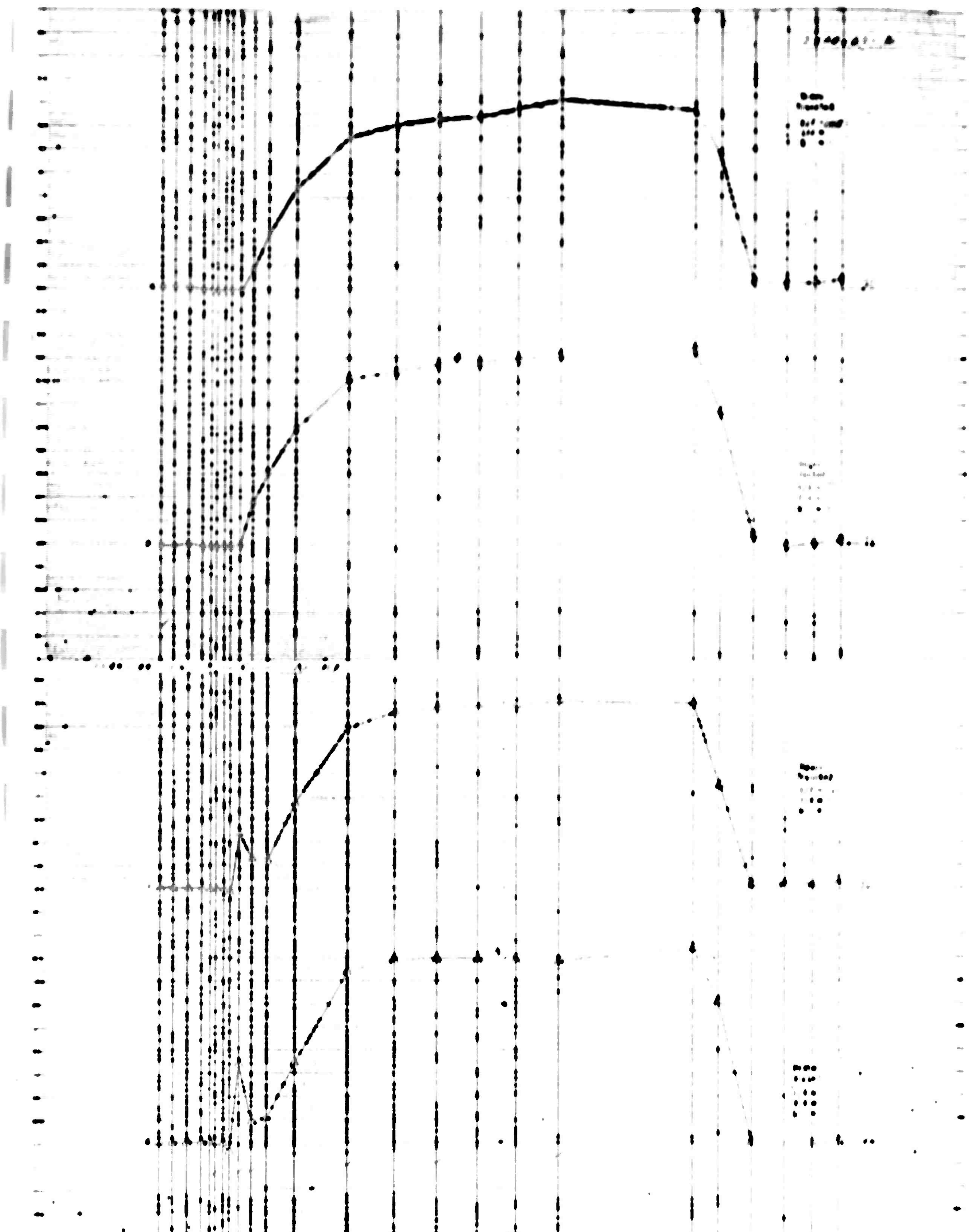

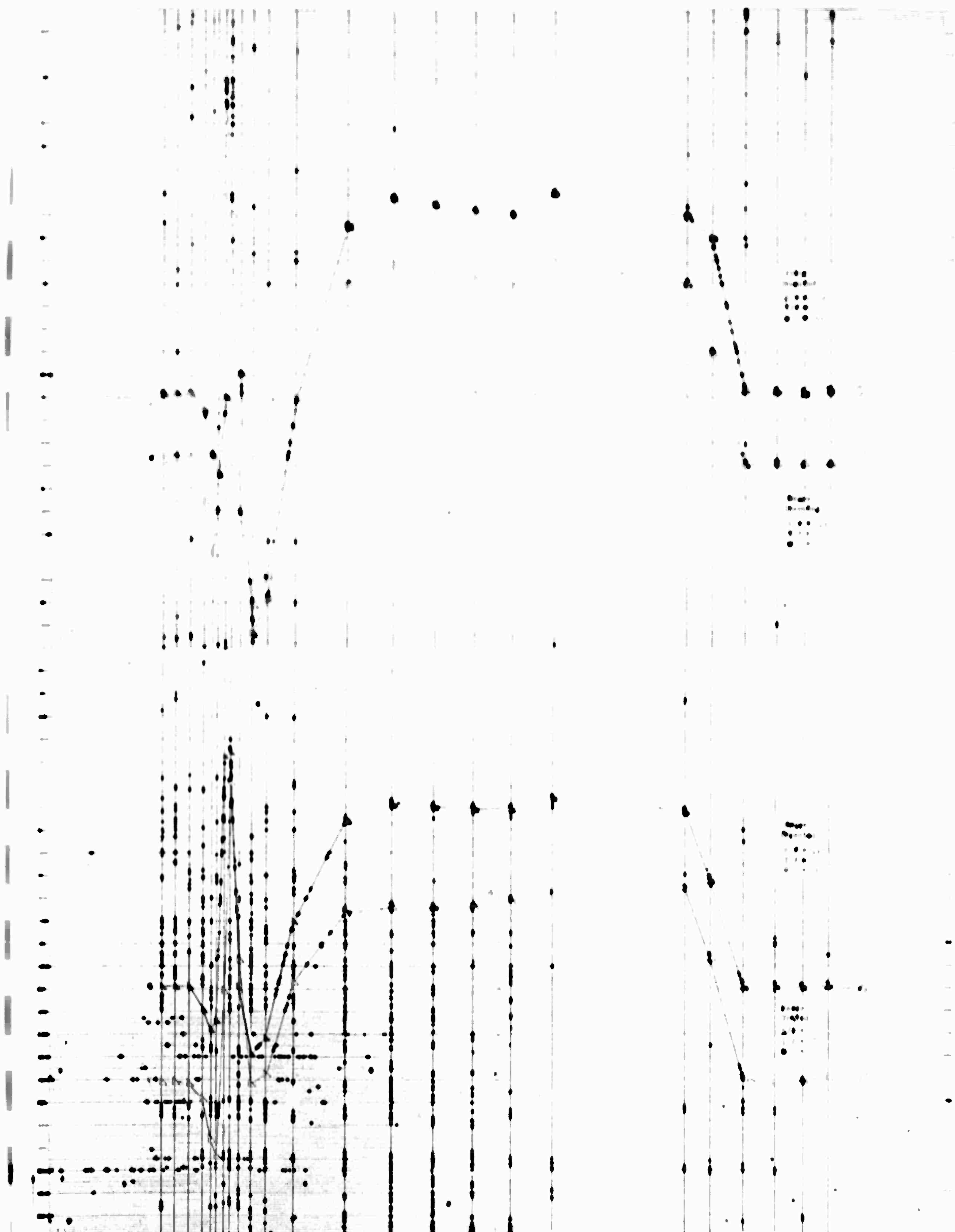

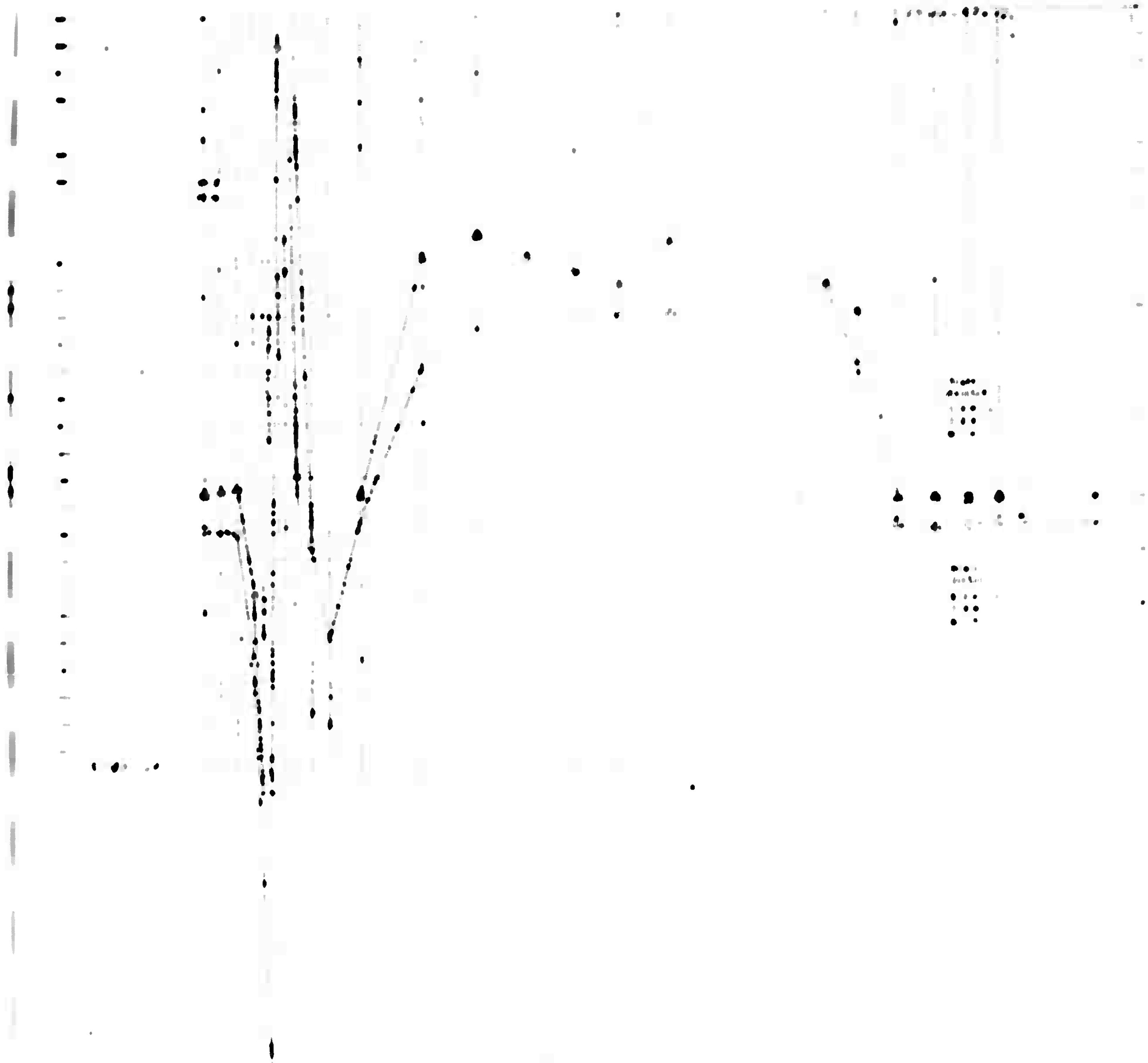

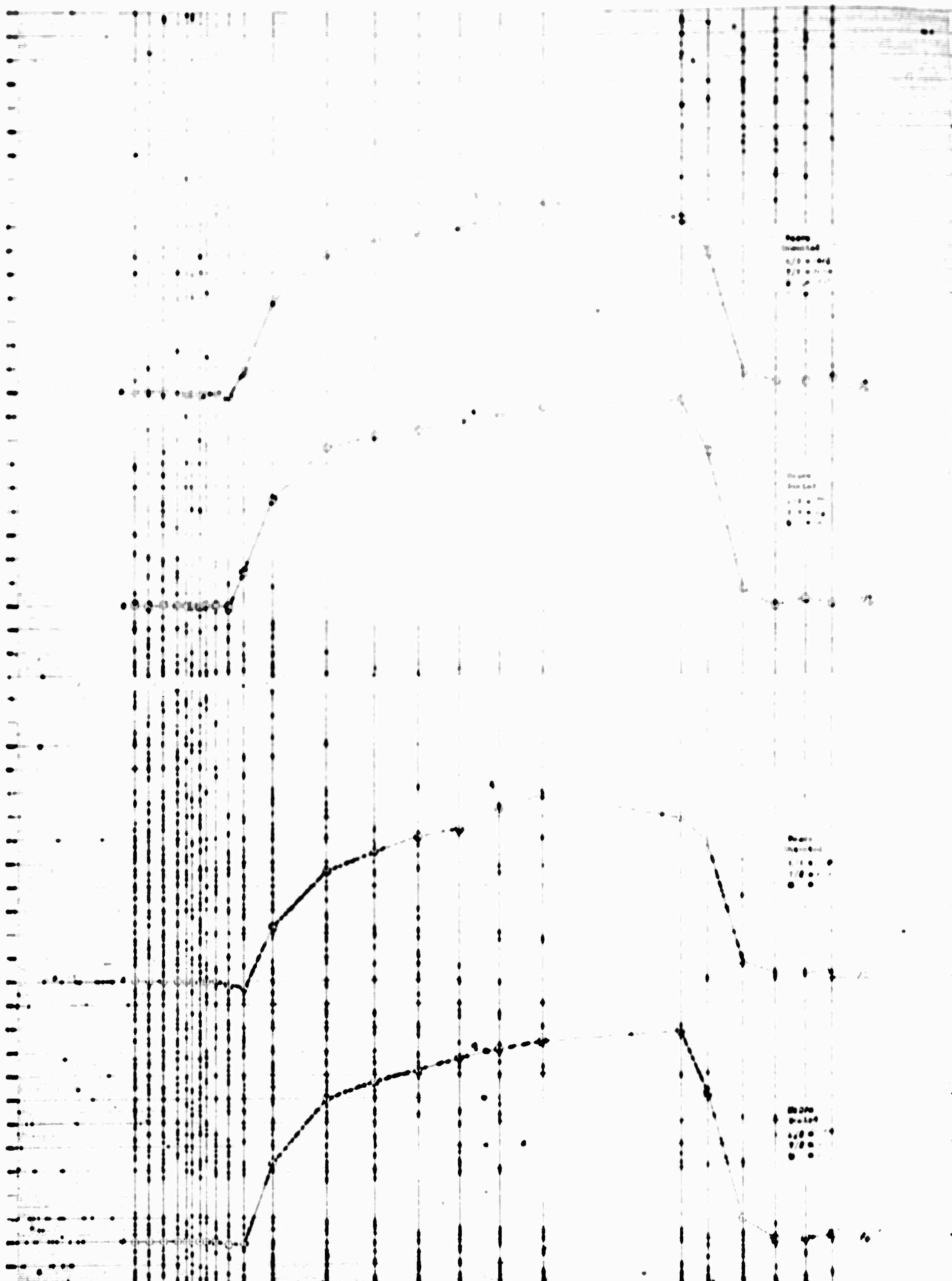

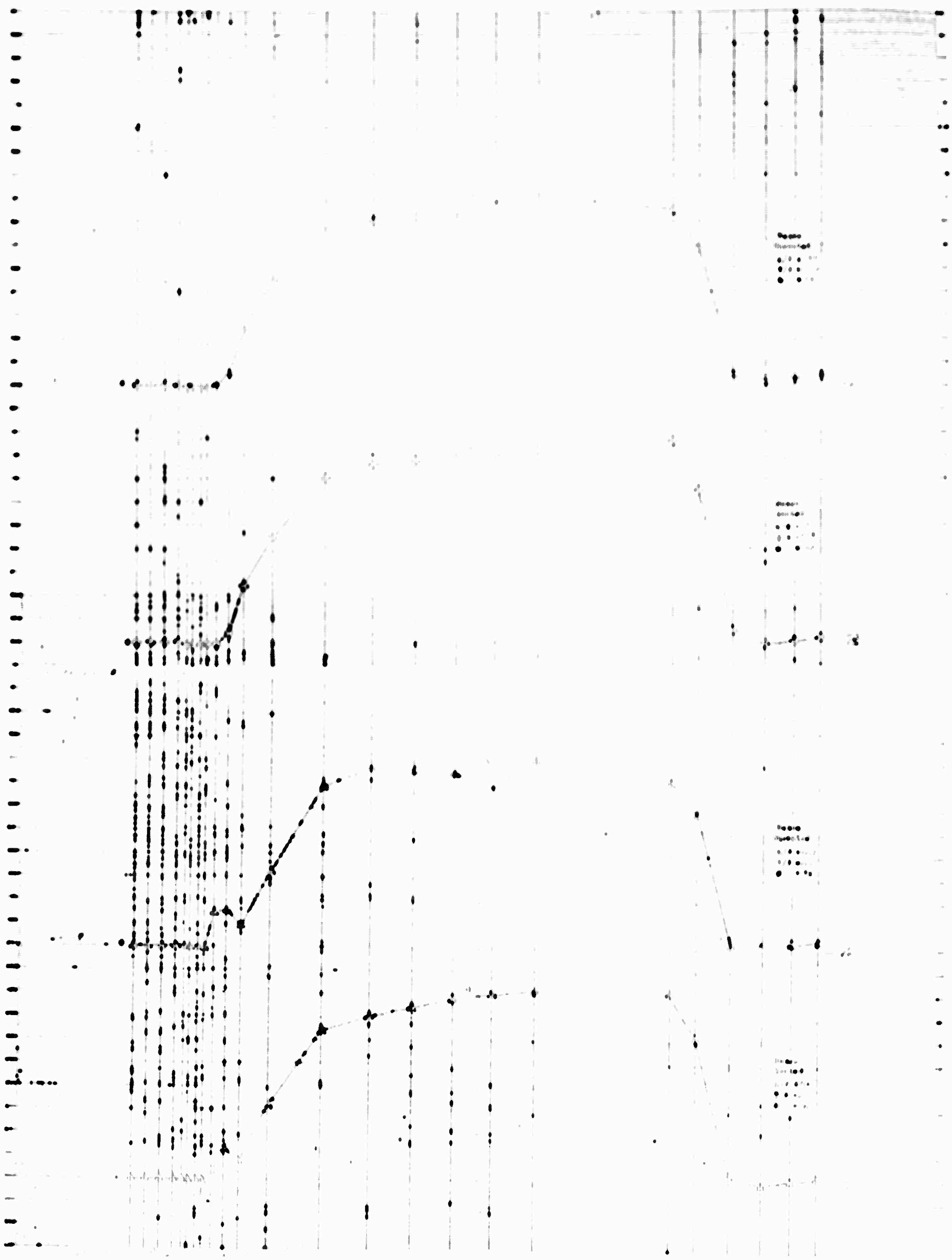

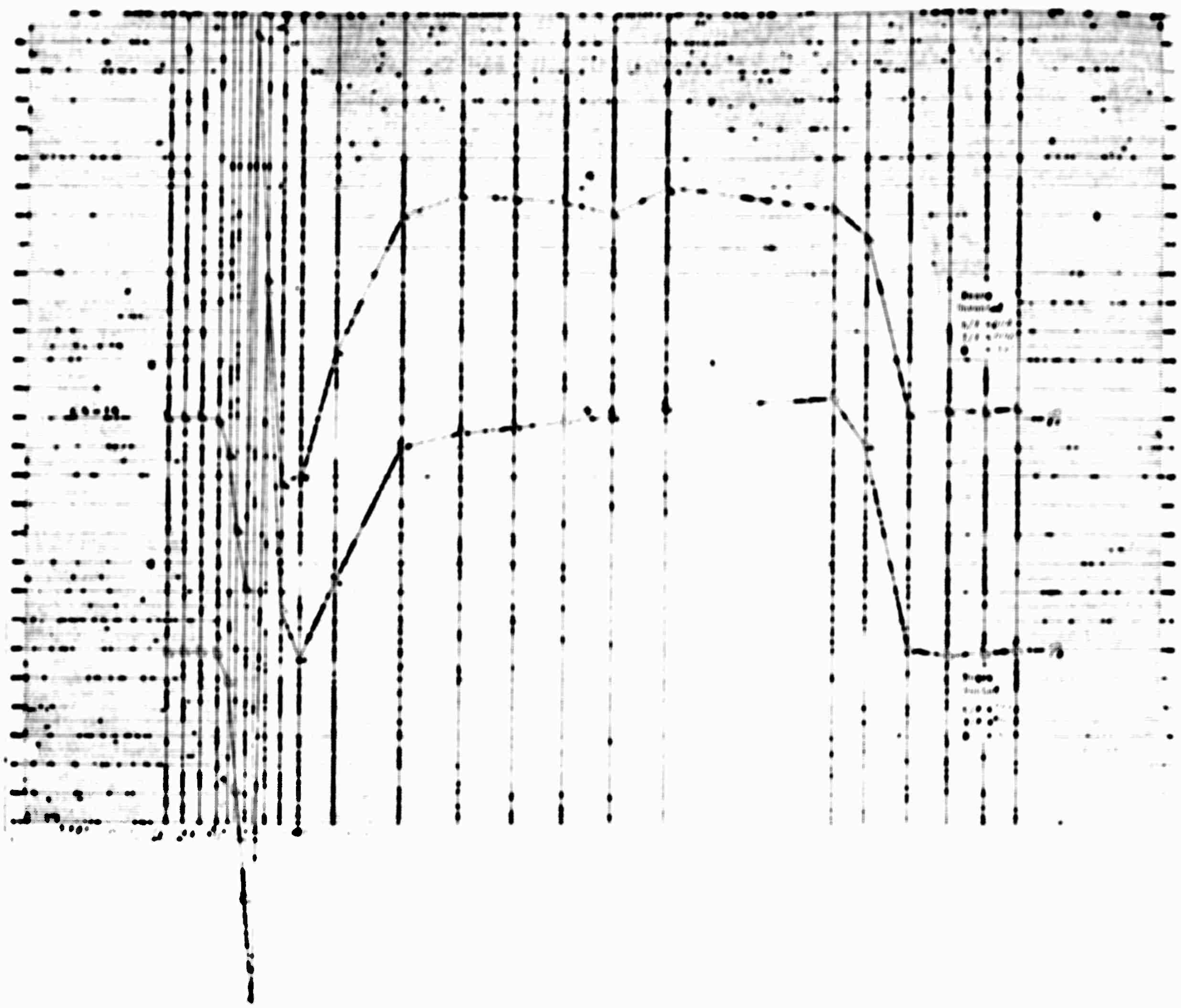

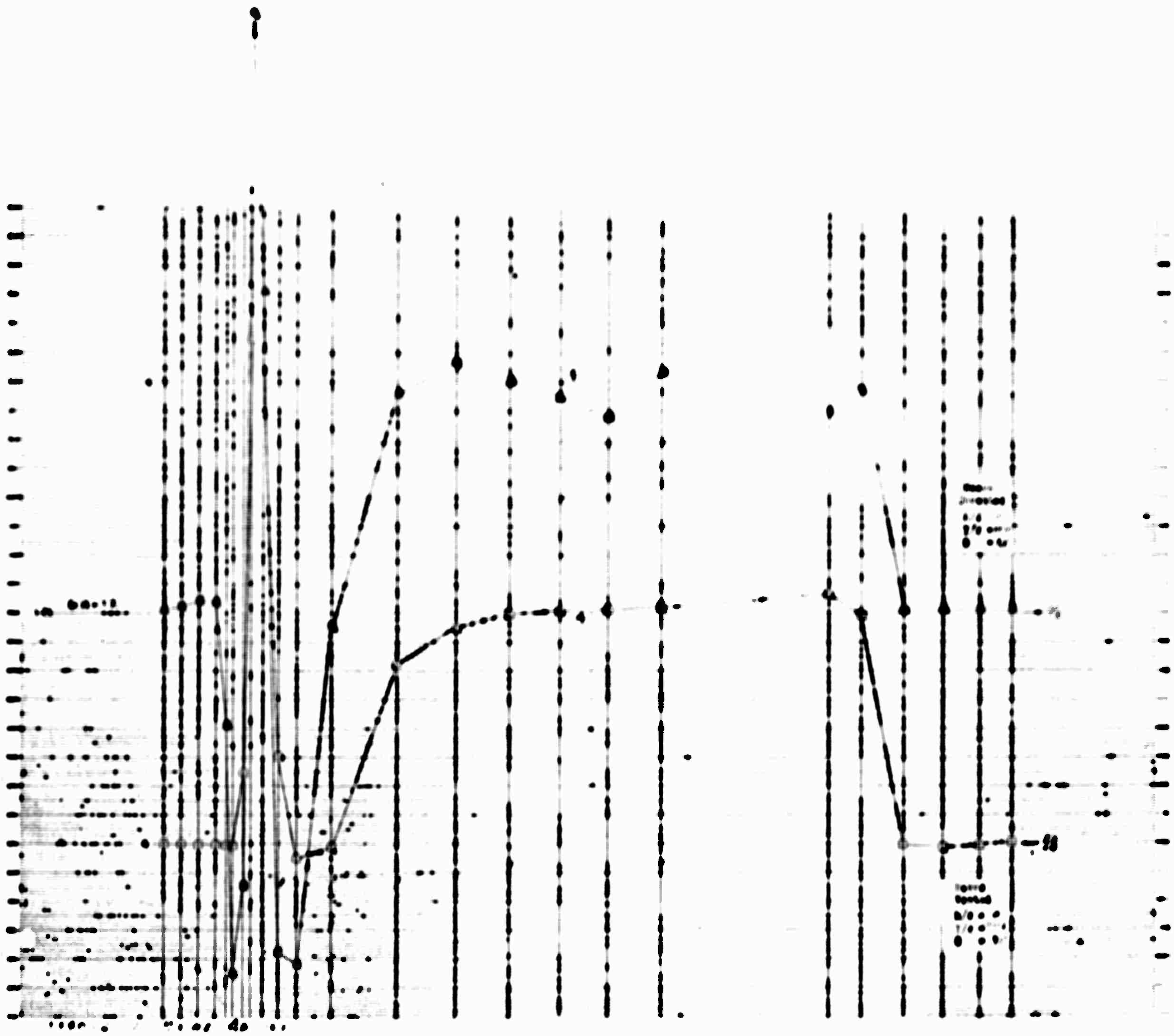

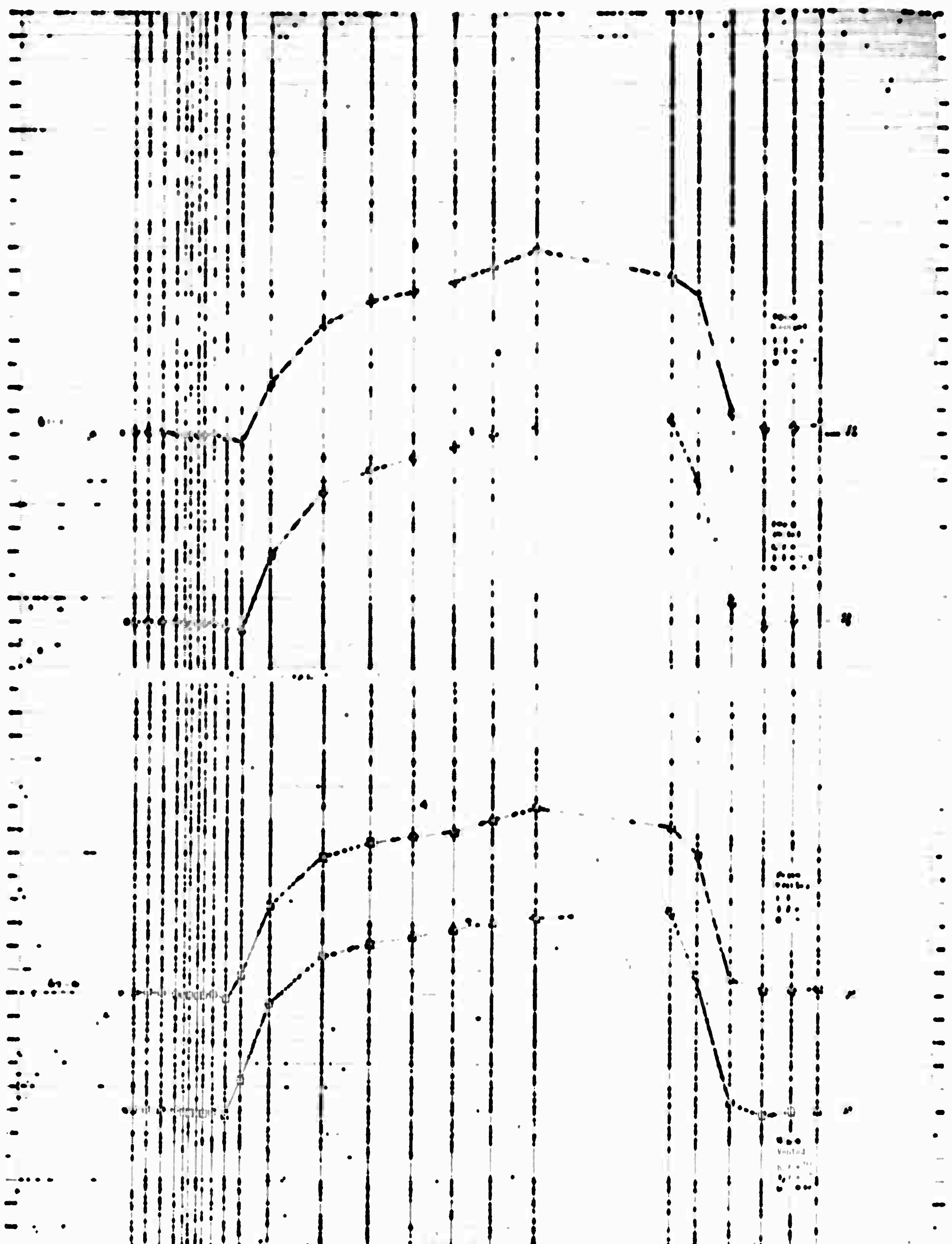

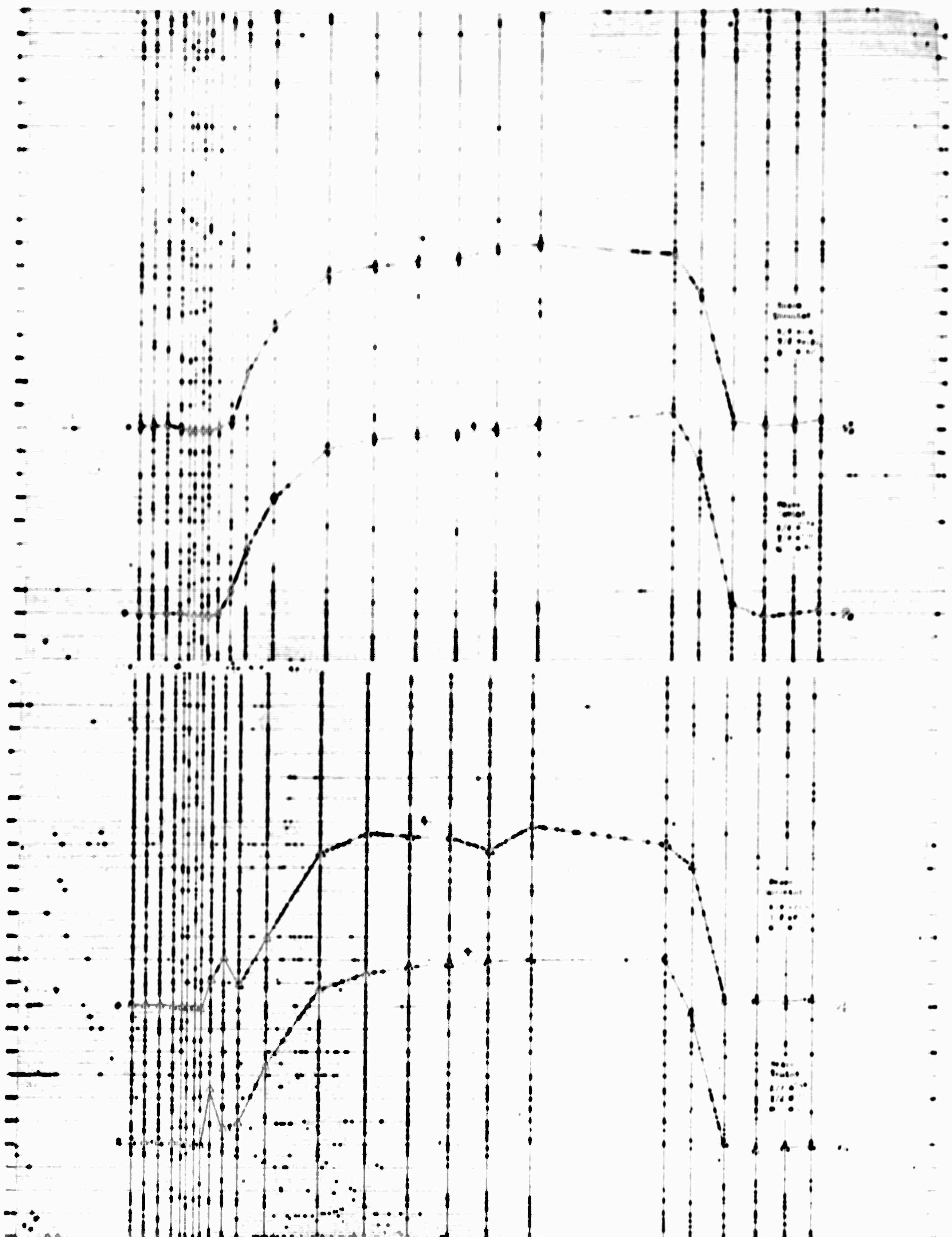

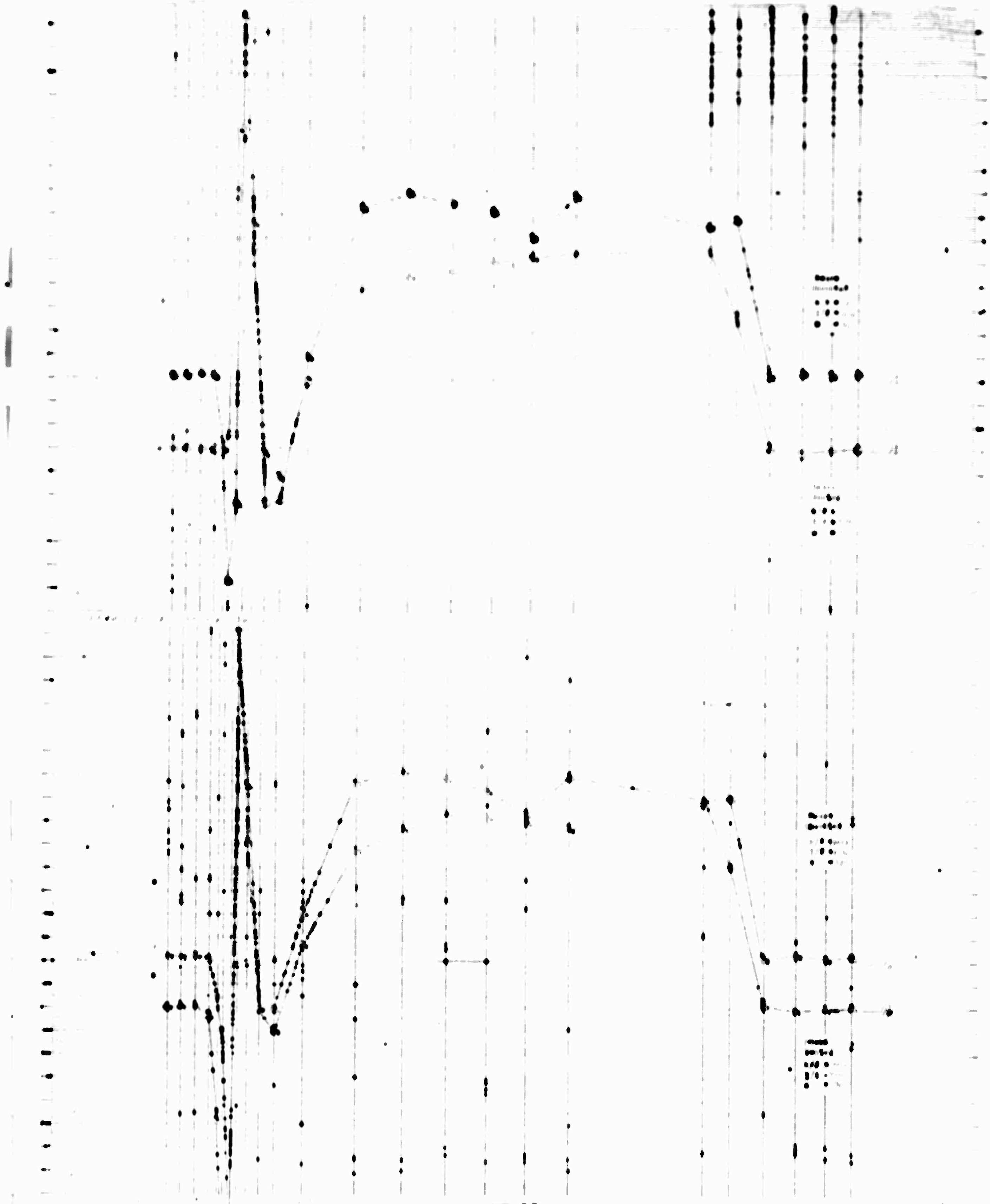

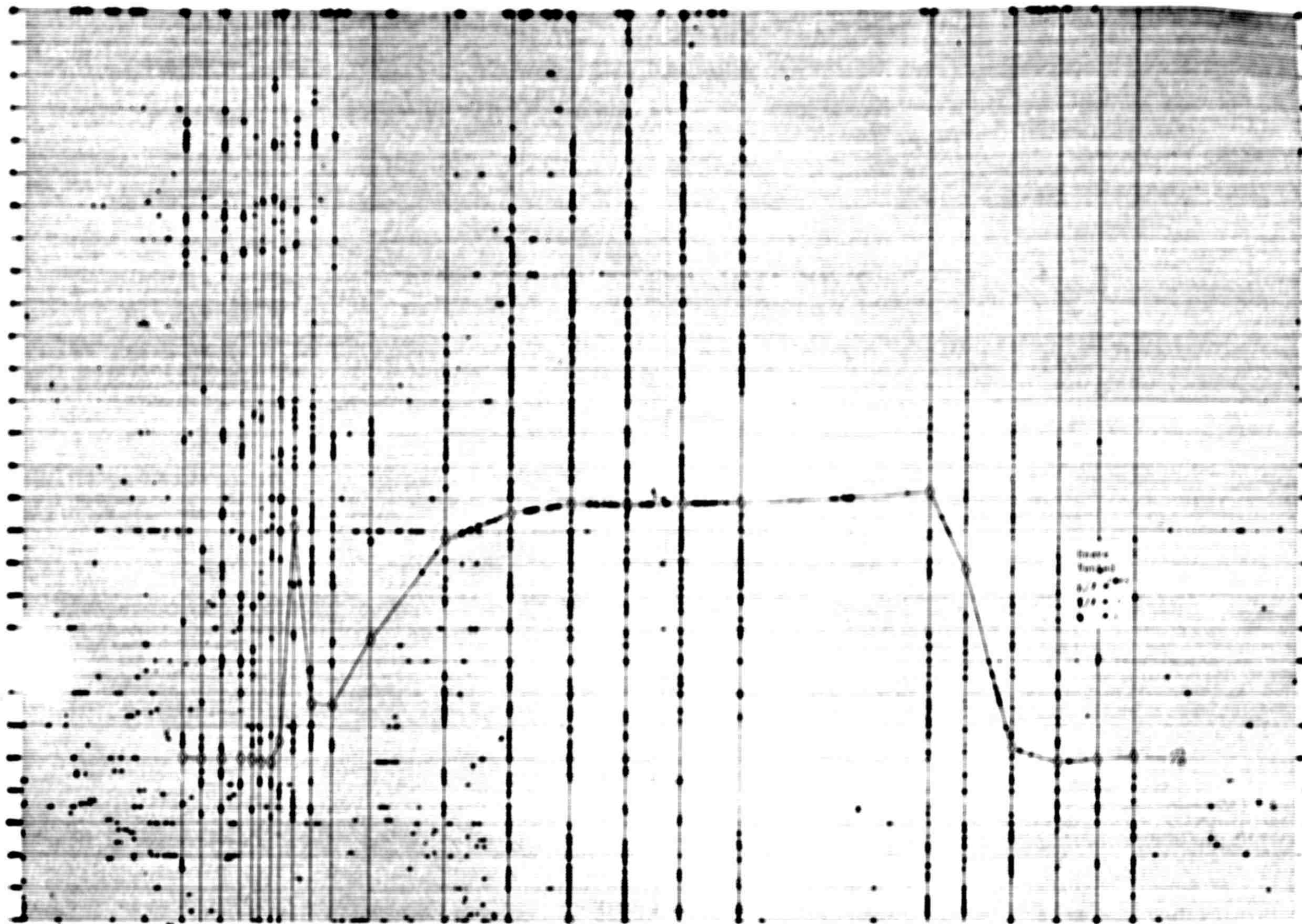

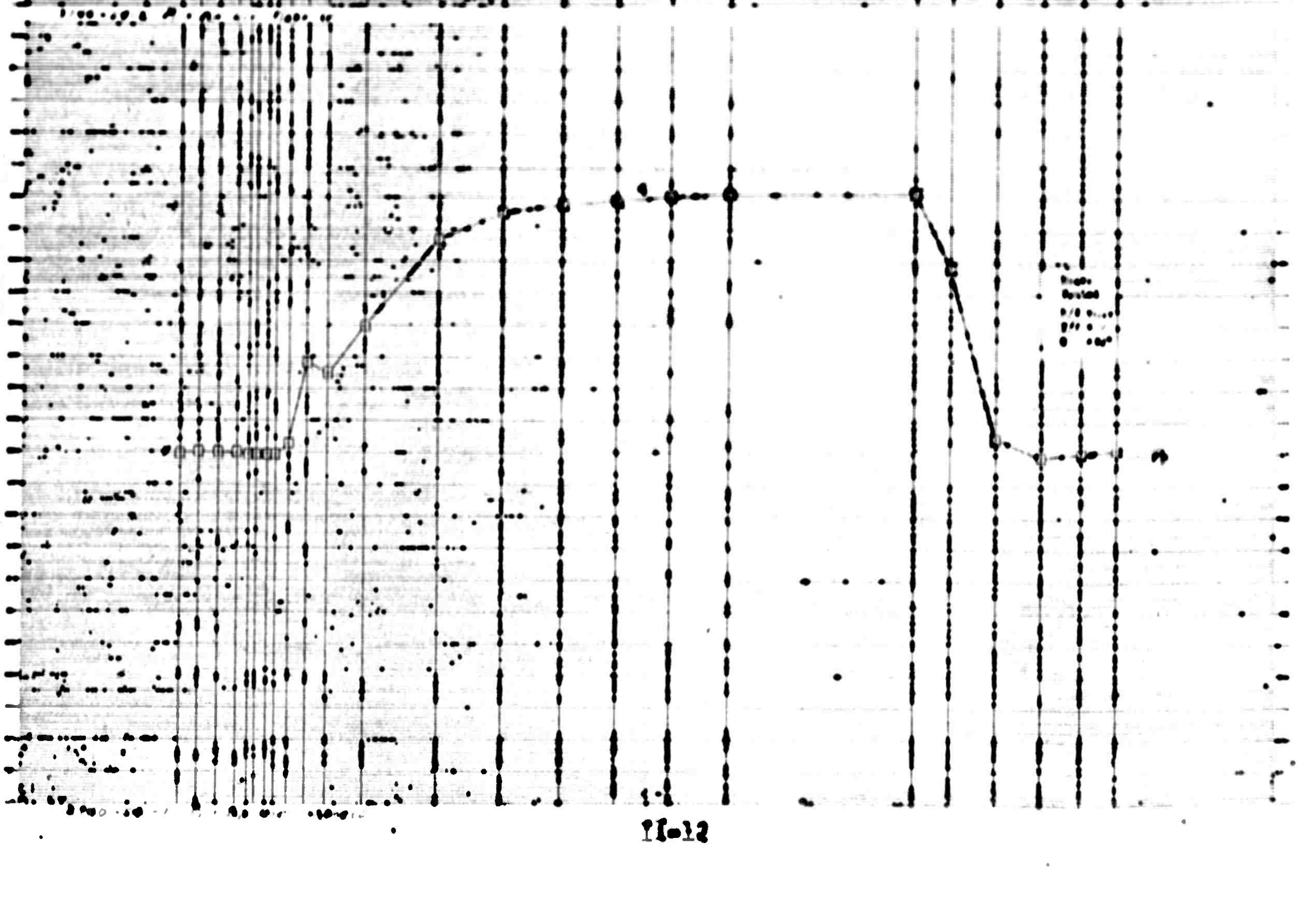

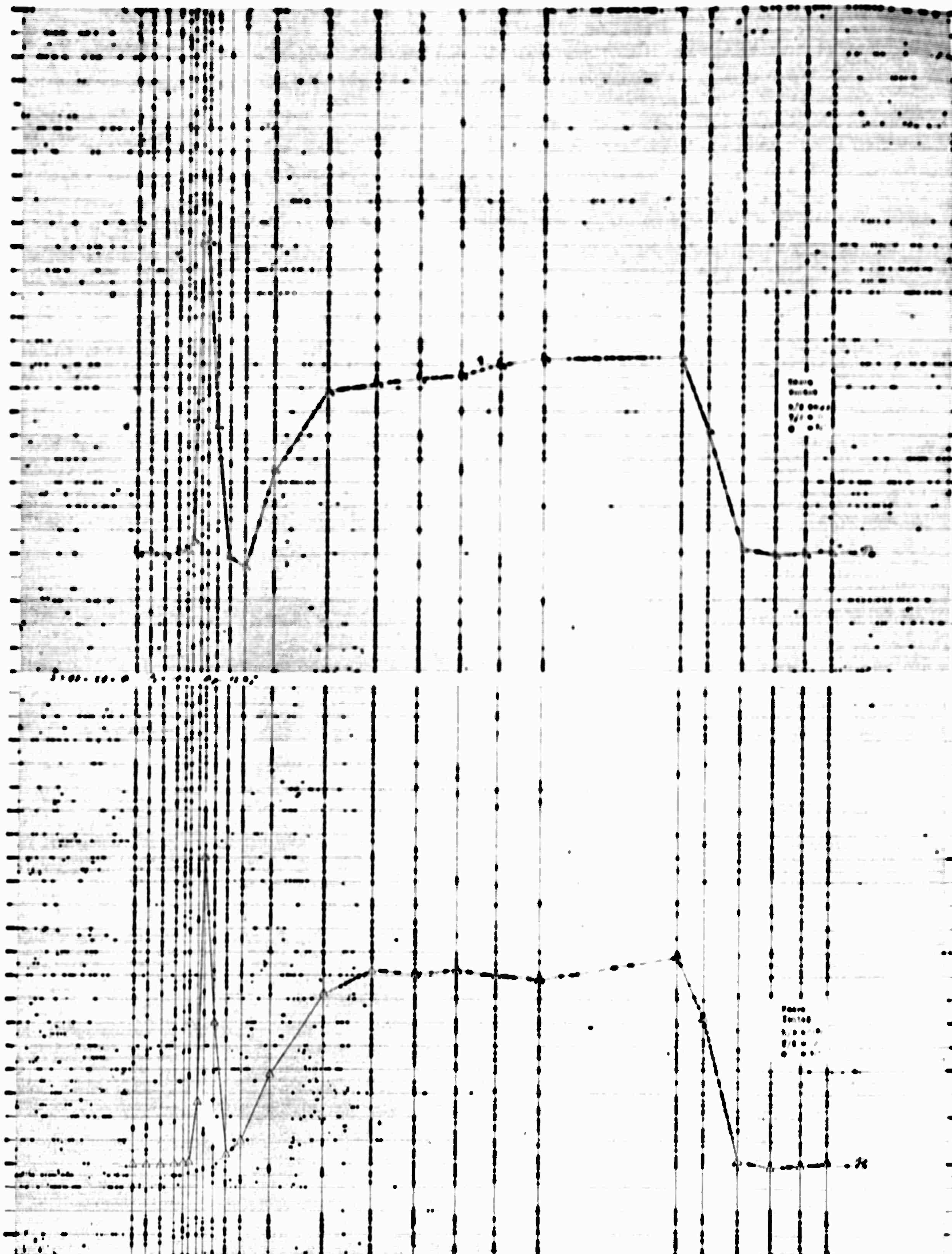

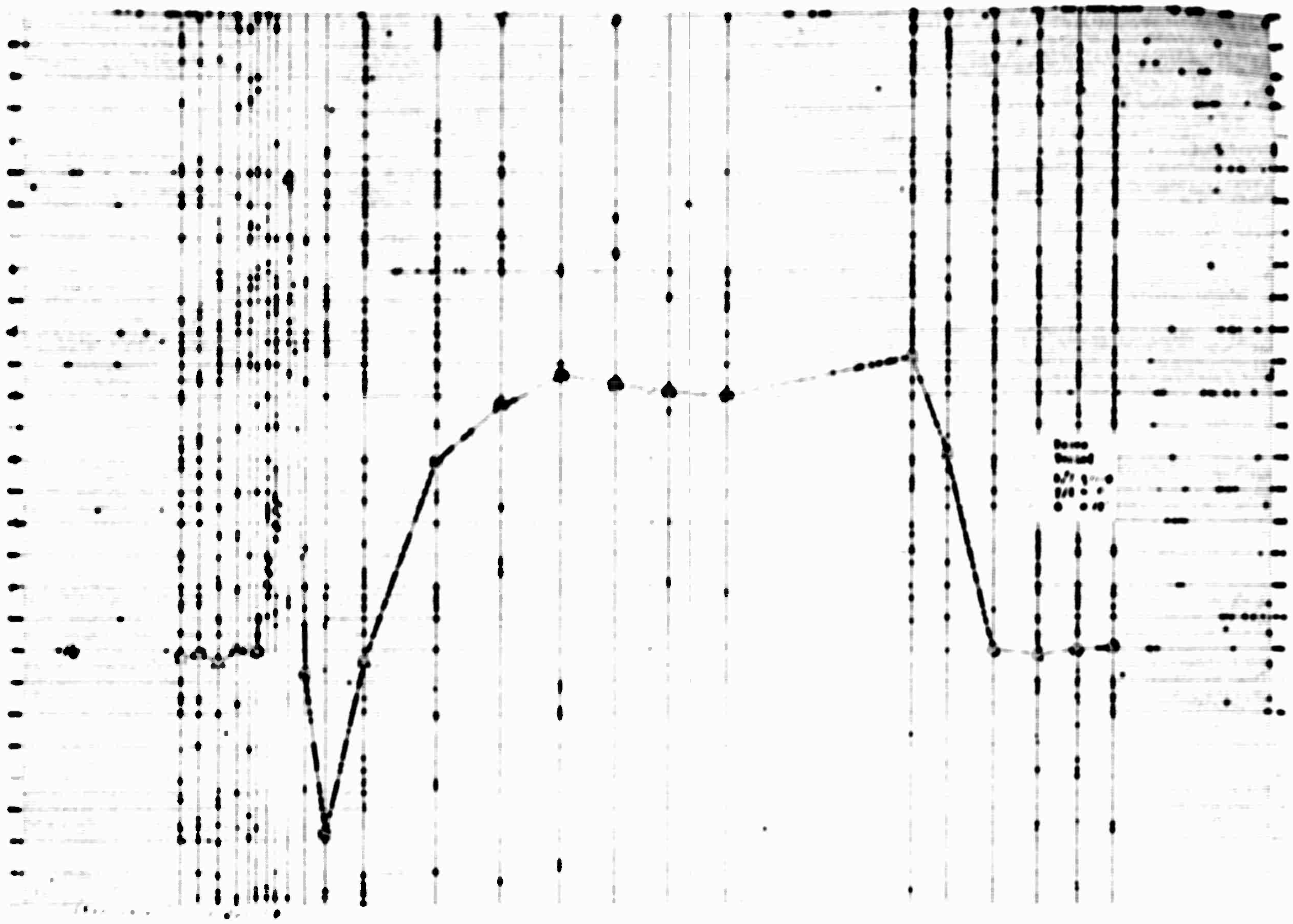

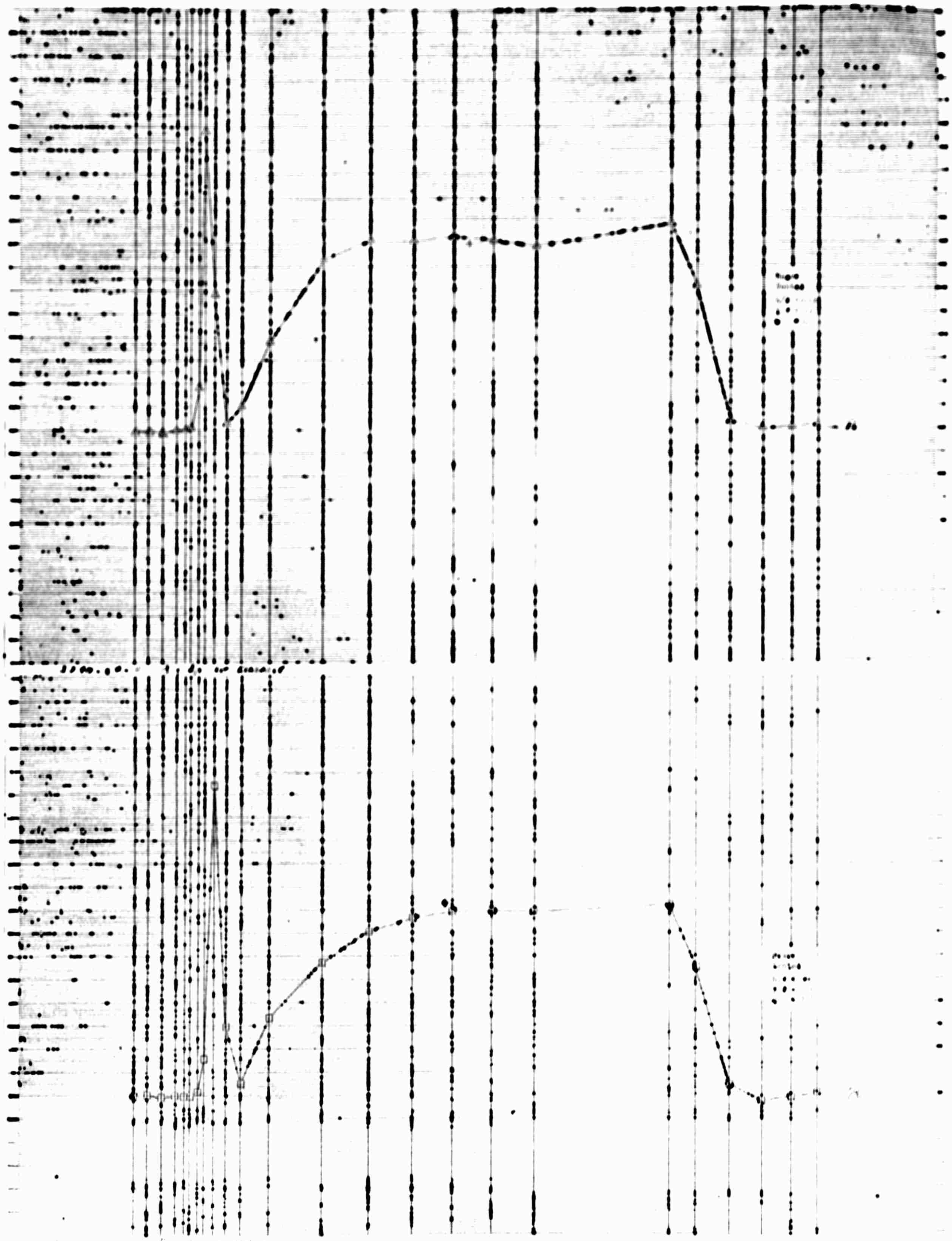

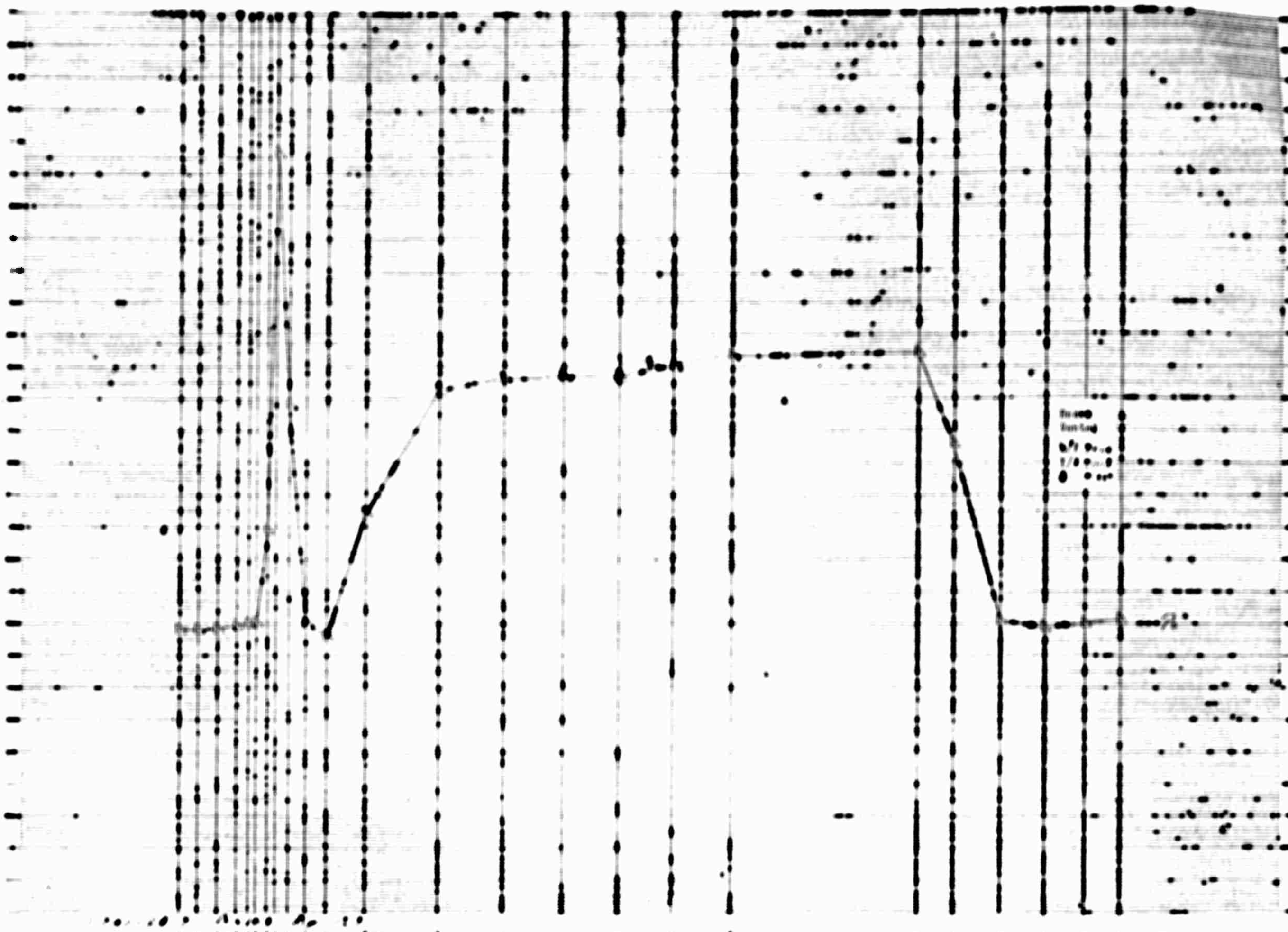

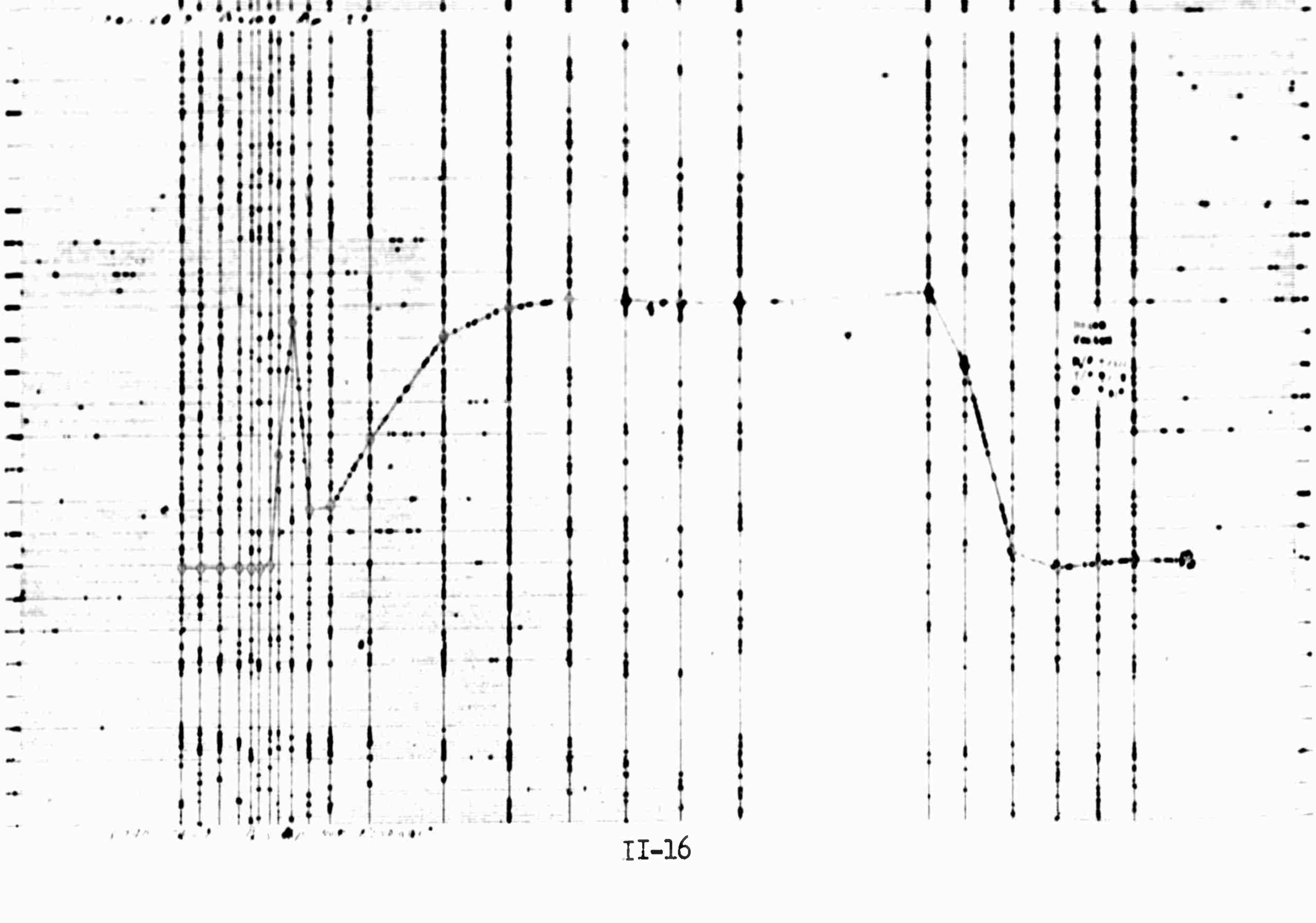

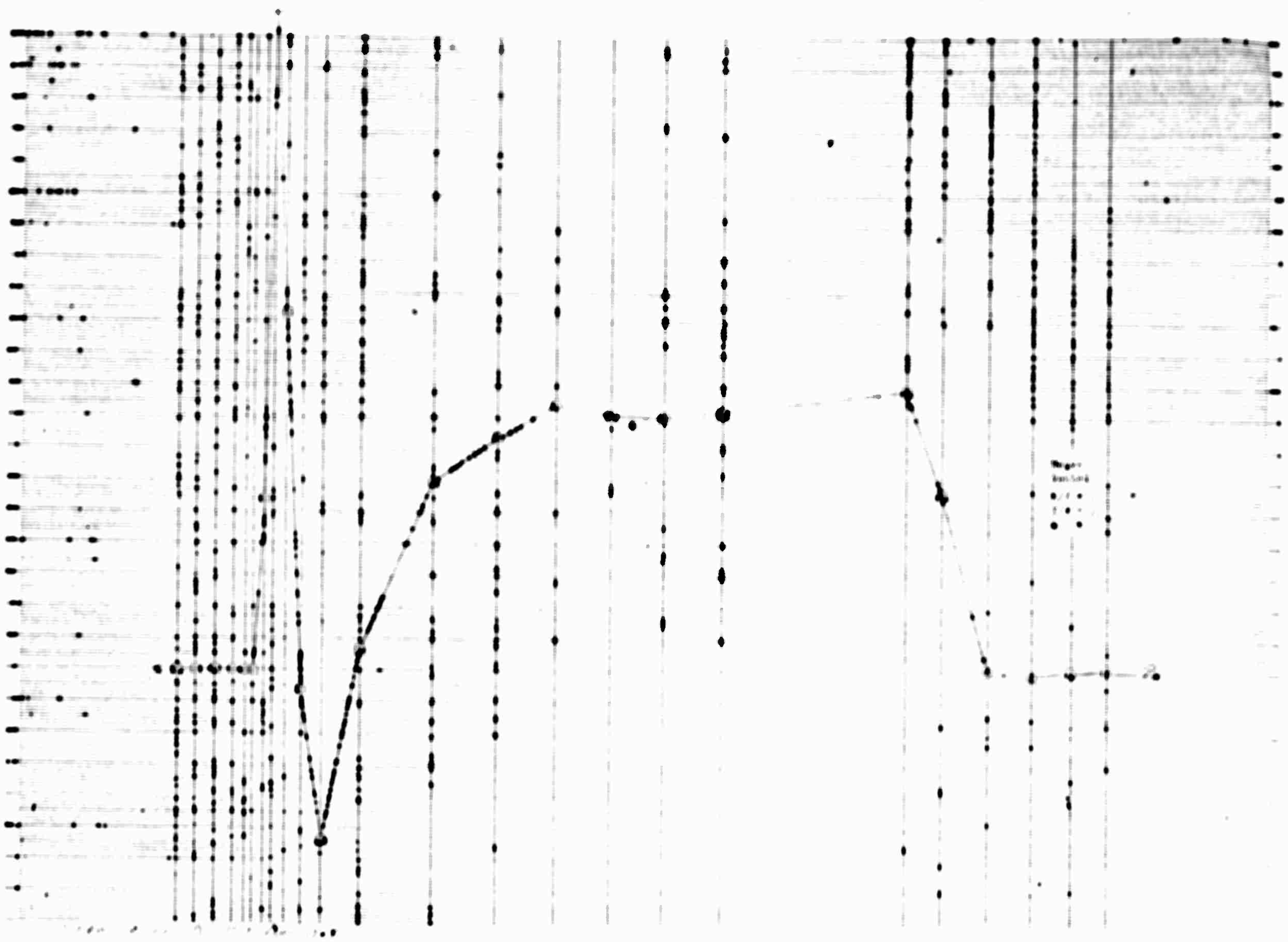

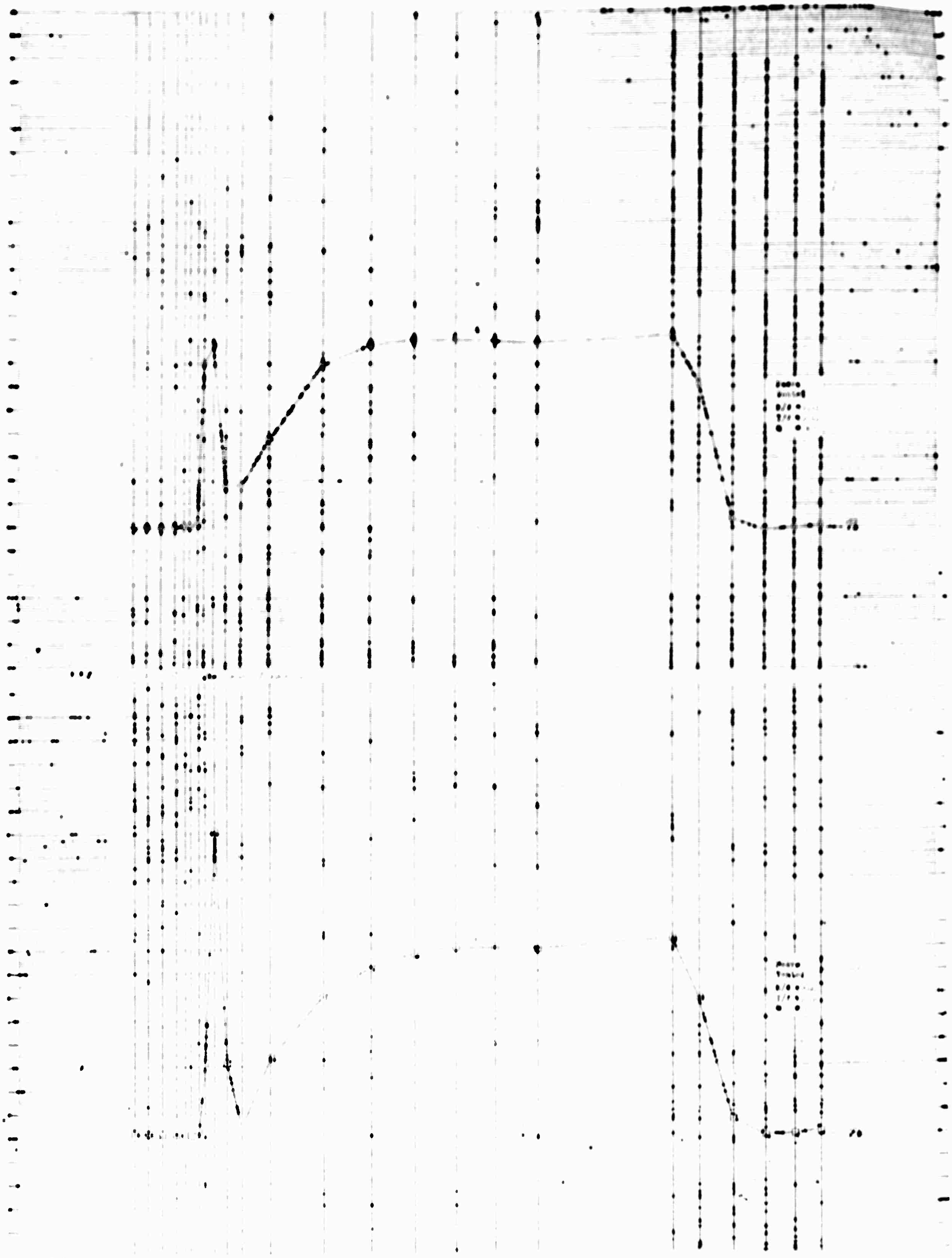

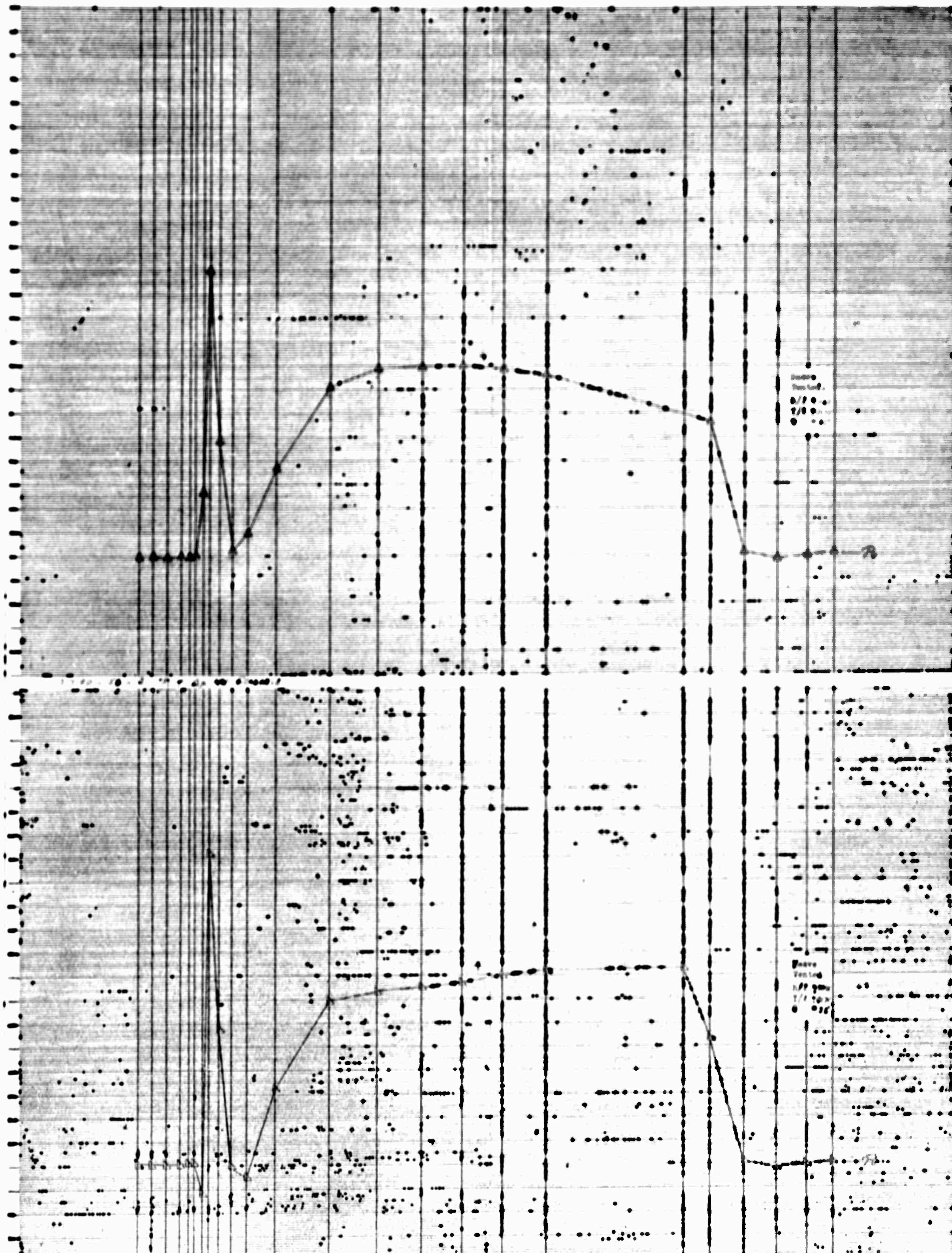

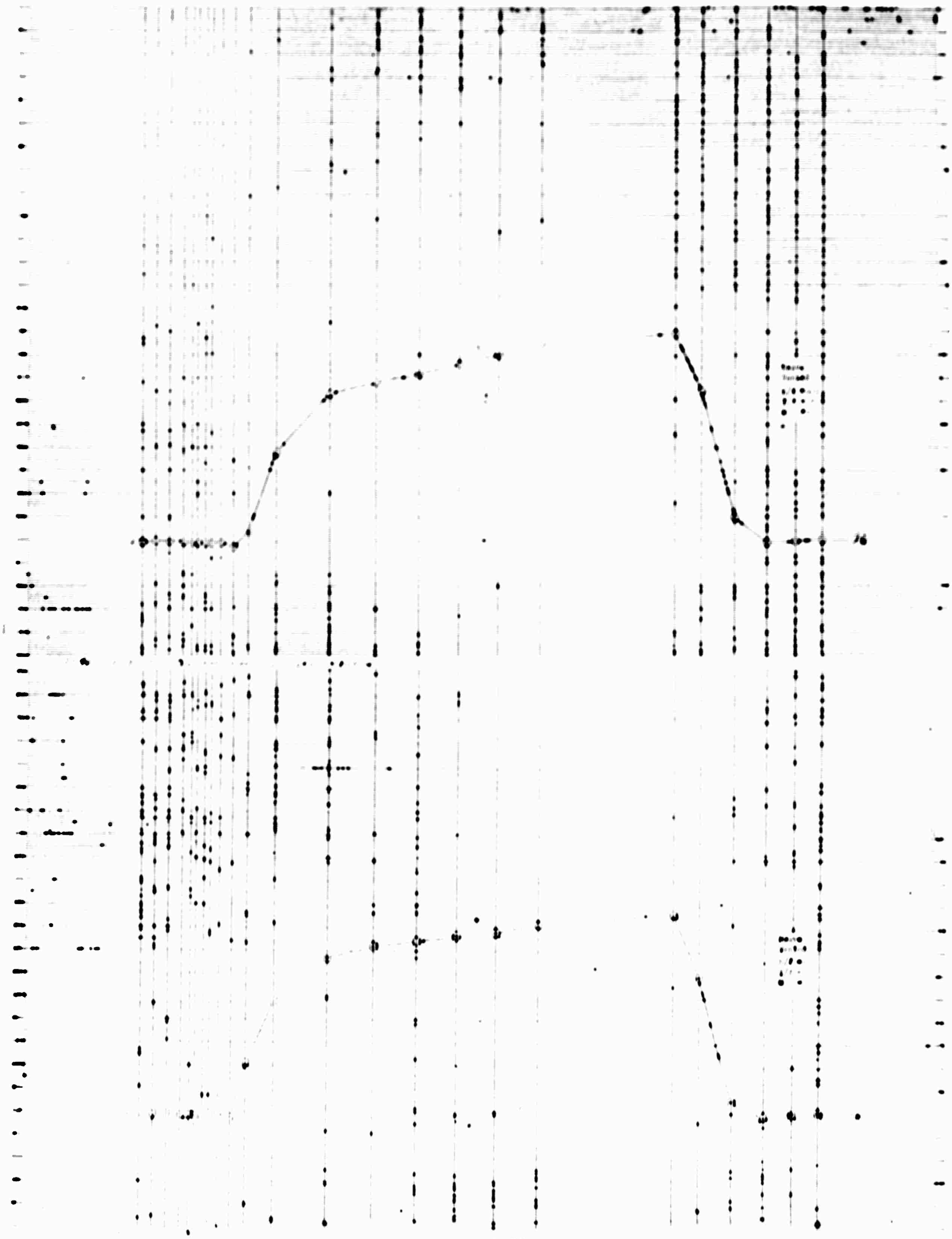

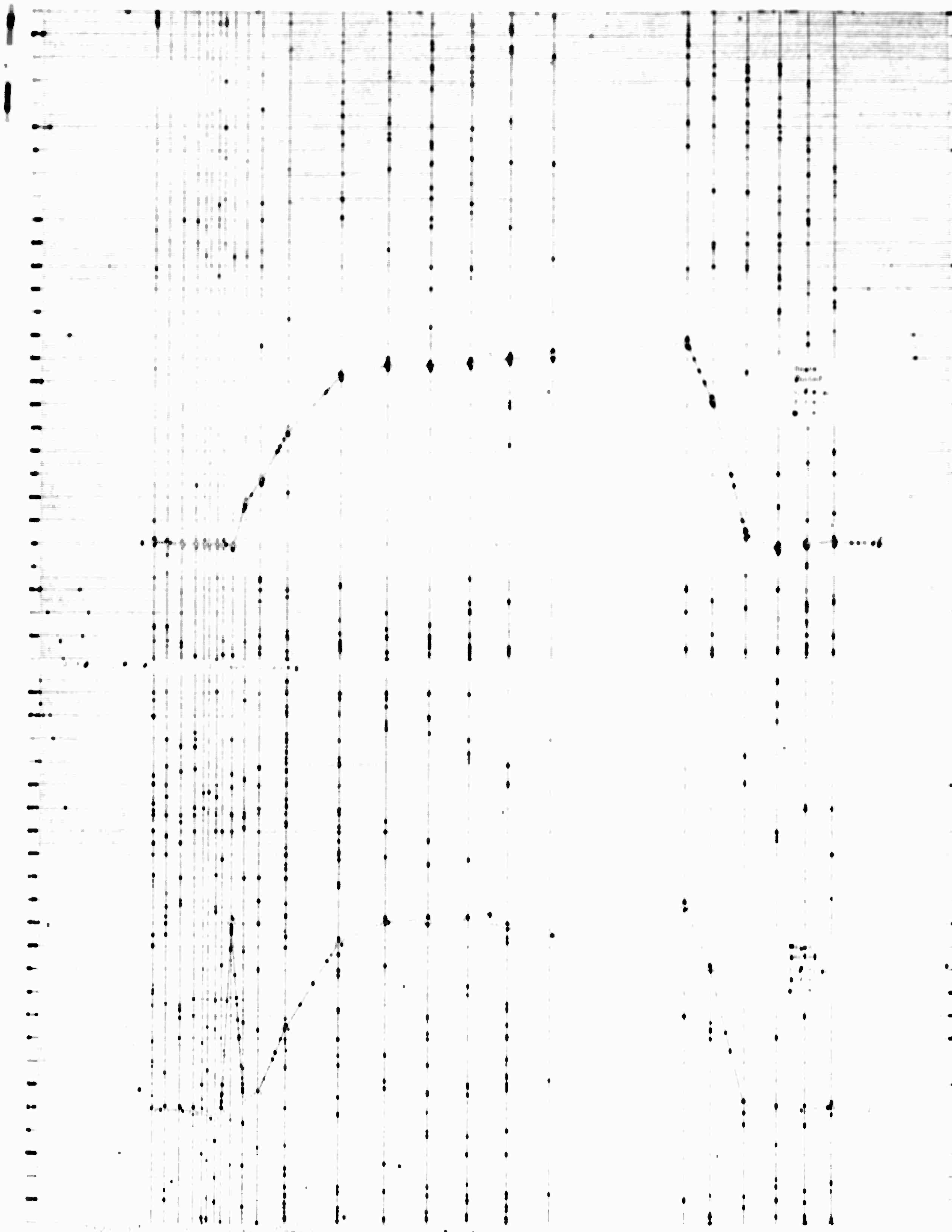

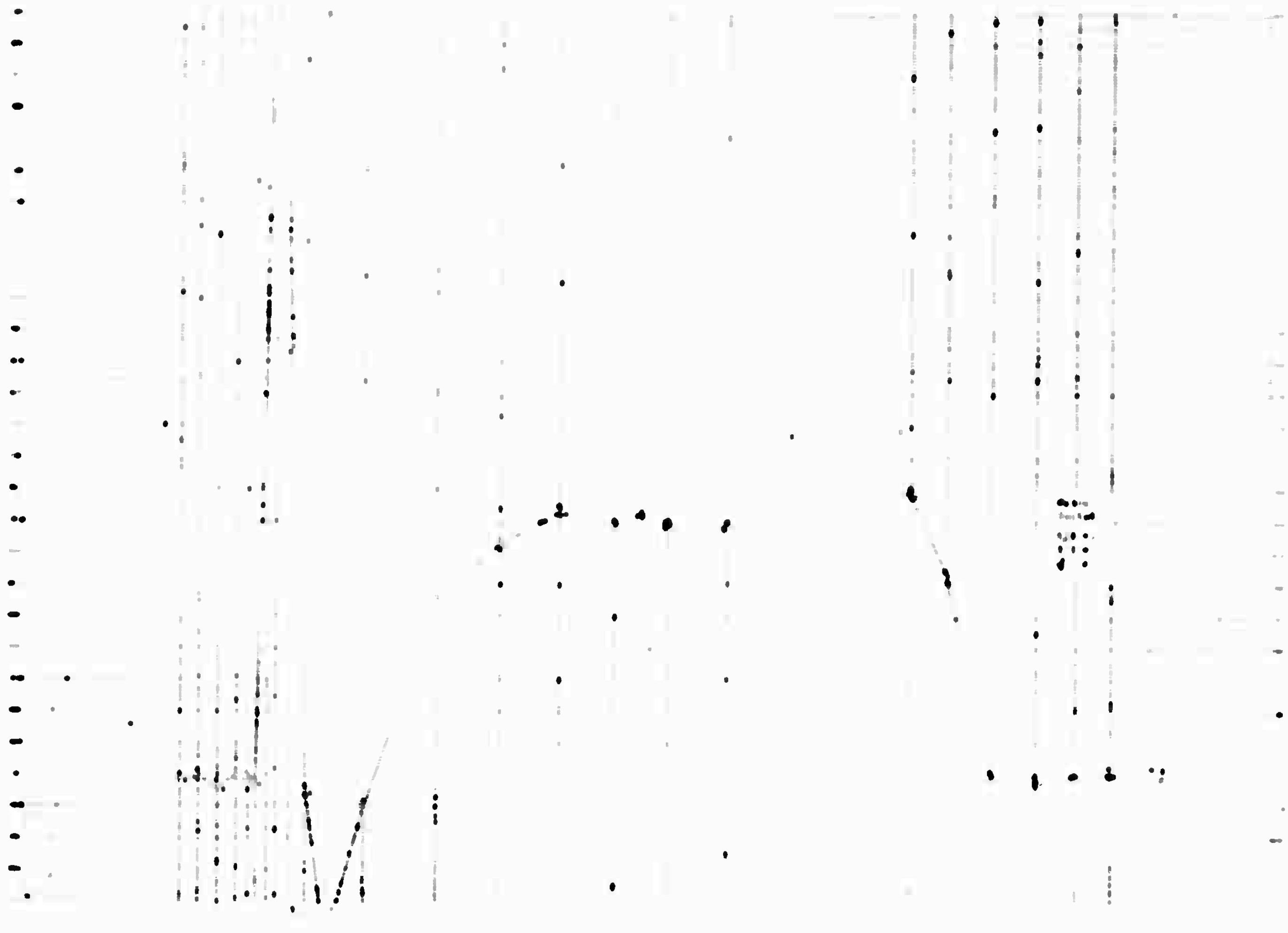

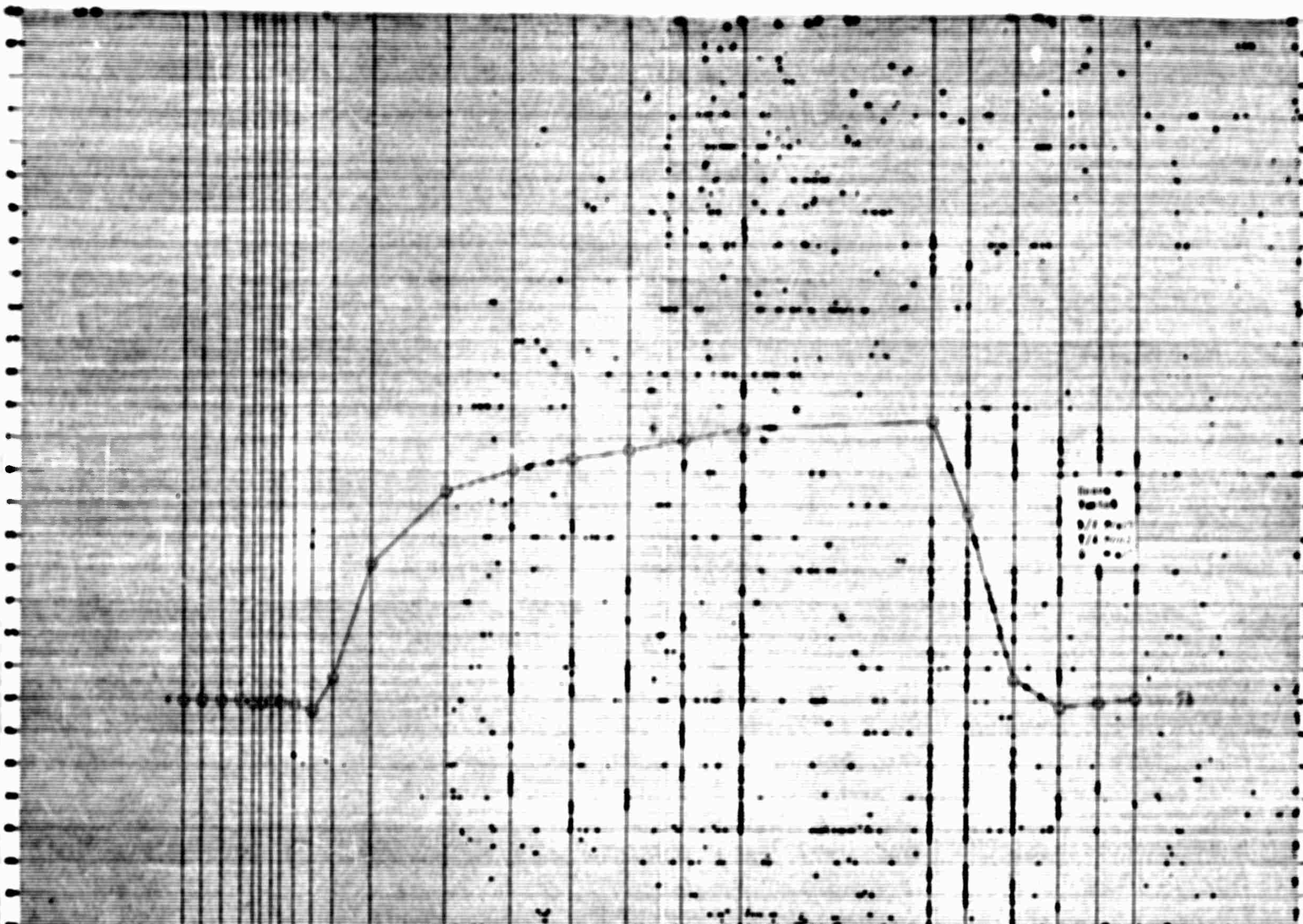

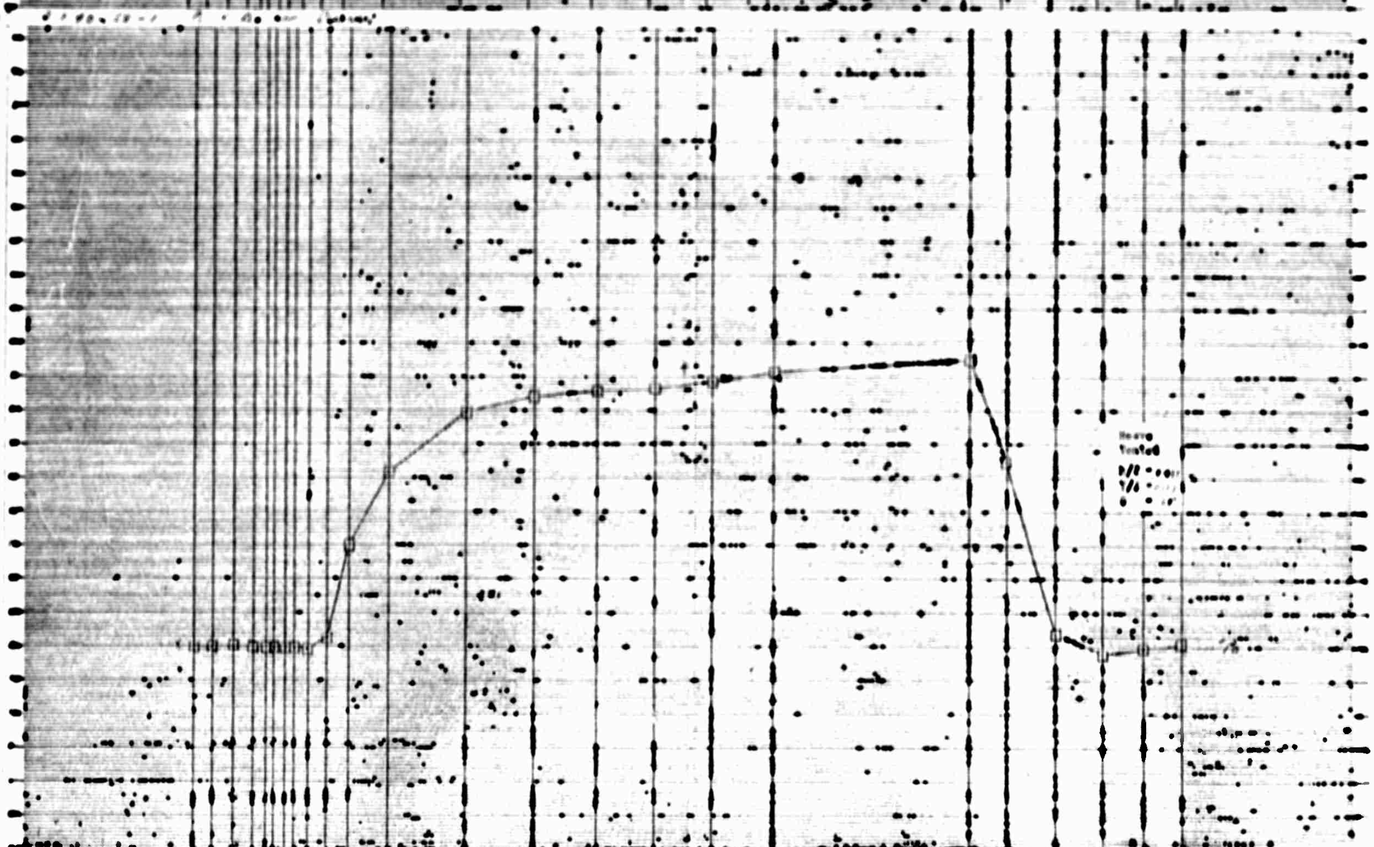

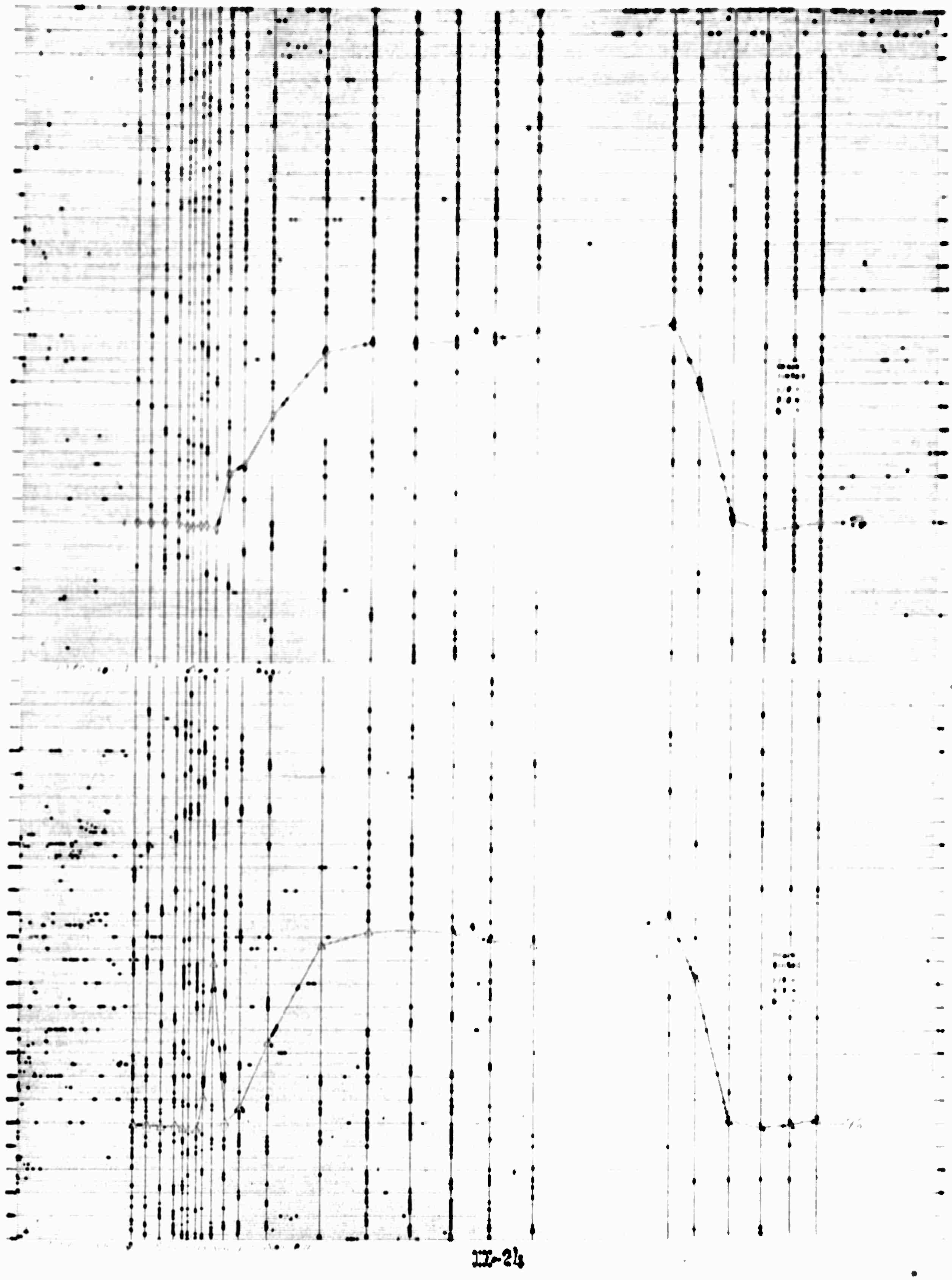

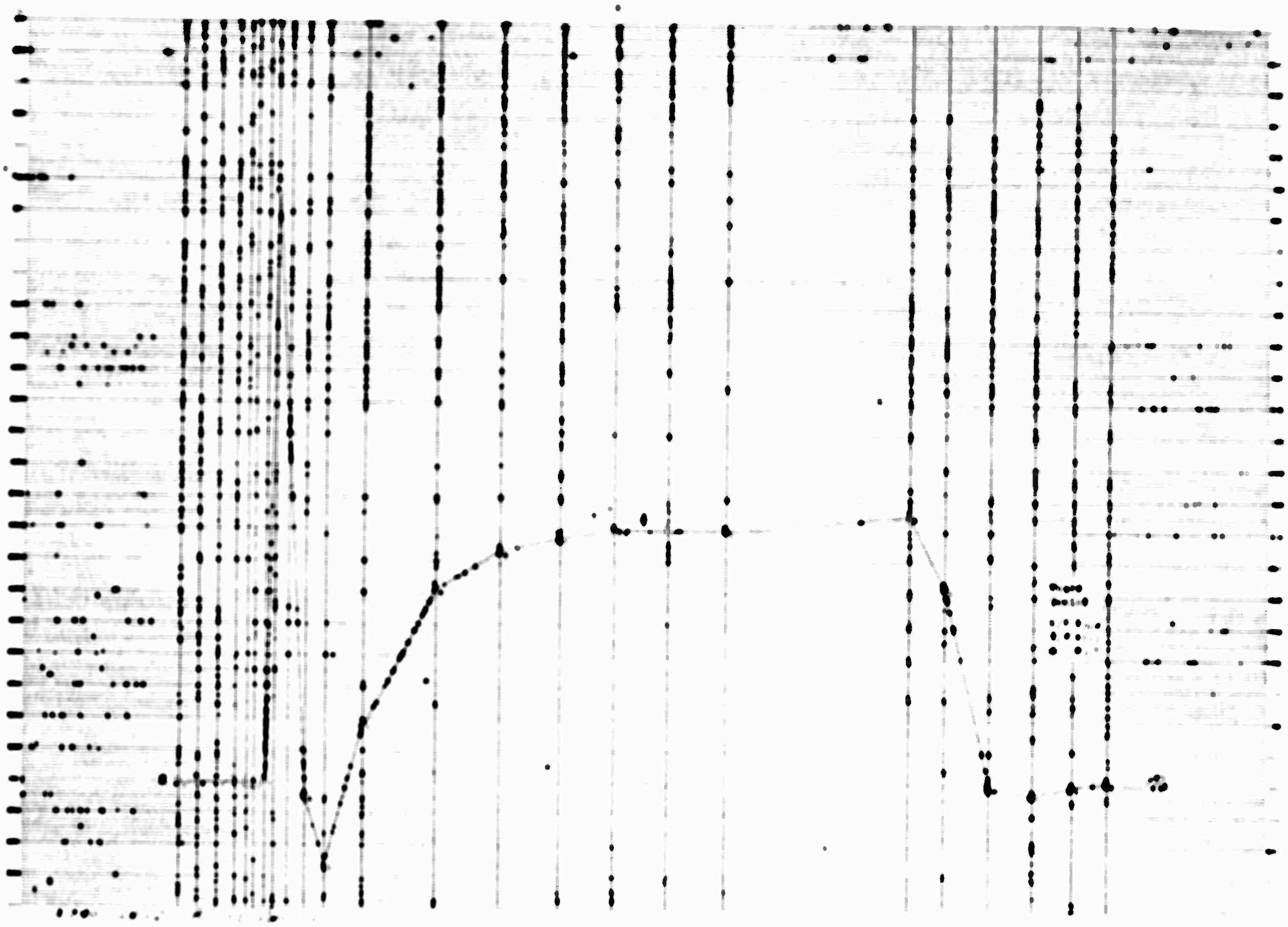

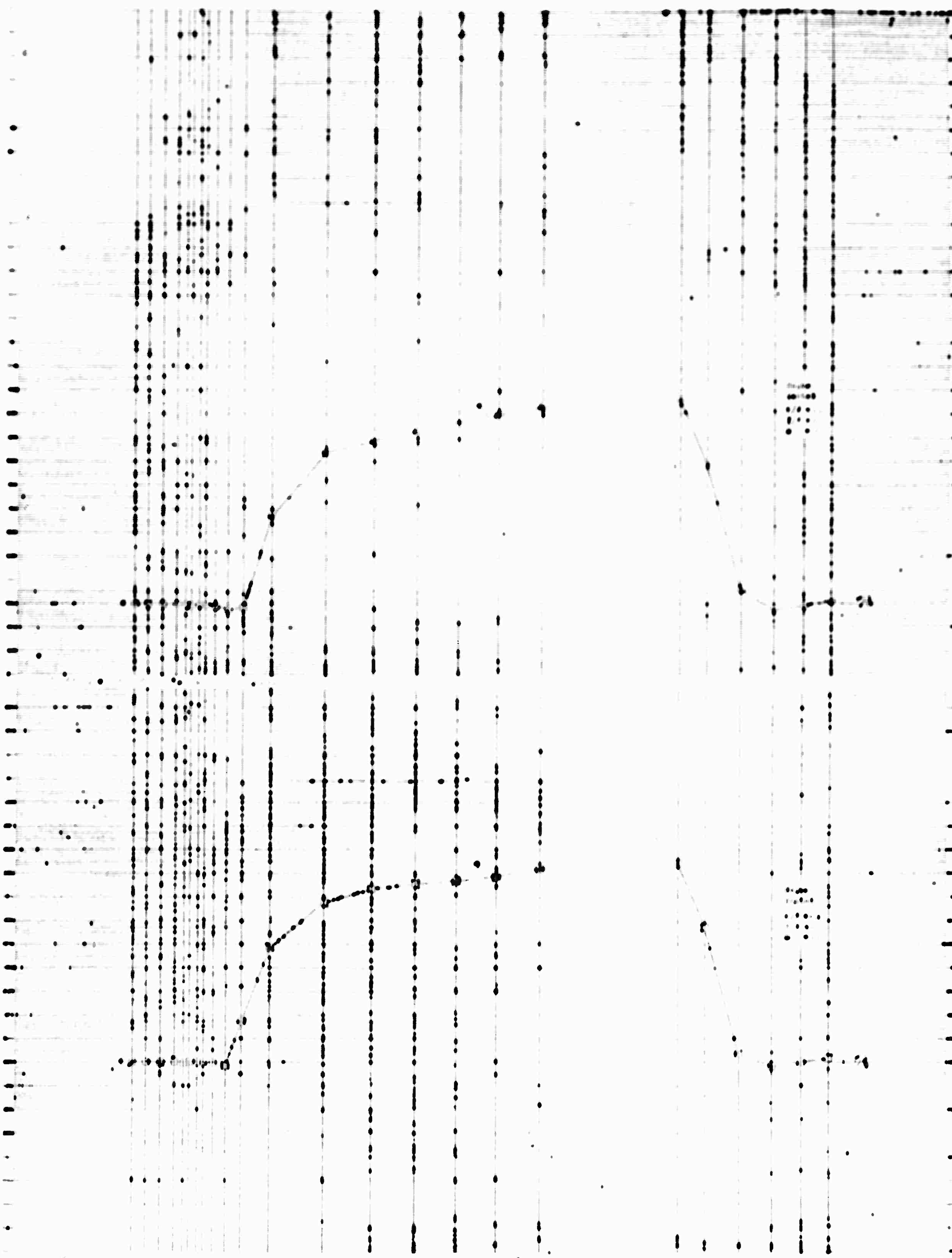

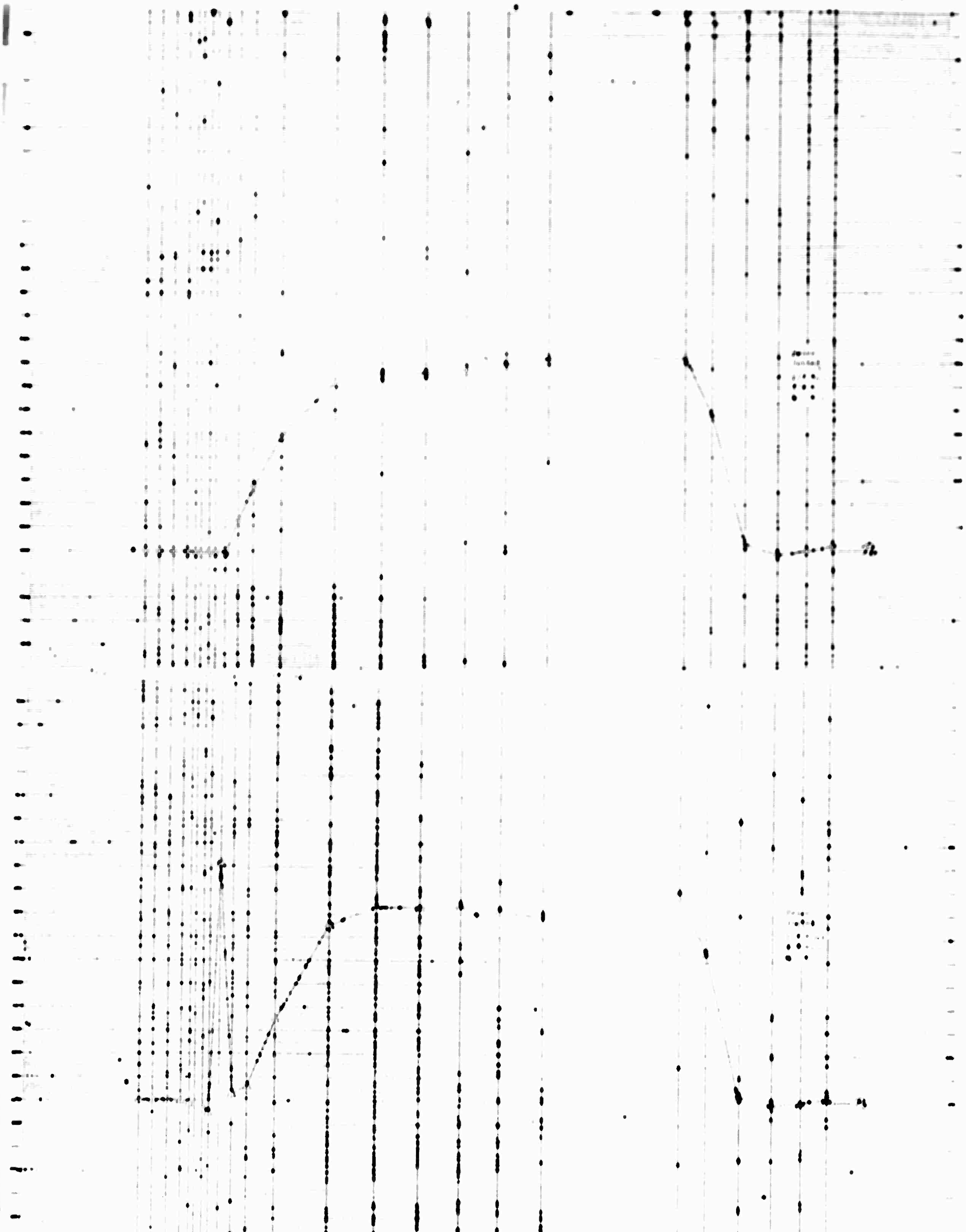

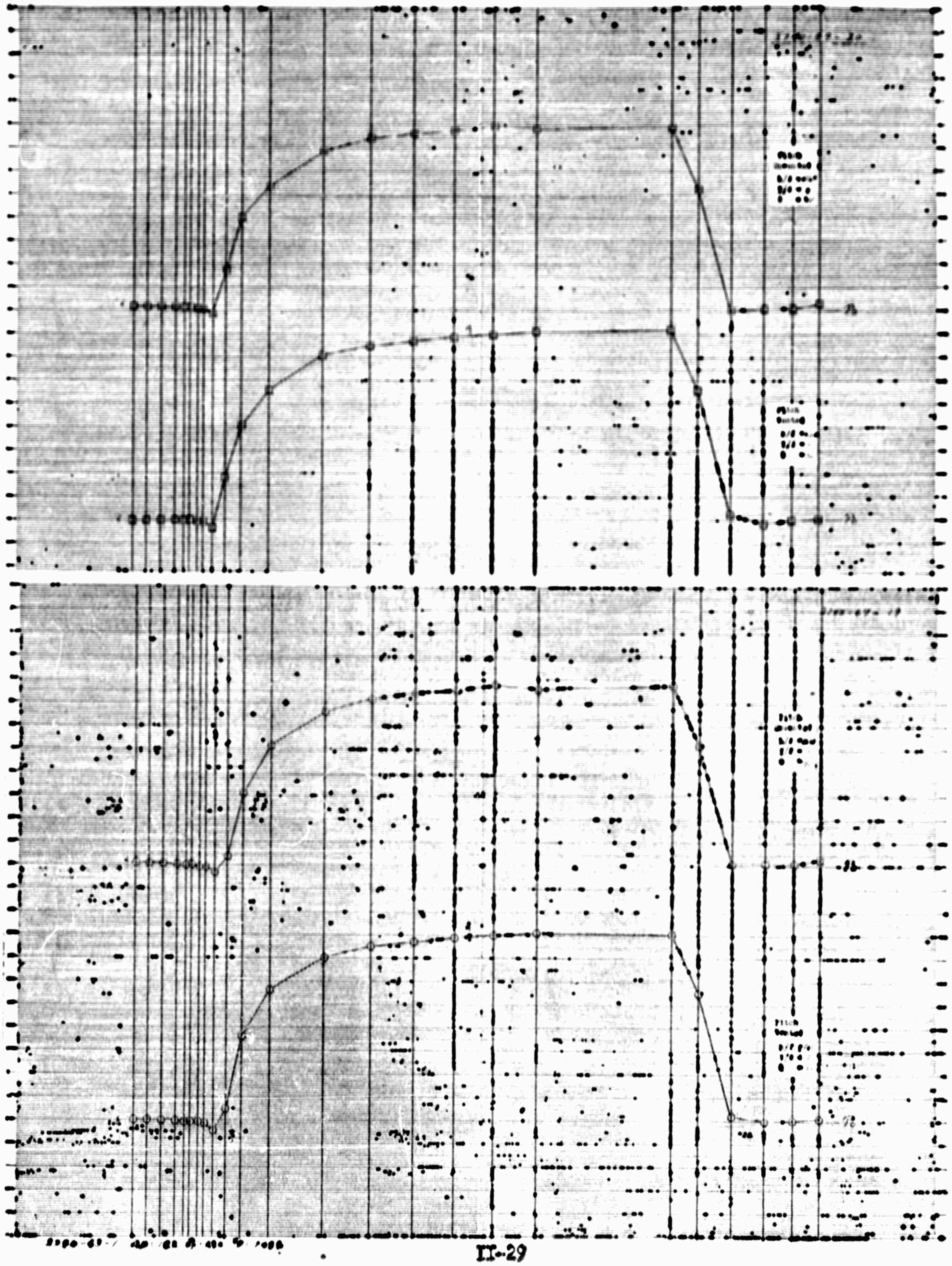

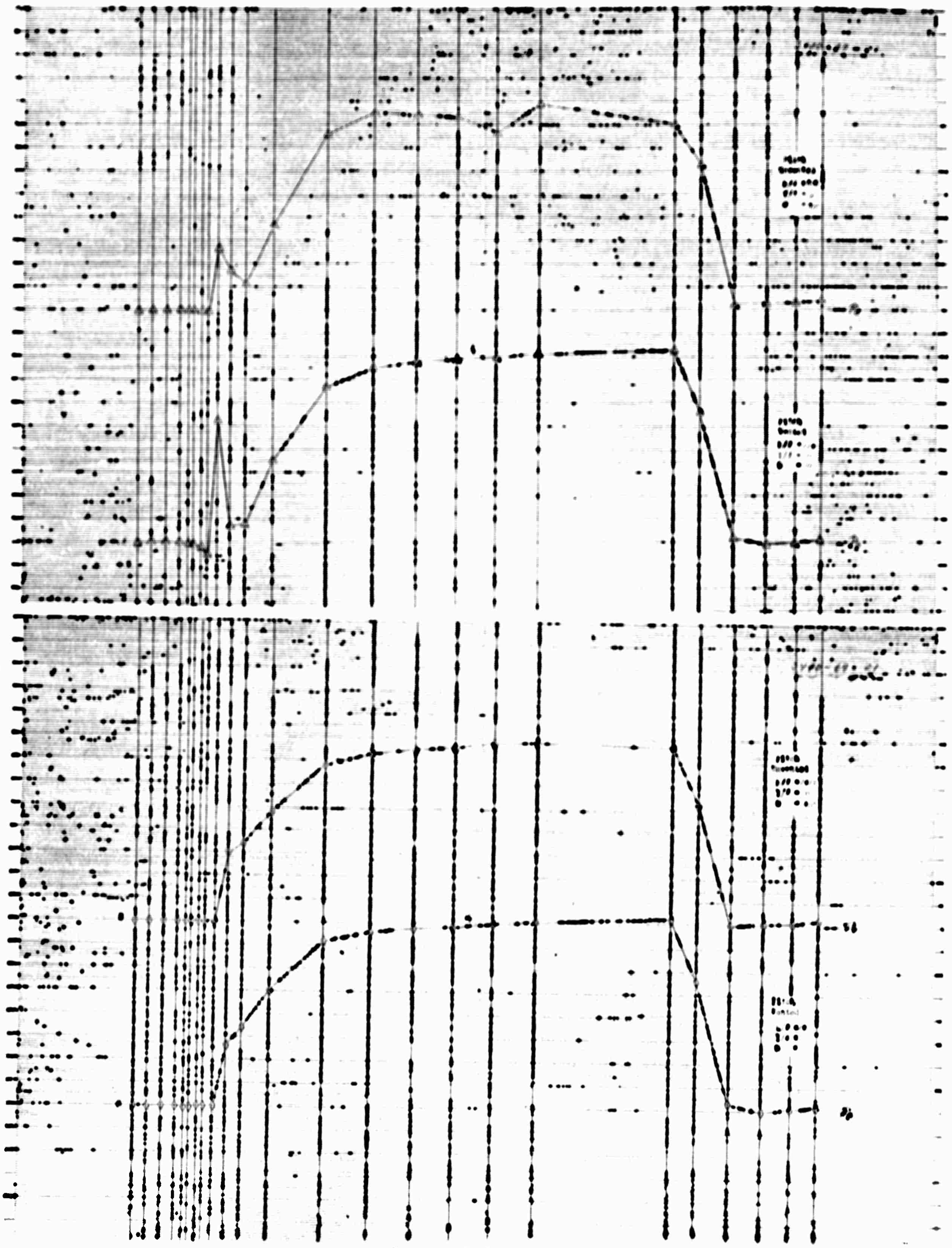

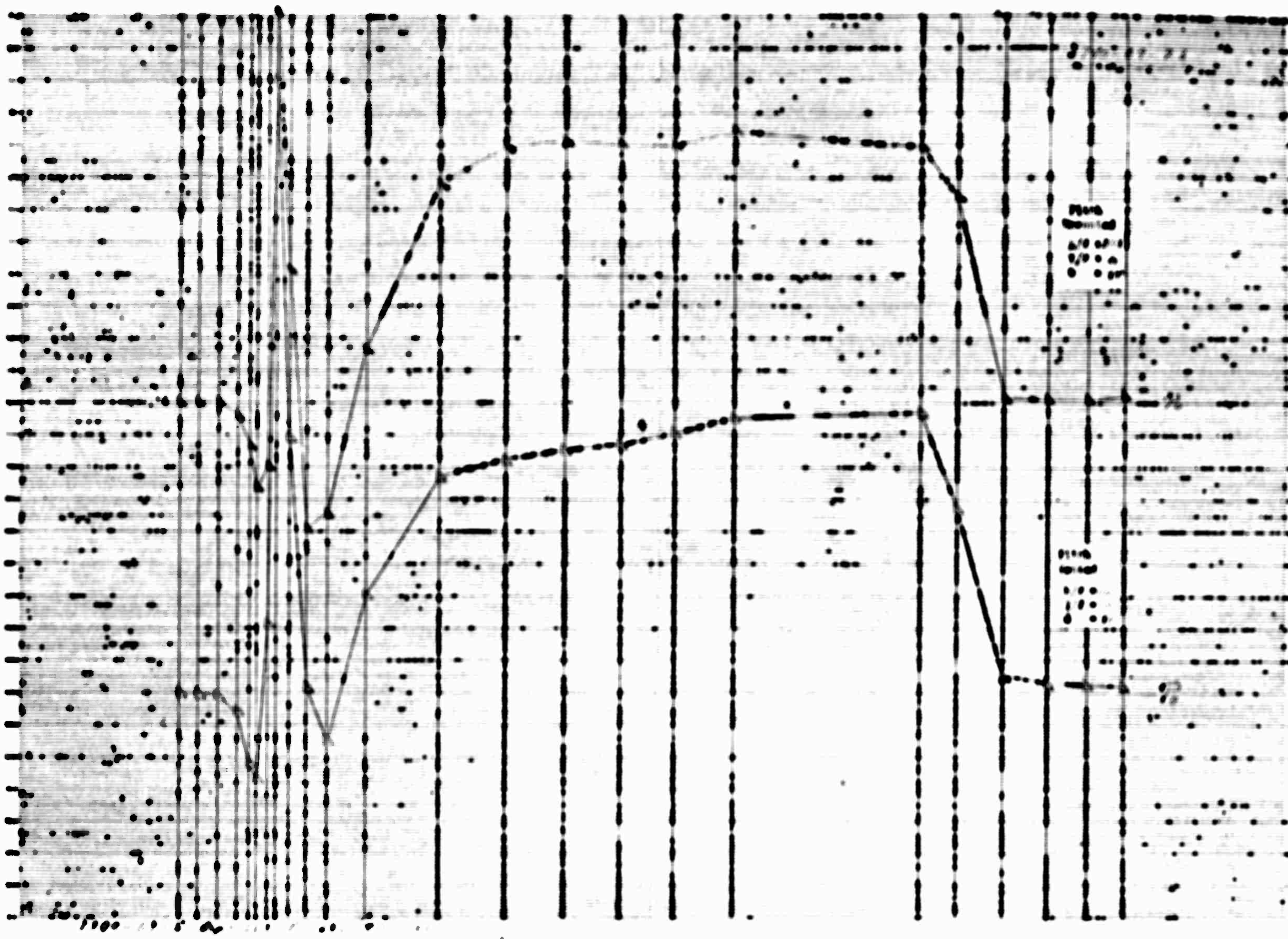

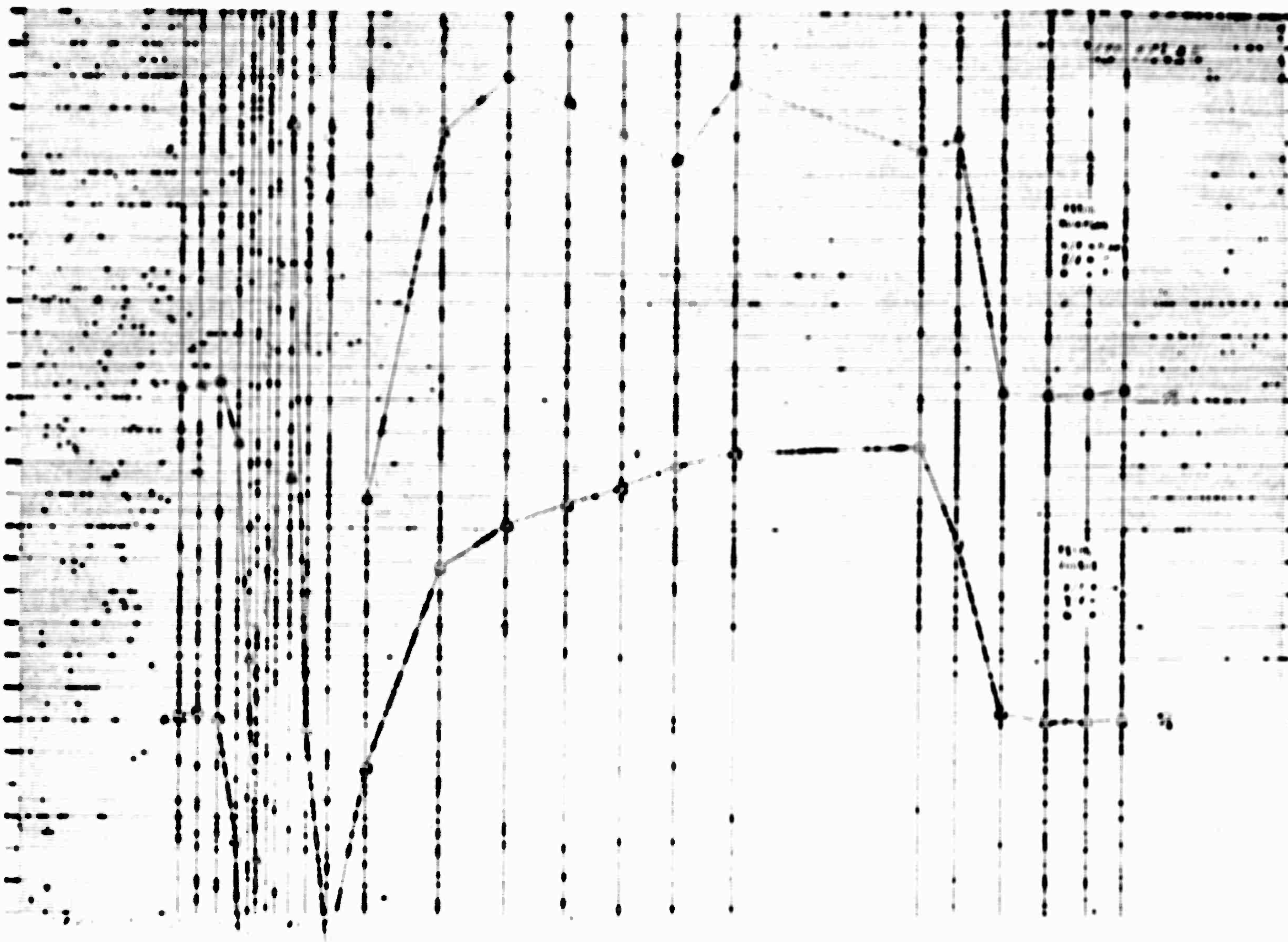

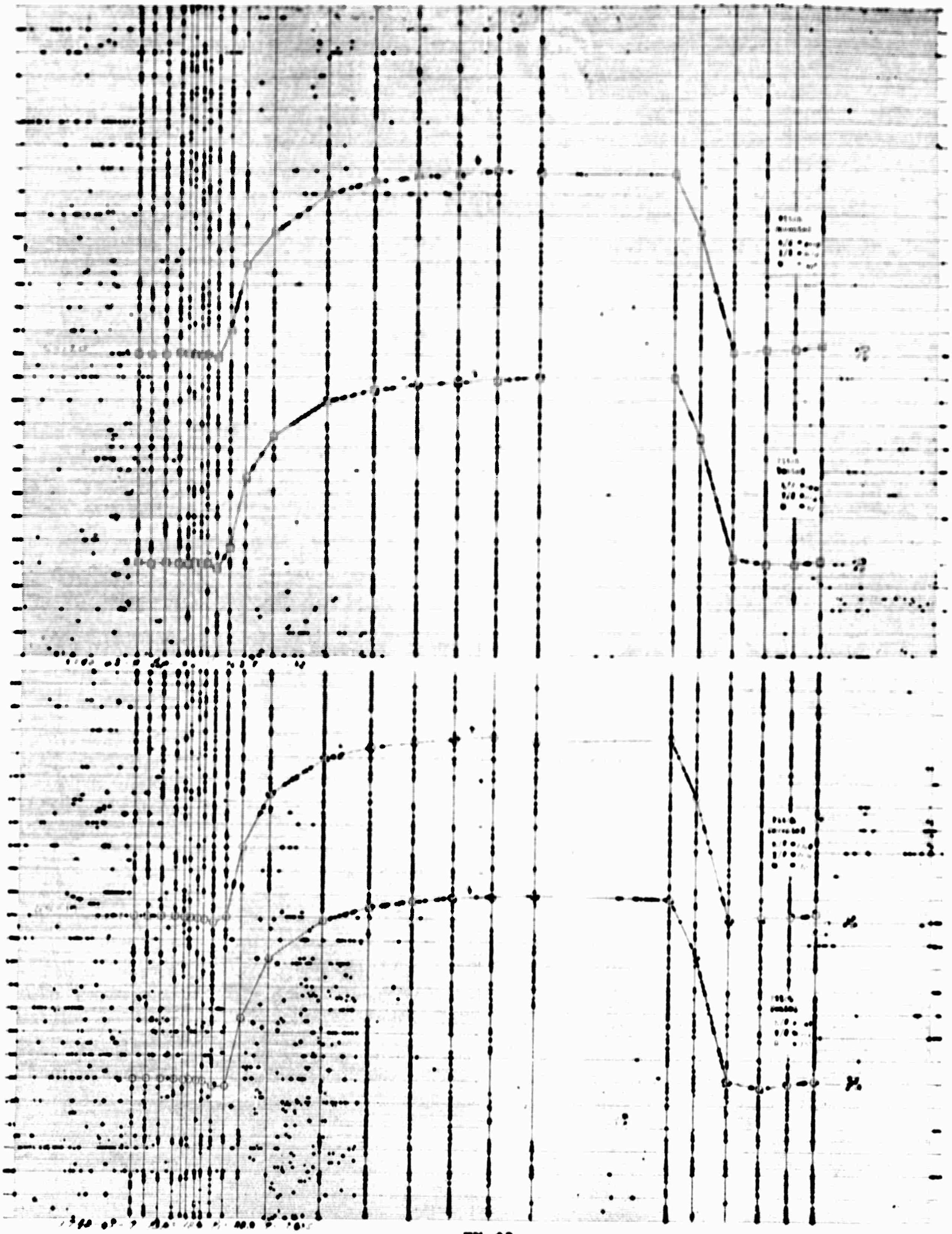

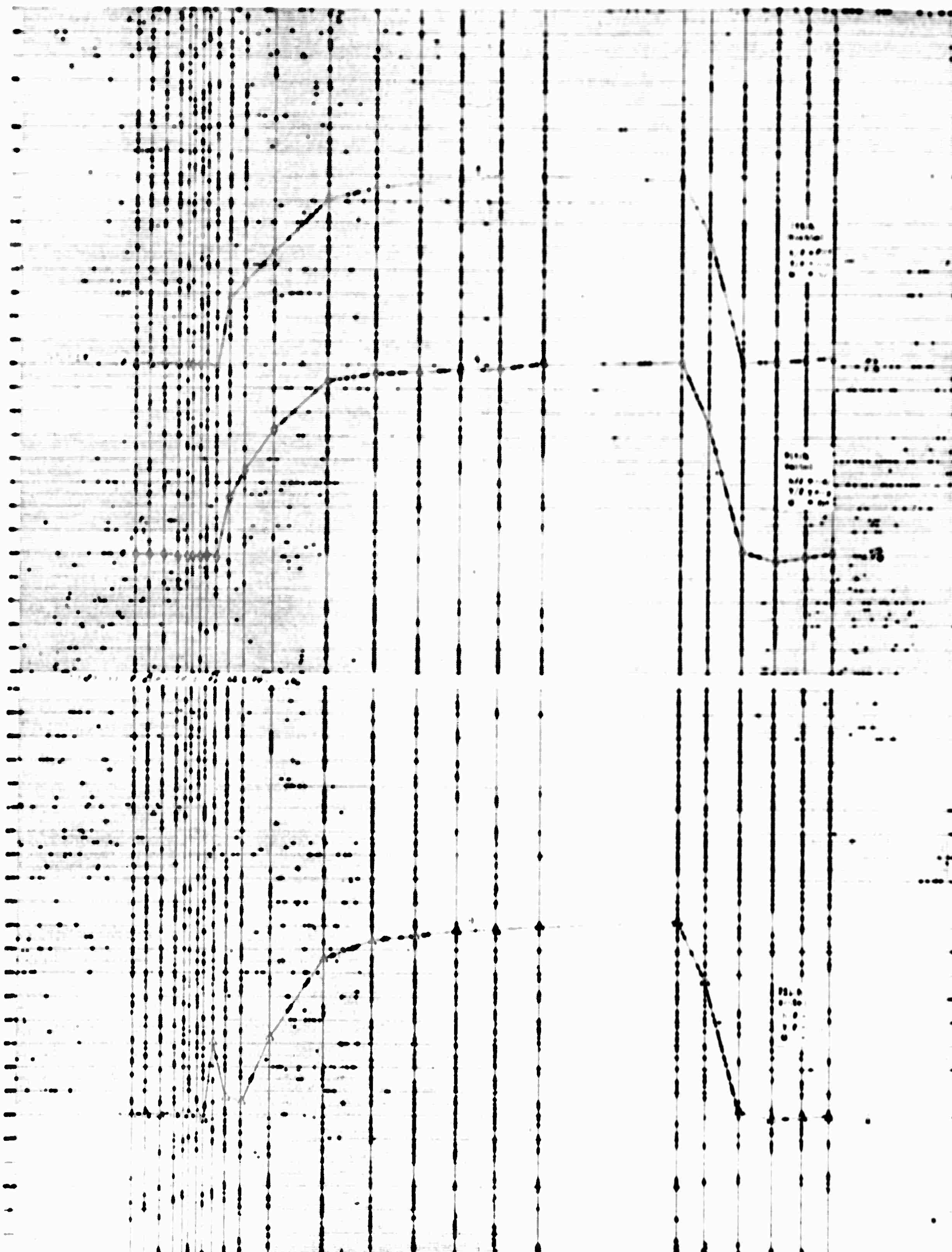

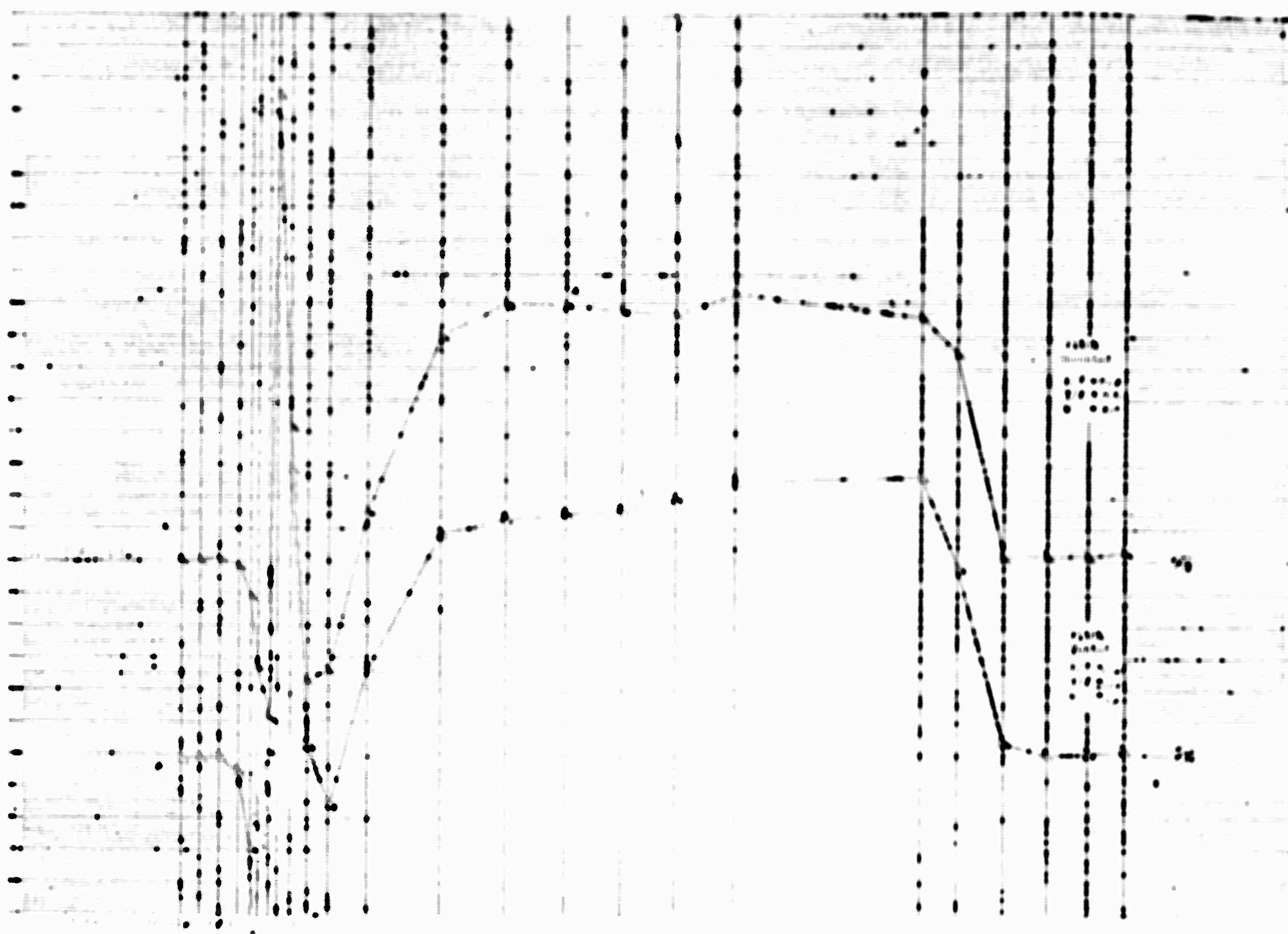

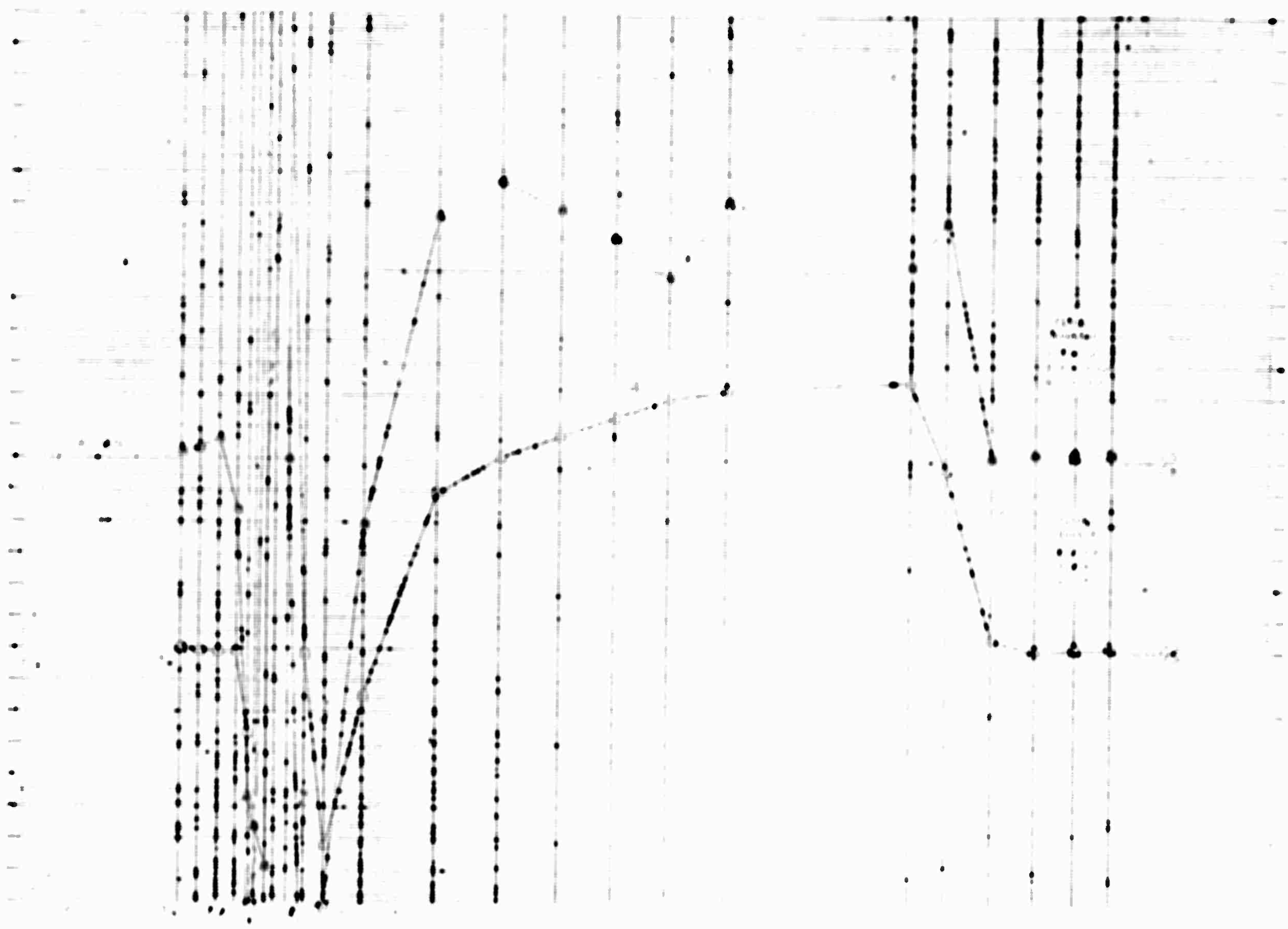

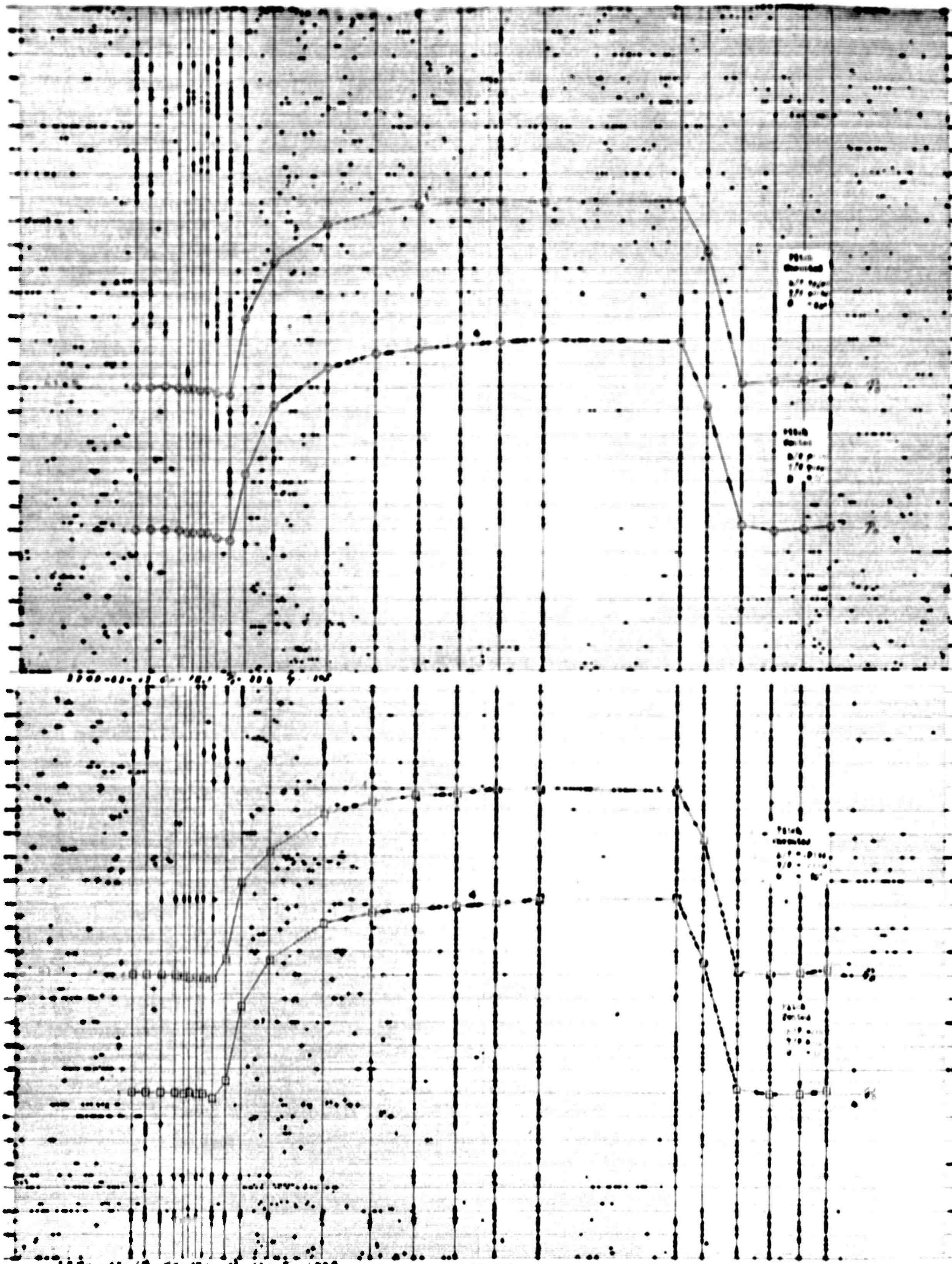

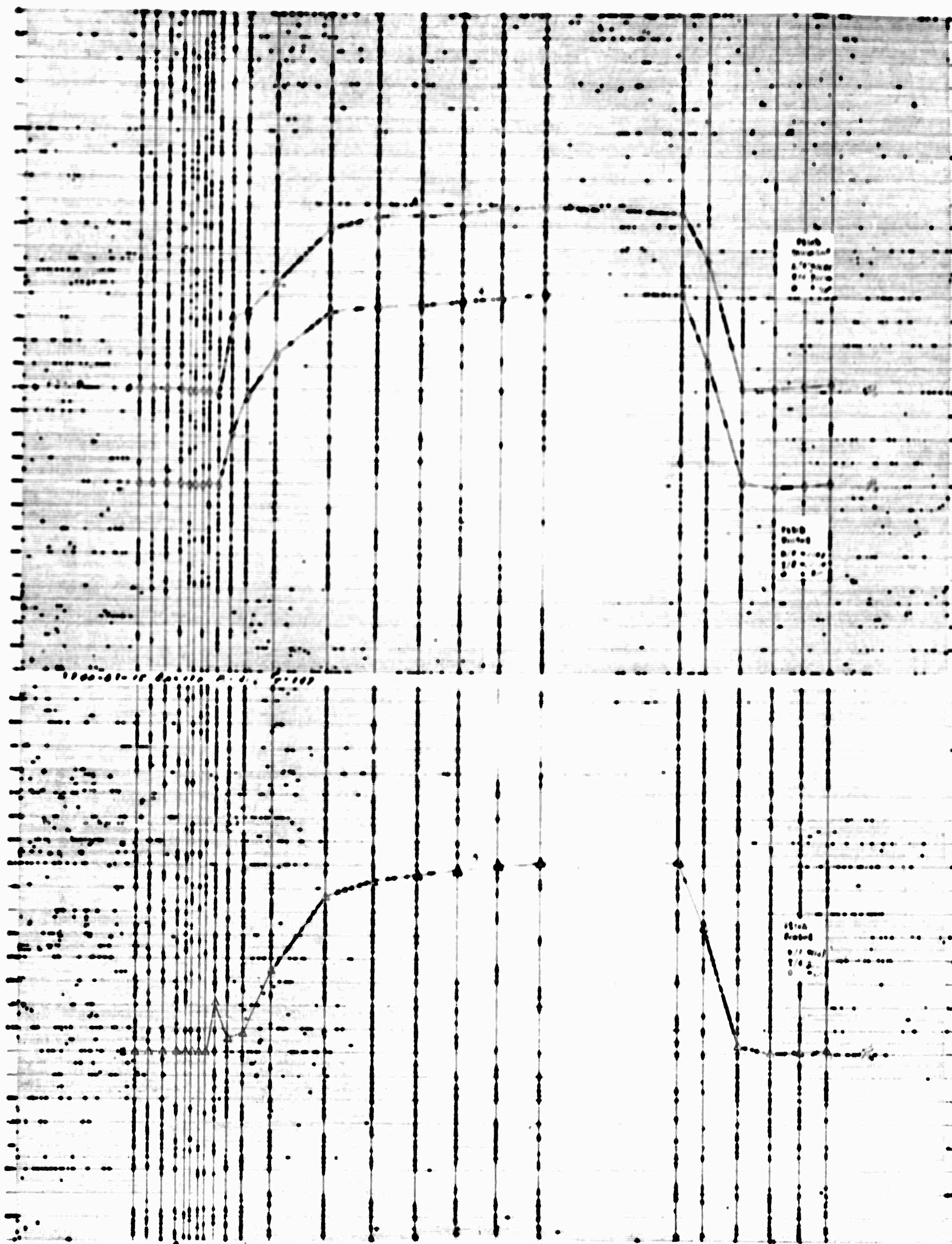

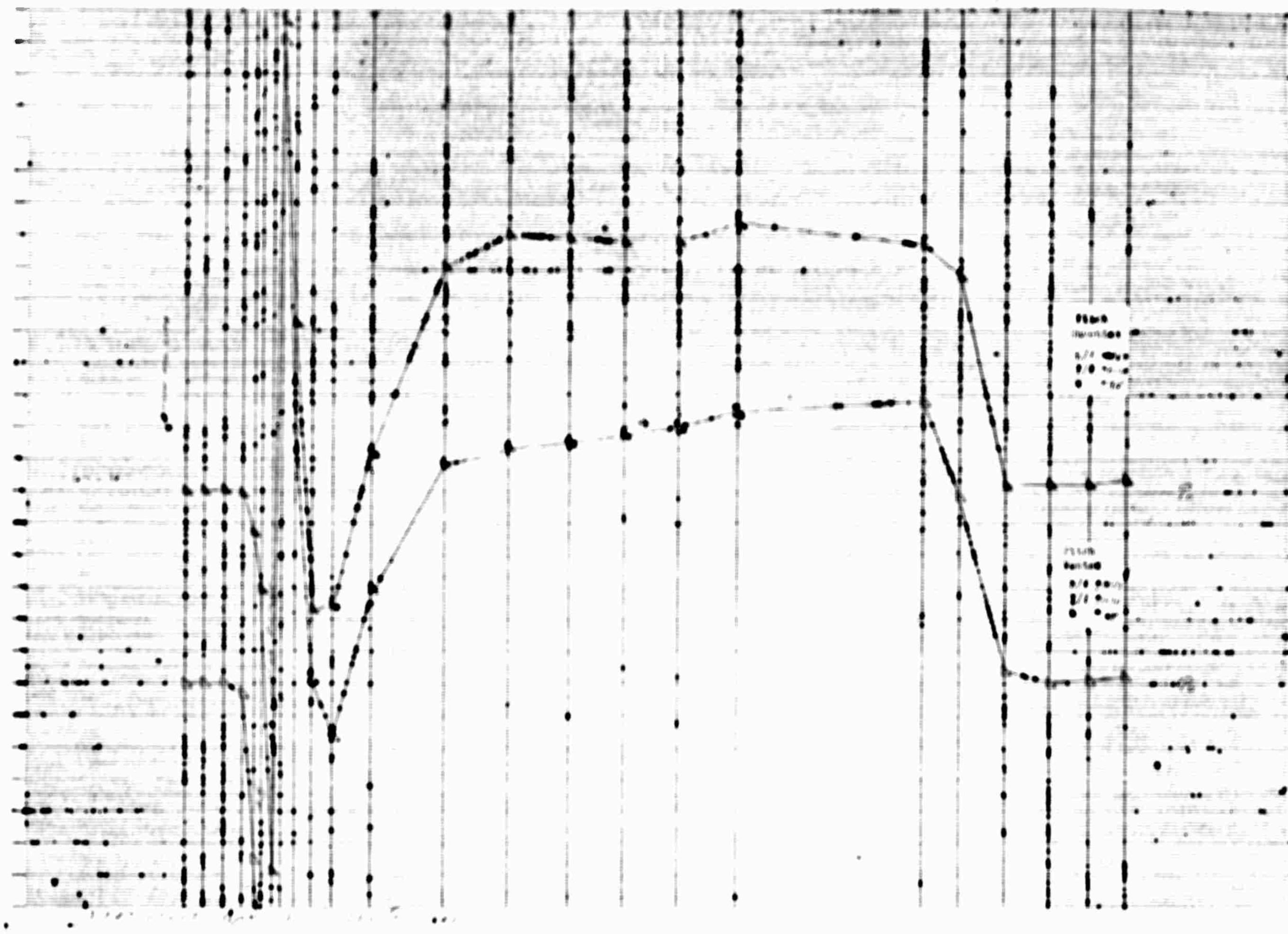

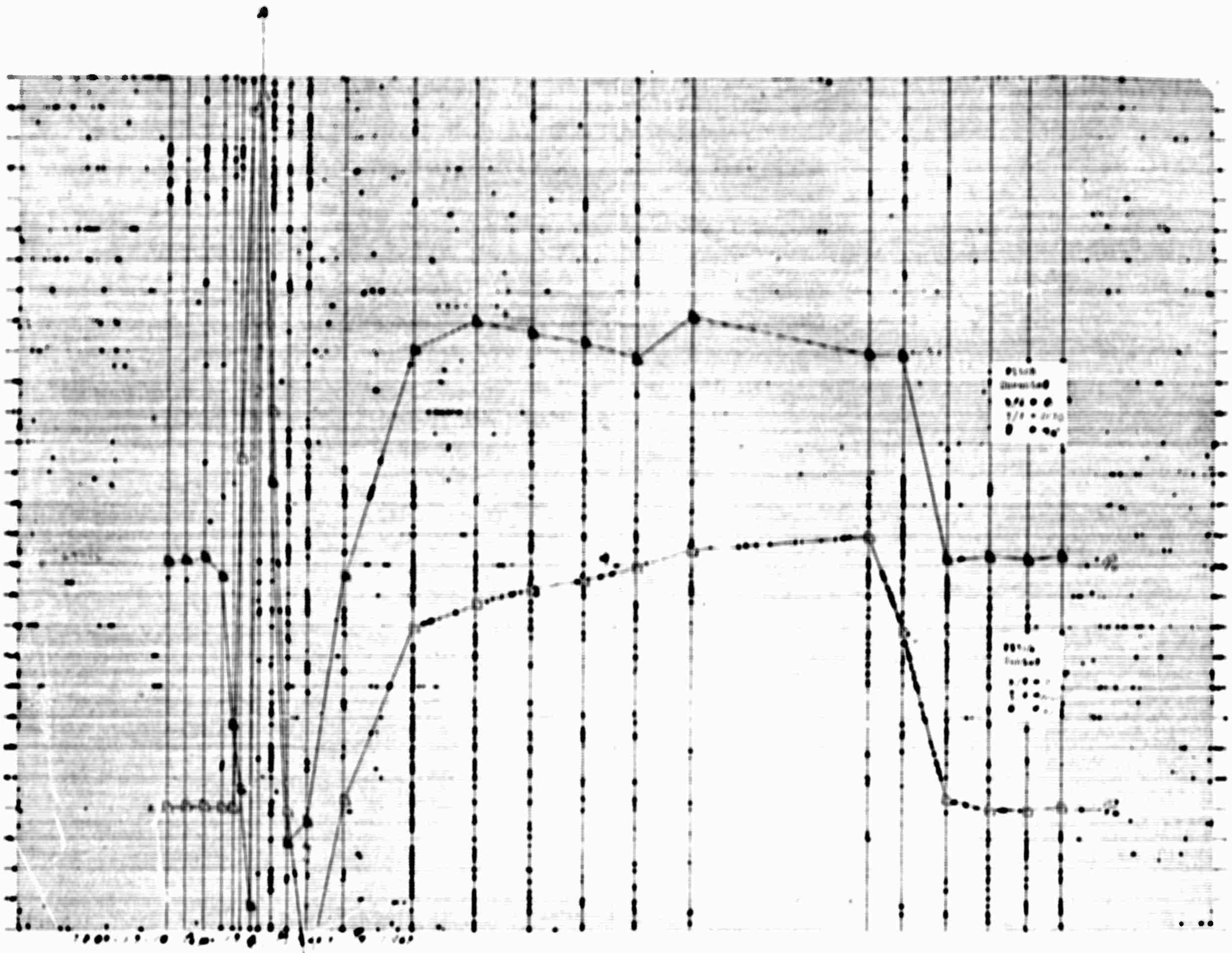

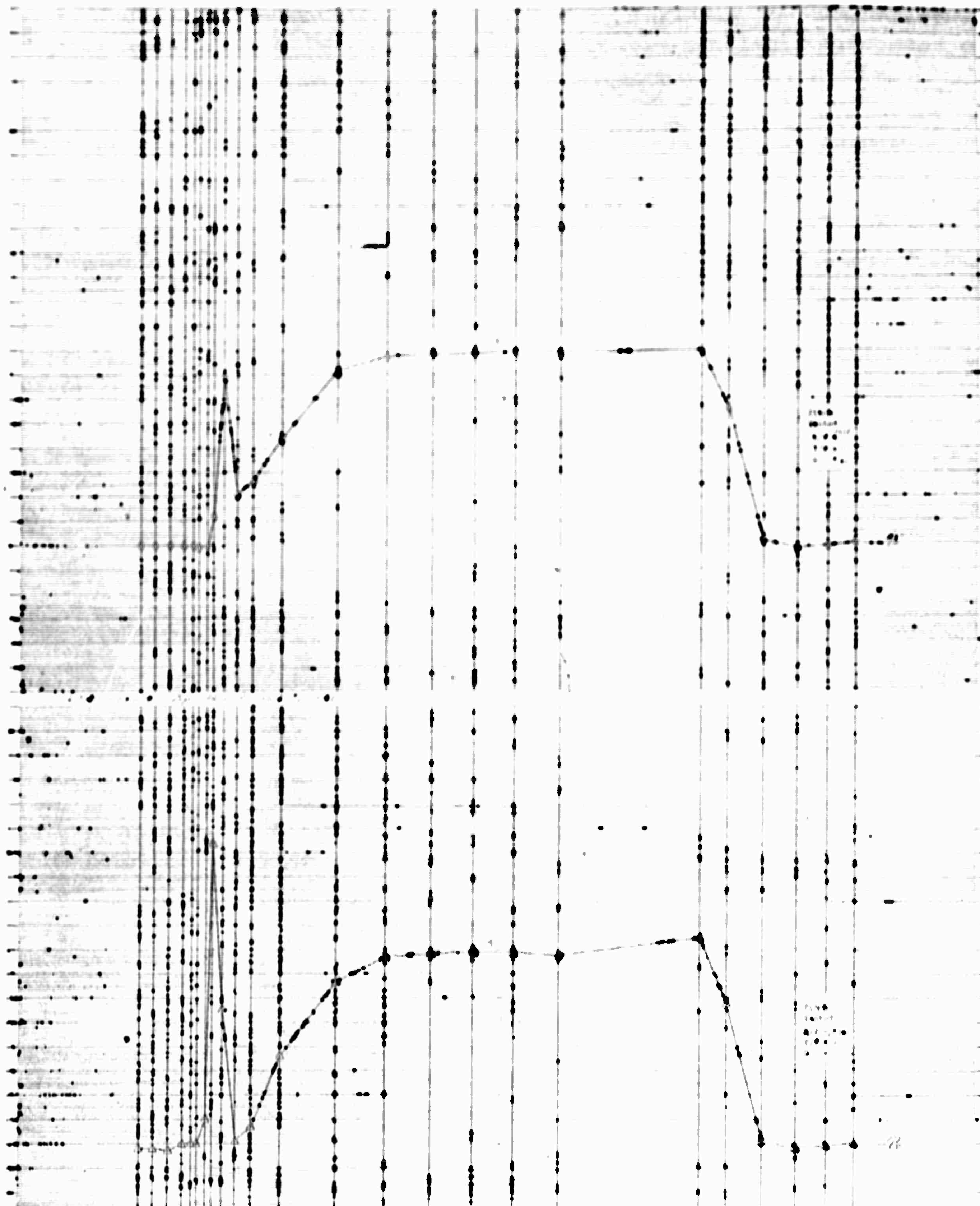

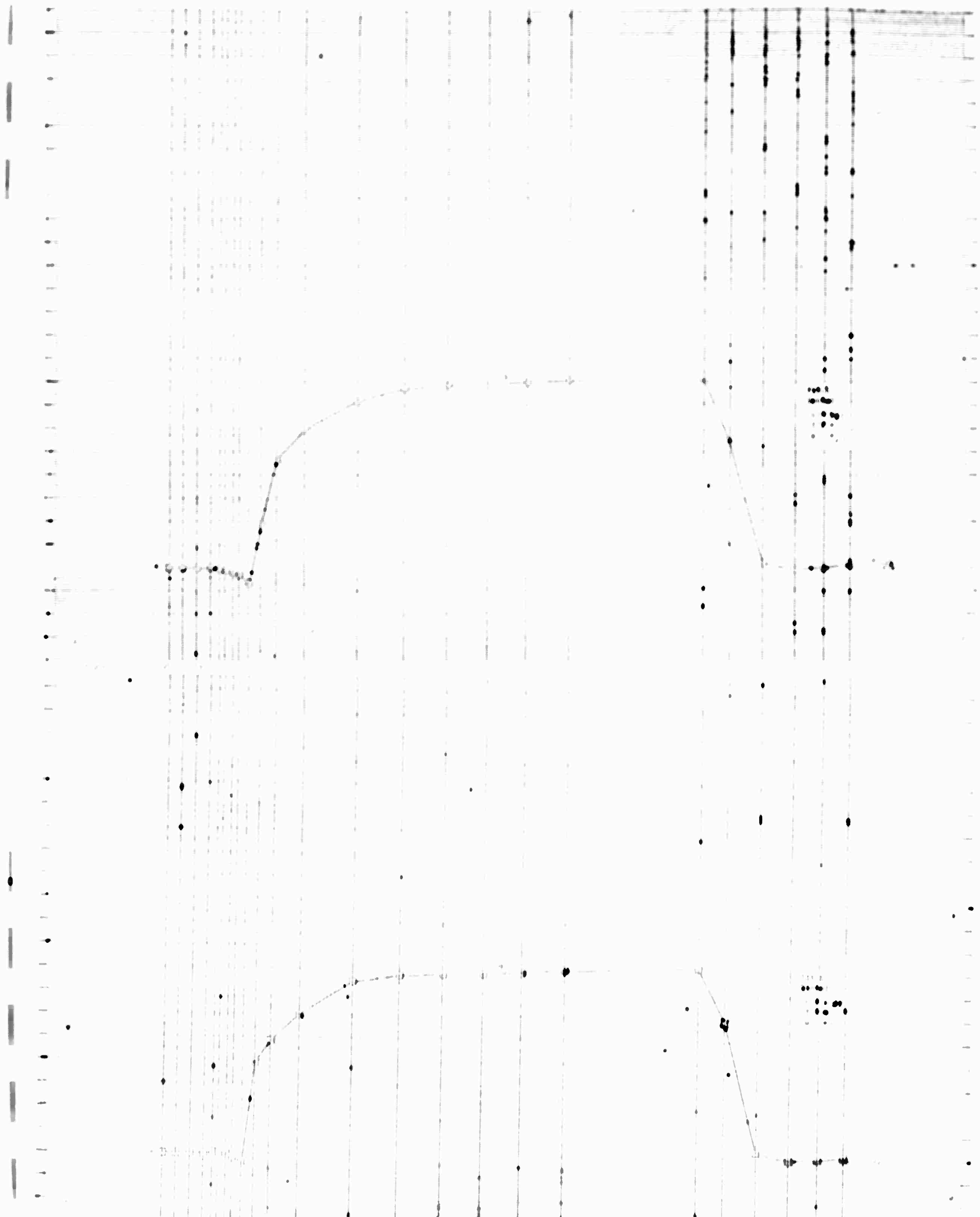

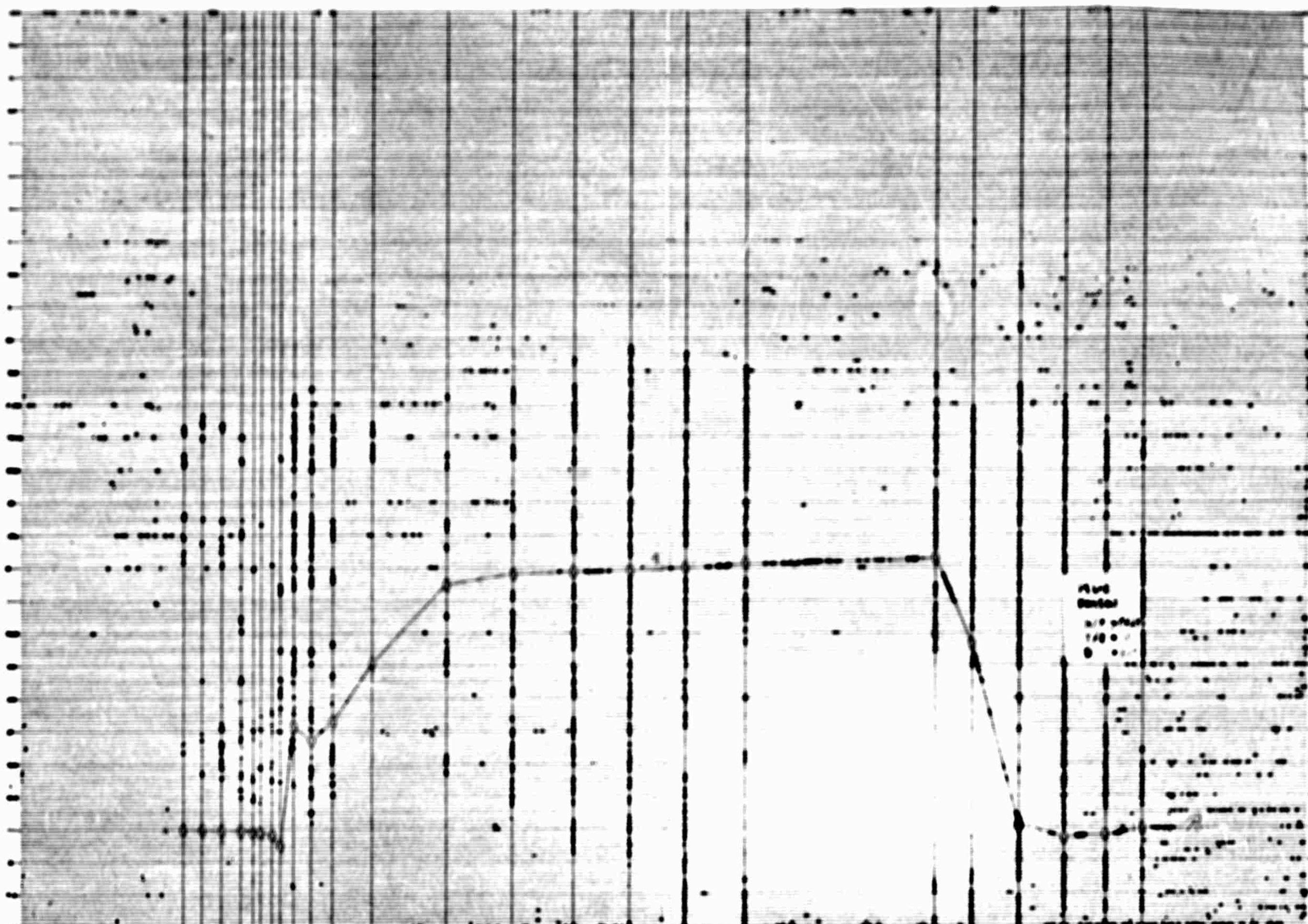

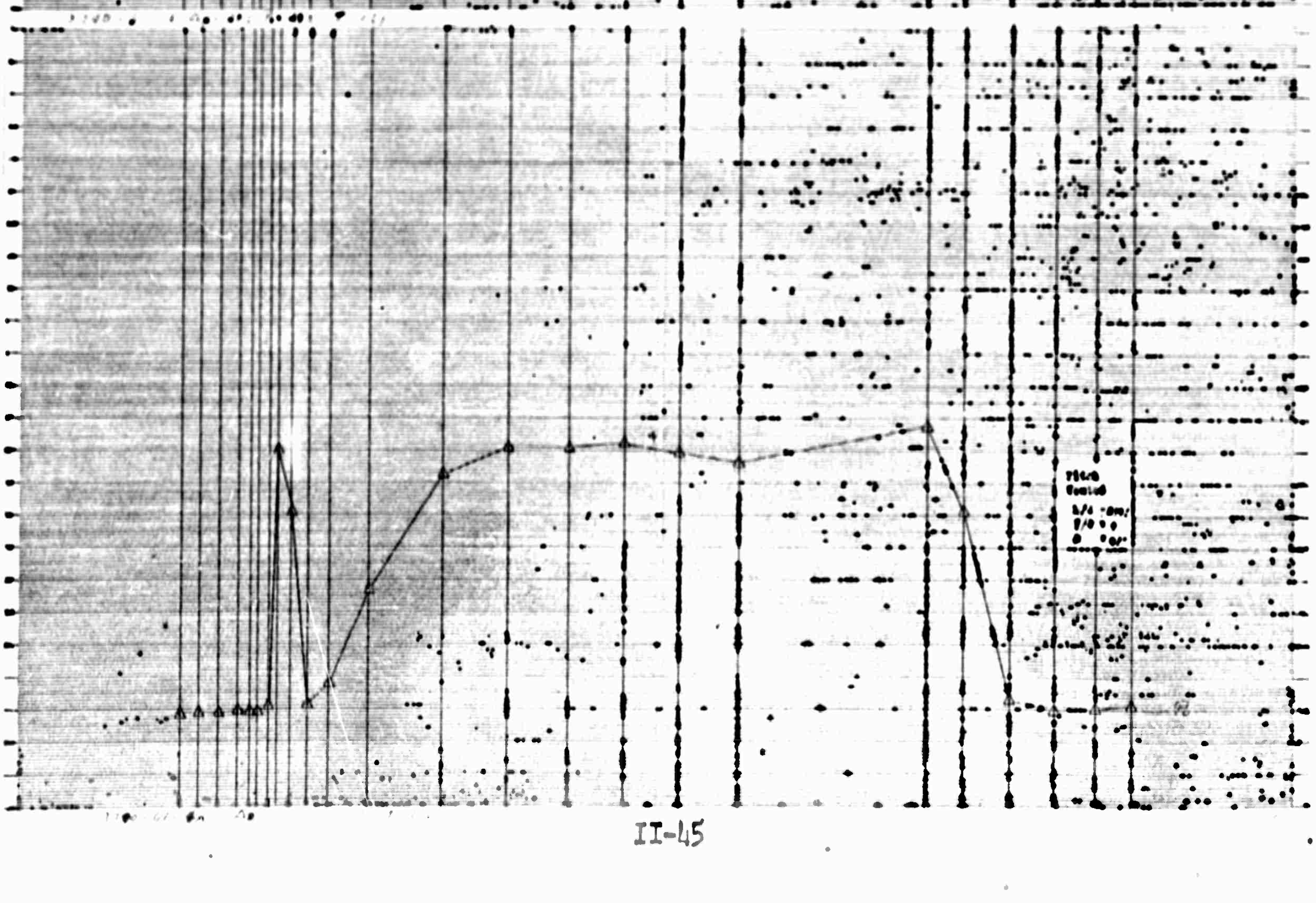

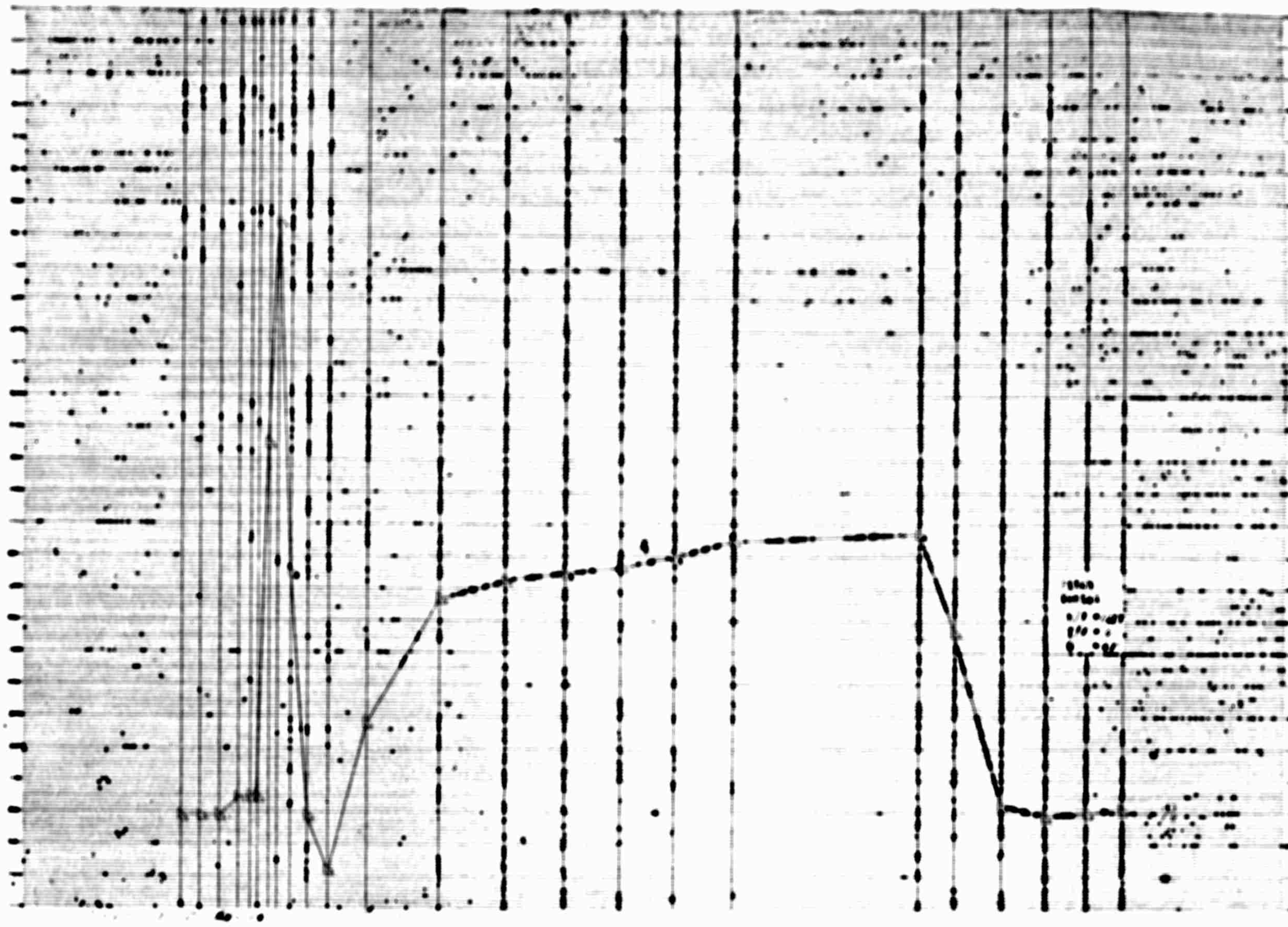

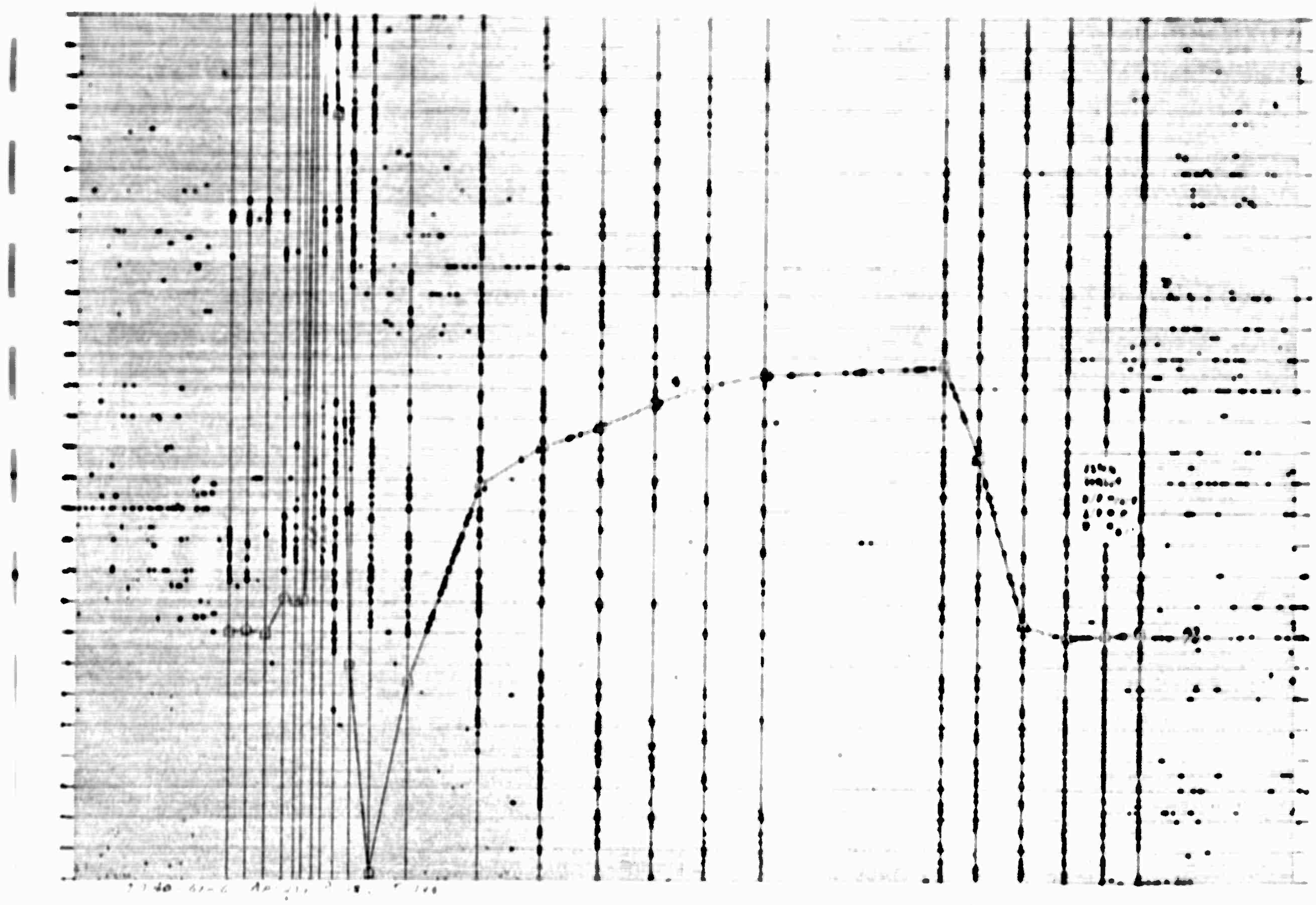

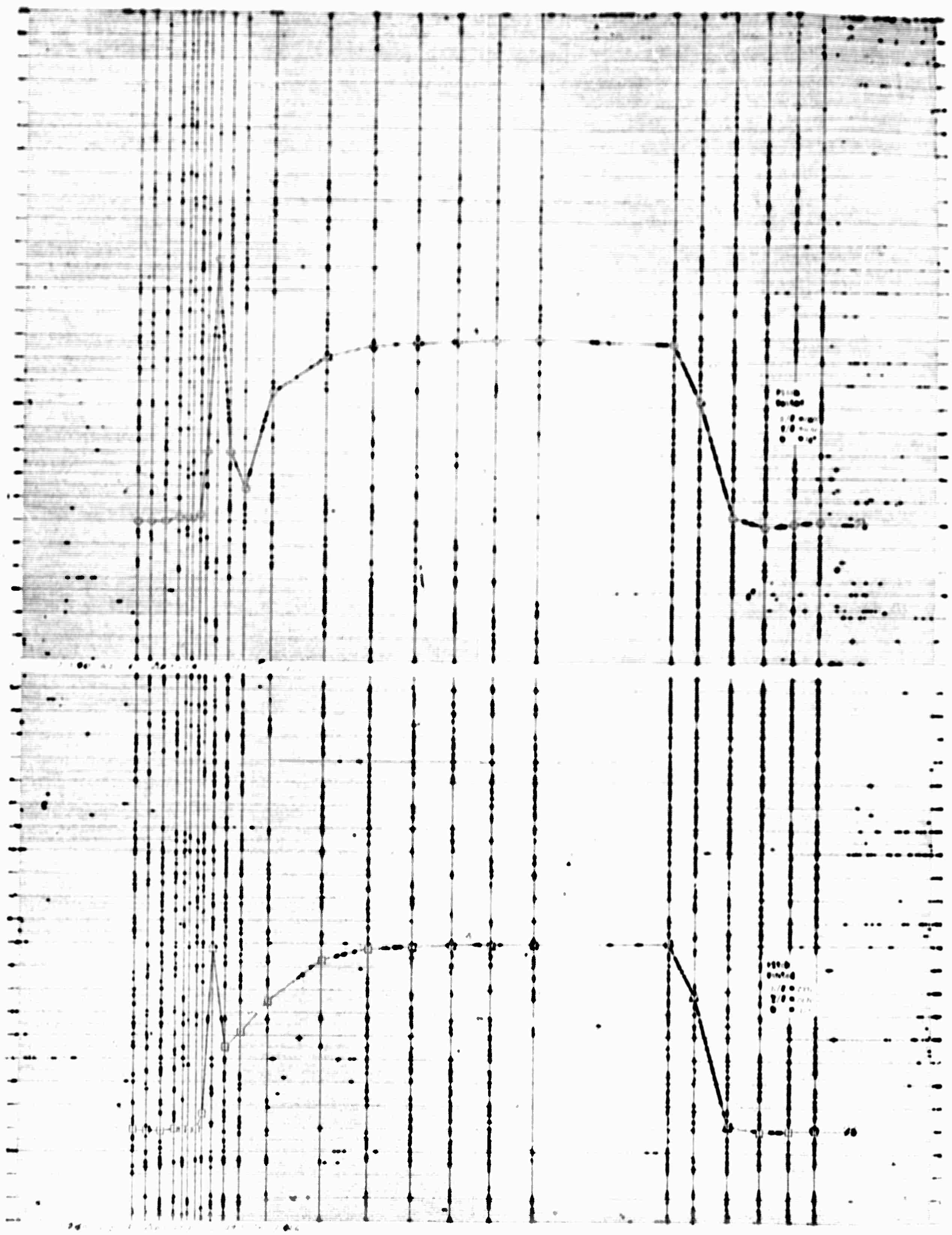

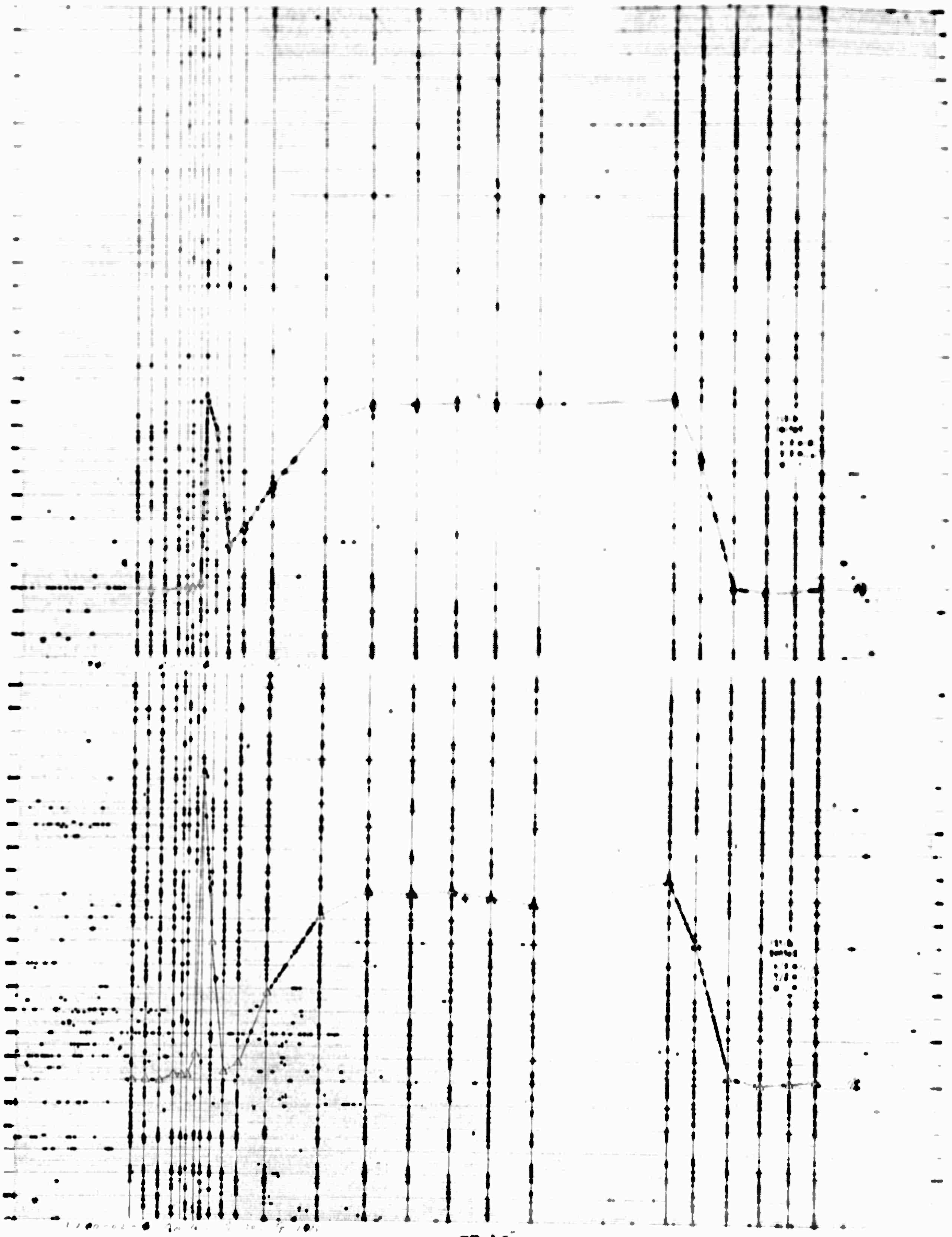

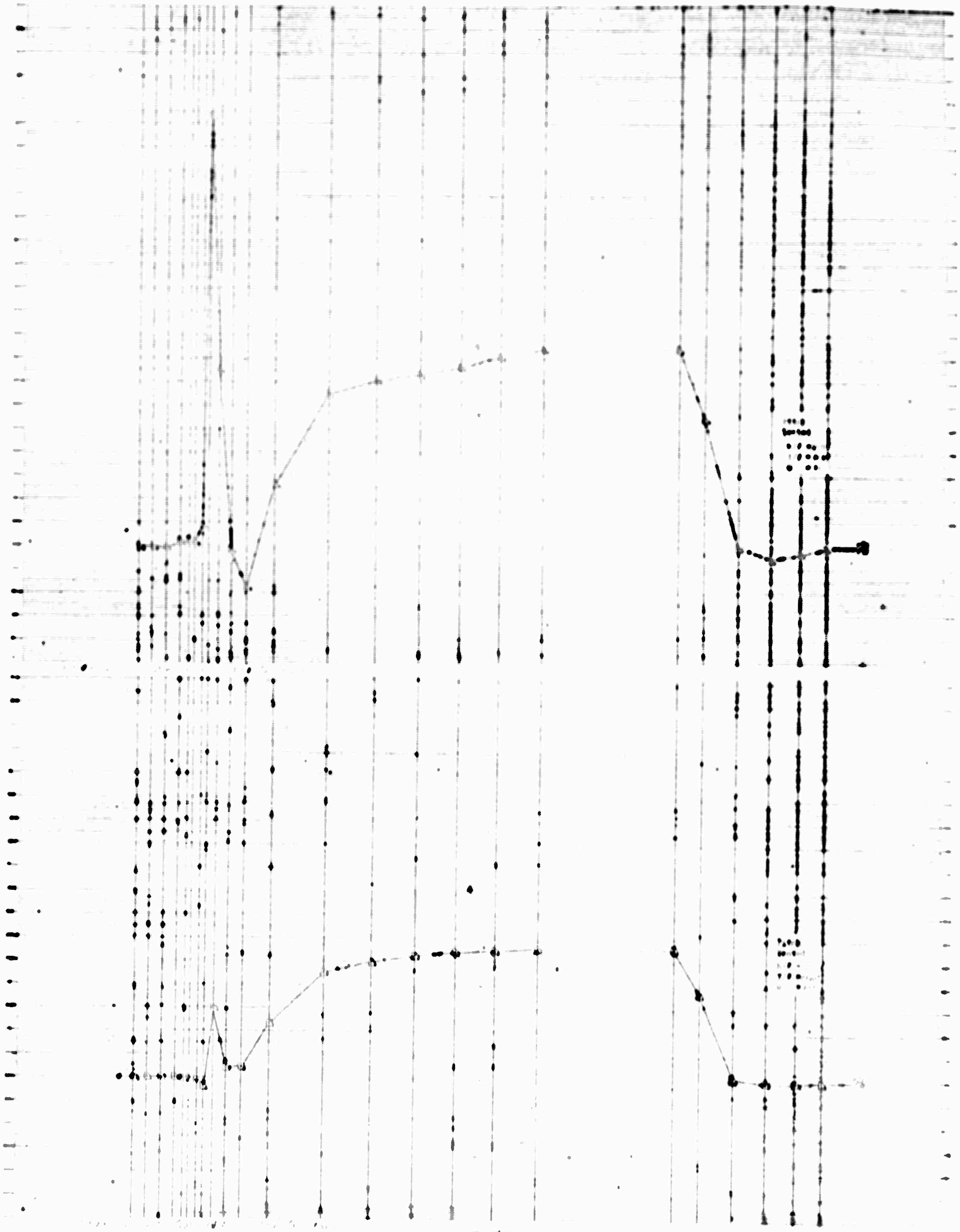

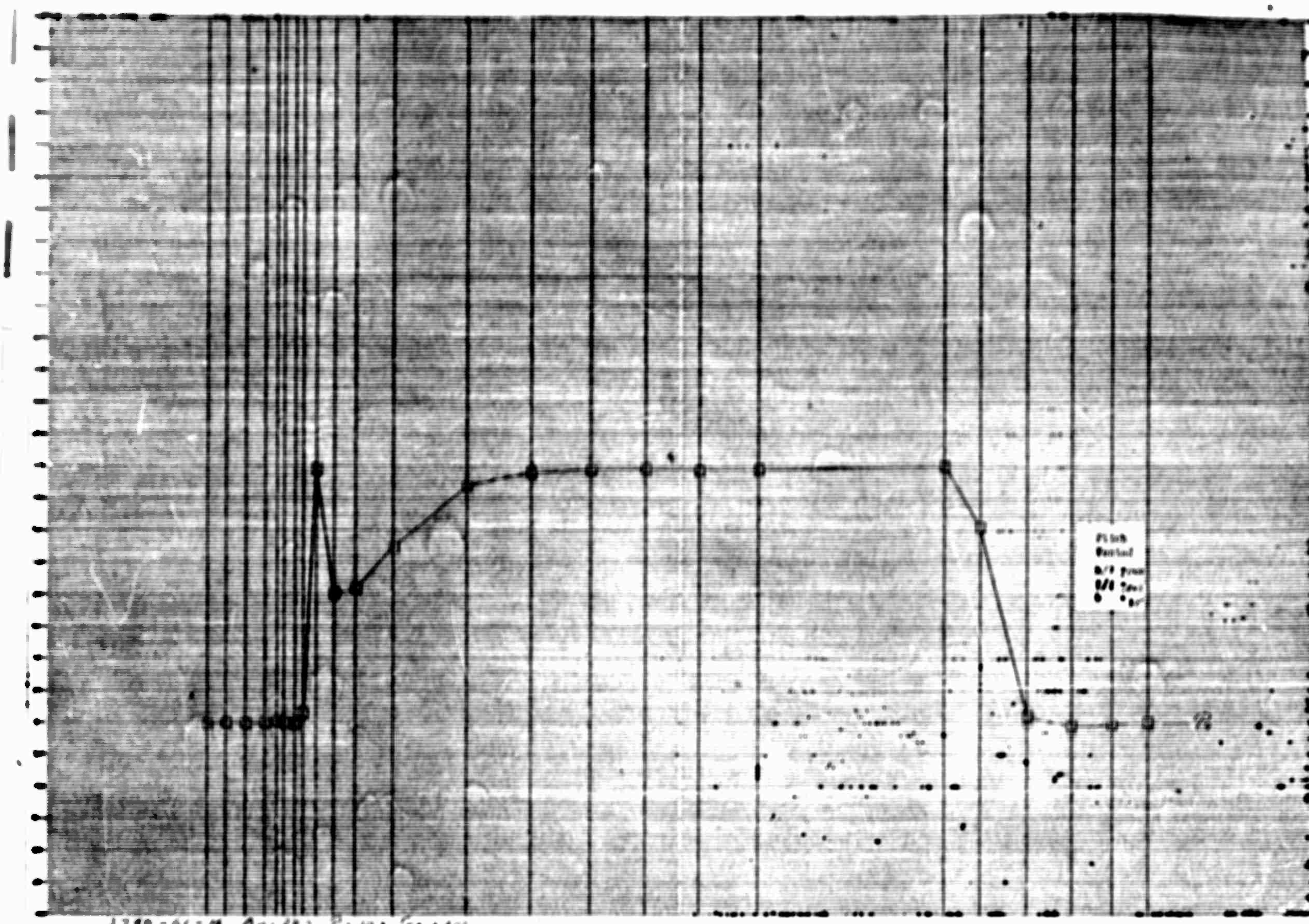

Pitch
Vented

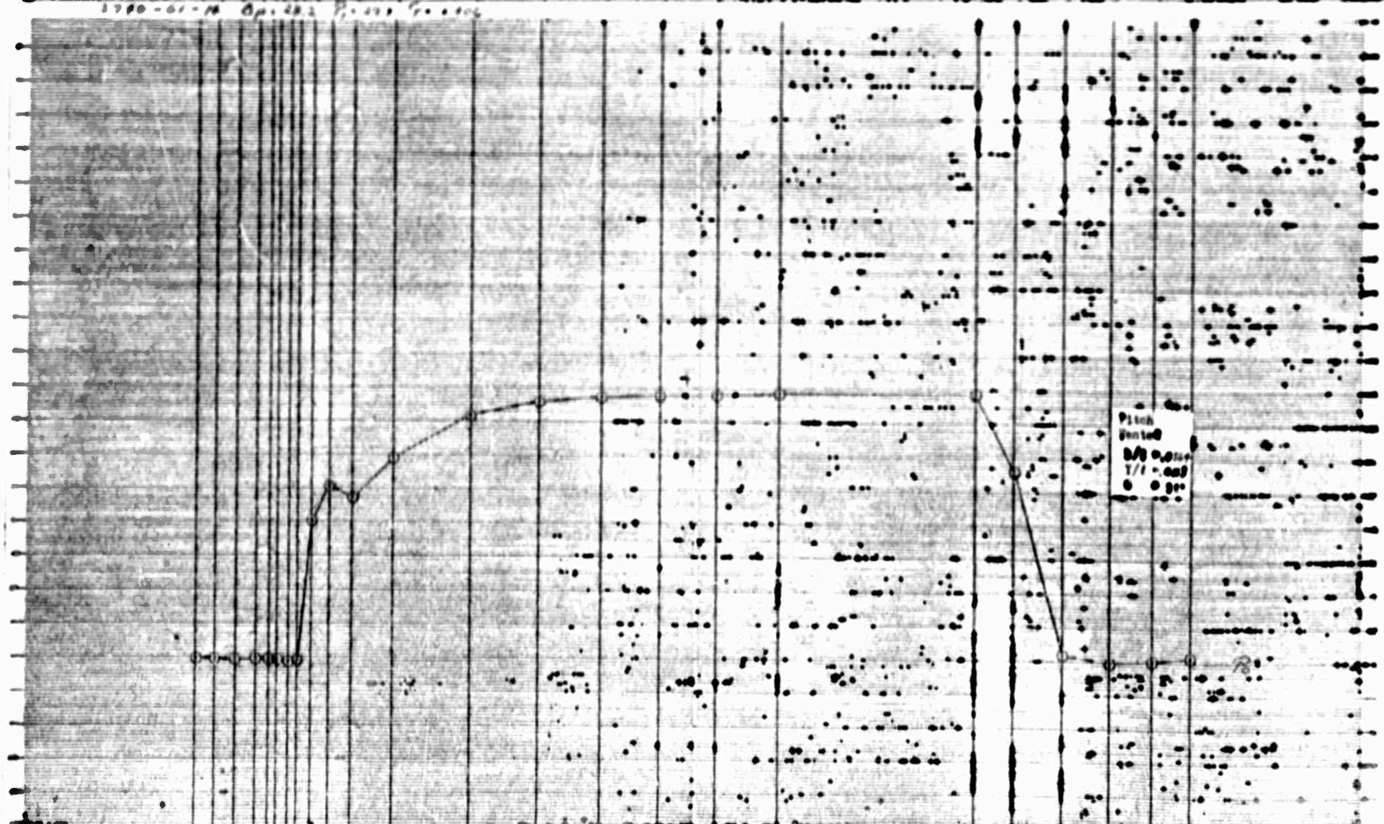

Pitch
Vented

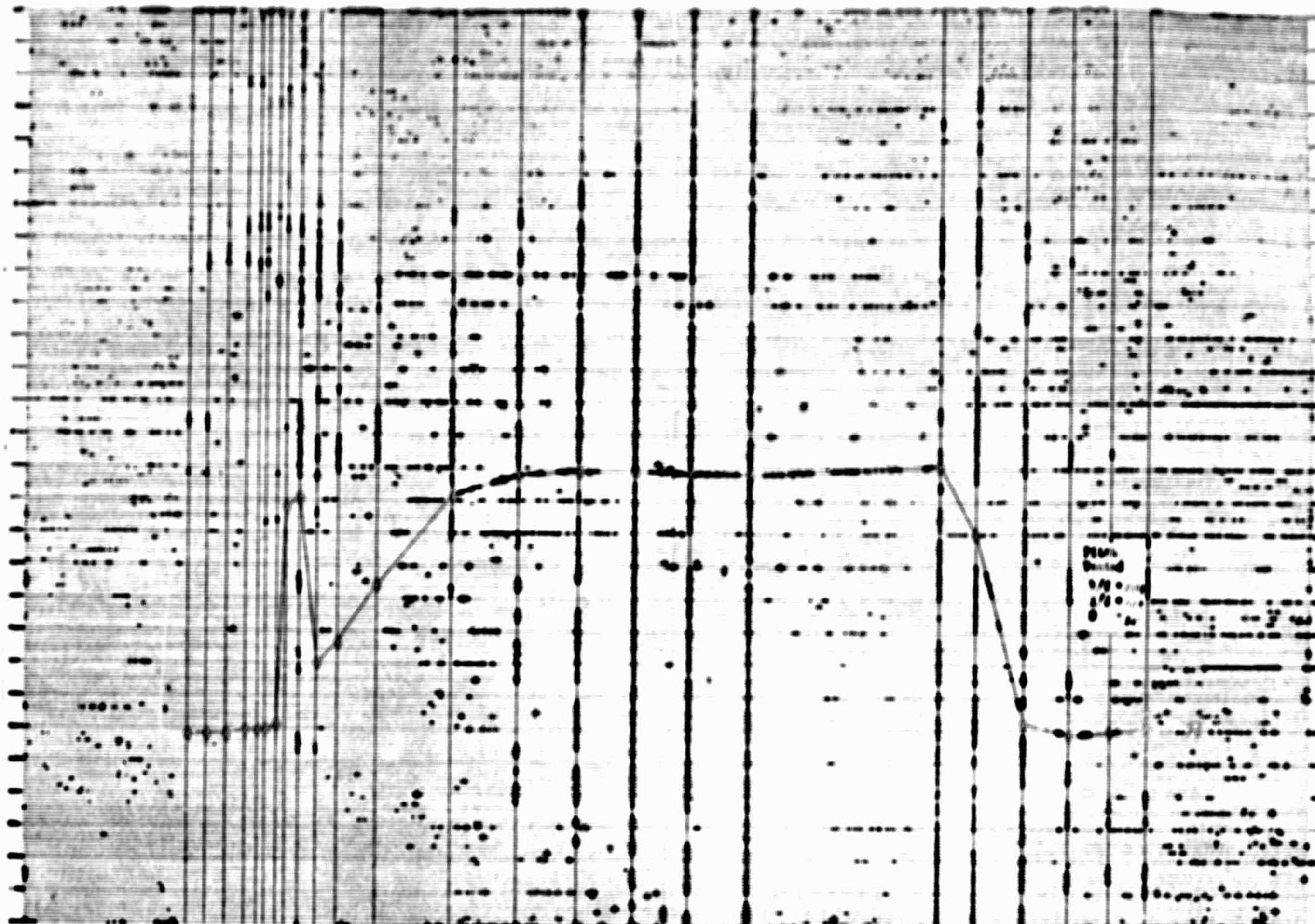

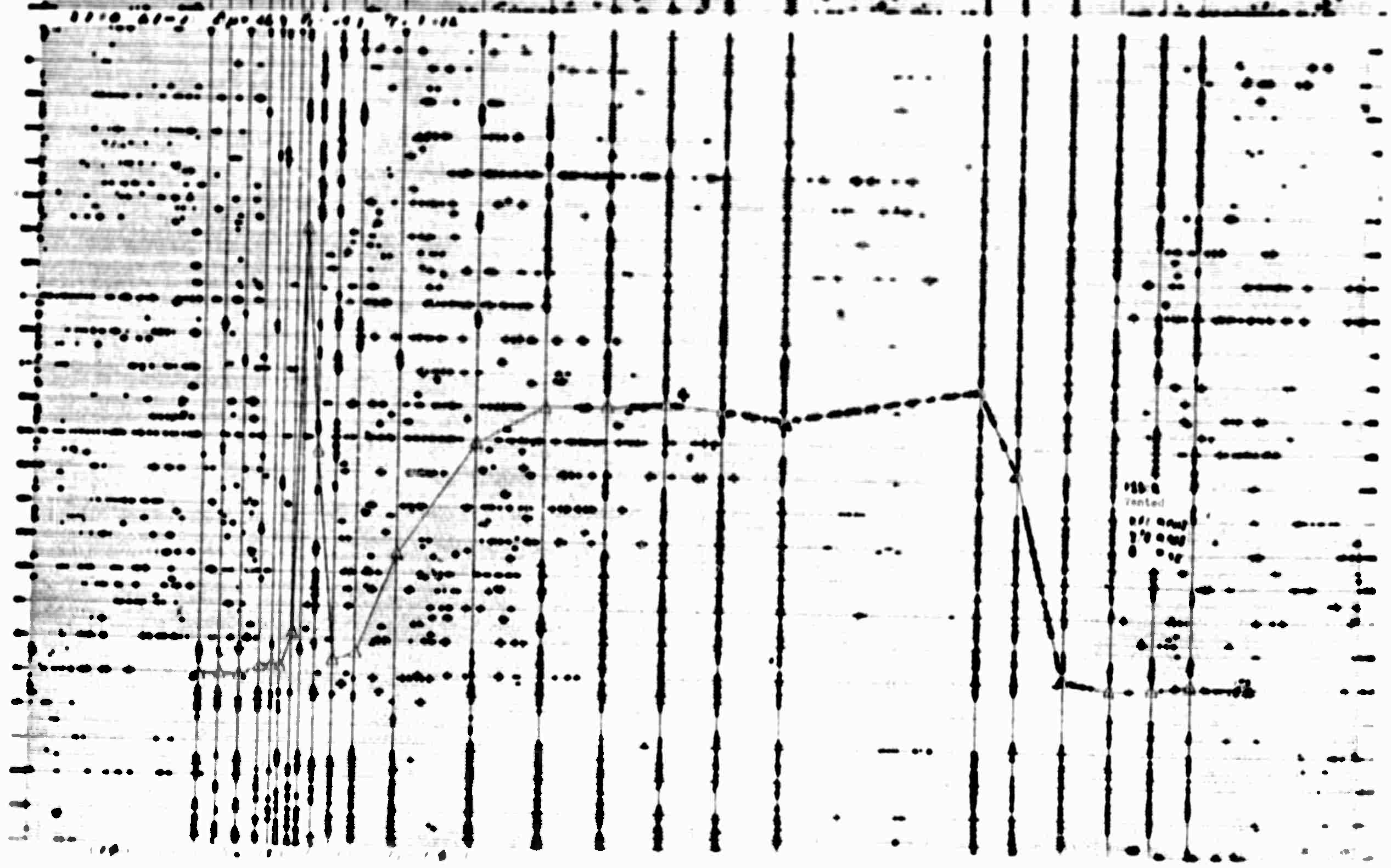
Vented